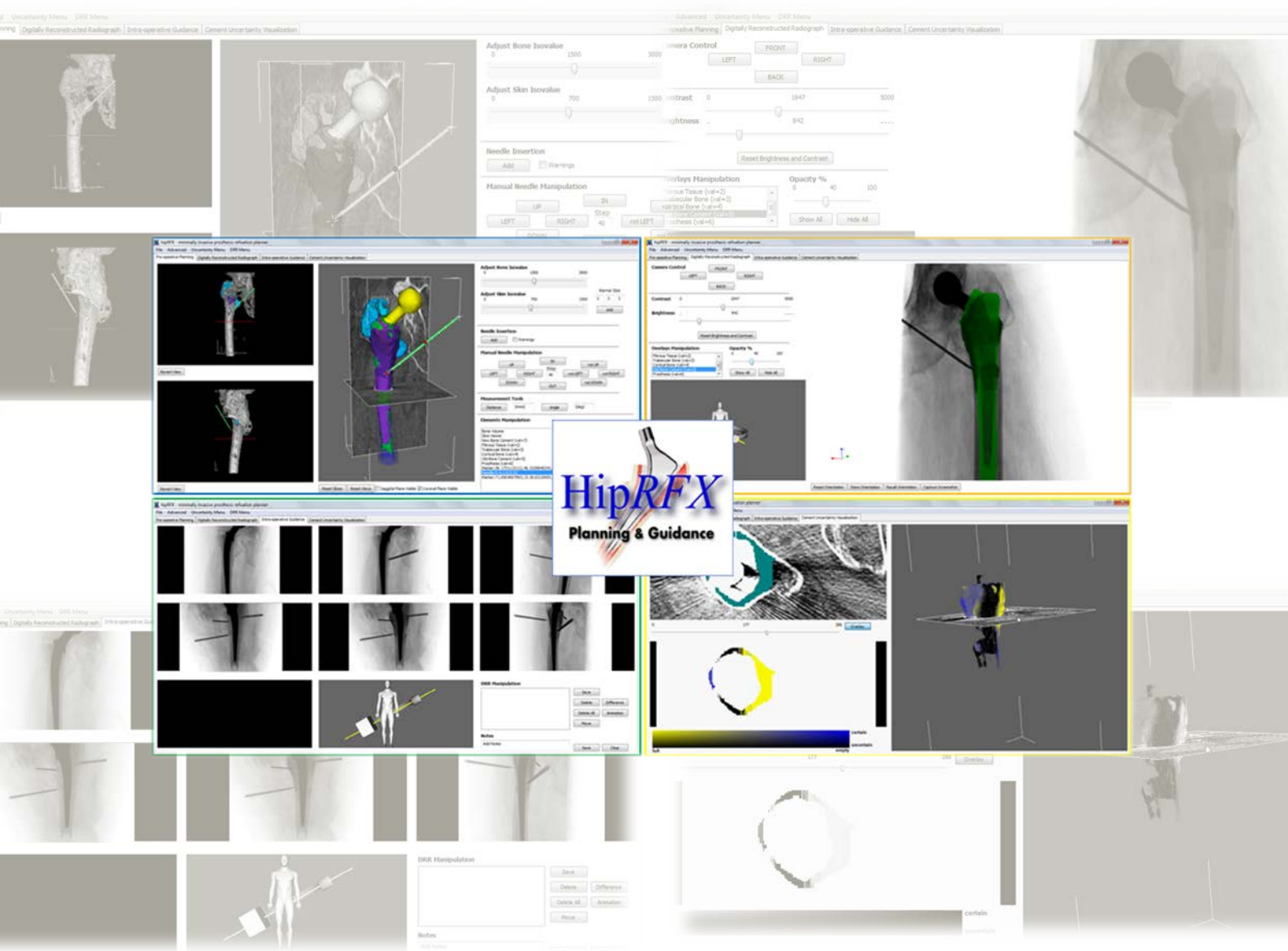


Visualization for the Planning and Guidance of Minimally Invasive Cement Injection in Orthopaedics

Master Thesis



Renata- Georgia Raidou

Visualization for the Planning and Guidance of Minimally Invasive Cement Injection in Orthopaedics

THESIS

submitted in partial fulfillment of the
requirements for the degree of

MASTER OF SCIENCE

in

BIOMEDICAL ENGINEERING

by

Renata-Georgia Raidou
born in Volos, Greece



Computer Graphics Research Group
Department of Intelligent Systems
Faculty EEMCS, Delft University of Technology
Delft, the Netherlands
www.ewi.tudelft.nl



Leiden University Medical Center
Department of Orthopaedics
Albinusdreef 2, 2333 ZA
Leiden, the Netherlands
www.lumc.nl

Visualization for the Planning and Guidance of Minimally Invasive Cement Injection in Orthopaedics

Author: Renata-Georgia Raidou
Student Number: 4125819
Email: R.G.Raidou@student.tudelft.nl

Abstract

Minimally invasive refixation by cement injection is a novel technique, performed at the Leiden University Medical Center for the revision of failed hip implants. During this procedure, the surgeon inserts needles into the periprosthetic space of the femur, to inject new cement for the fixation of the prosthesis. For that, two intra-operative imaging modalities are used: computed tomography (CT) and fluoroscopy. Still, this combination is not optimal, because of the inherent disadvantages of both modalities. The surgeons would appreciate a better workflow, to avoid computed tomography intra-operatively and to follow a fluoroscopic-based procedure, only.

In striving towards this goal, we implemented HipRFX, an integrated system for planning and guiding minimally invasive refixation. In our planning approach, the surgeon performs the operation virtually, using data from a single pre-operative CT scan. Then, the system uses the information from the plan, to simulate pseudo-fluoroscopic images. These images realistically imitate how the plan would ideally look on the fluoroscopic monitor. Intra-operatively, we propose a stepwise guidance approach. The surgeon uses the two-dimensional simulated radiographs with additional information embedded, as guidelines for the operation. Post-operatively, HipRFX offers cement filling uncertainty visualization, for the assessment of the outcome of the surgery.

In order to test our implementation, we conducted a domain expert review, during which we simulated the visual environment of a refixation procedure. Additionally, we performed other user-in-the-loop validations, concerning the user interface design and, especially, cement filling uncertainty visualization. The final evaluation of the HipRFX workflow was an in situ experiment, on 5 cadaver legs.

Our main contribution is a first practical investigation of a complete system, to assist orthopedic surgeons in planning, guiding and assessing minimally invasive refixation procedures. This new workflow has advantages over the current approach, where CT and fluoroscopy are combined, but also over a fluoroscopic-only approach. Our system is based on a single pre-operative CT scan and does not require intra-operative scanning, or new hardware. Moreover, we introduced cement filling uncertainty visualization, as a means of post-operative assessment, based on pre-operative information. To our knowledge, this is a novel domain that can offer new insight into the cement filling of the periprosthetic space. Our secondary contribution emerges from the results of our evaluations, which can be used in further research.

Thesis Committee:

Chair:	Prof.Dr.Ir. B.P.F.Lelieveldt, LUMC / Faculty EEMCS, TU Delft
Committee member:	Dr. C. P. Botha, Faculty EEMCS, TU Delft
Committee member:	Dr. F.M. Vos, Faculty TNW, TU Delft
Committee member:	D.F. Malan, M.Sc., LUMC / Faculty EEMCS, TU Delft

Preface

This Master Thesis is my last big step towards obtaining a Master of Science in Biomedical Engineering at the Delft University of Technology. This work was held in collaboration with the Leiden University Medical Center (LUMC). It aims at providing surgeons with a better workflow and a new insight into the data of patients that must undergo minimally invasive refixation of loosened hip prosthesis by cement injection.

My project was a wonderful “journey” that lasted ten months. Yet, it would not have been possible or that exciting if my “co-travelers” had been different. It was an opportunity to experience new things and broaden my horizons towards new directions. I am grateful that I had the best people next to me.

Firstly, I would like to thank Charl Botha for giving me the opportunity to work on this project, for his enthusiasm, encouragement and guidance. I would also like to thank François Malan, my daily supervisor, for his support and contribution to the project and, especially, for being so motivational. Our cadaver experiment was an once-in-a-lifetime experience. Additionally, I would like to thank Prof. Dr. Rob G.H.H. Nelissen, for his enlightening feedback during the evaluations, for being always enthusiastic and eager to help and, especially for his immense help with performing the cadaver experiment. This would not have been conducted, without the contribution of a number of people: Dr H.J.L. van der Heide and Marc Nieuwenhuijse, for placing the prostheses; Fred A.H. van Immerseel from the LUMC Anatomy Department for taking good care of our “subjects”; Noeska Smit, our enthusiastic radiographer on the day of the experiment; Edward Valstar, who had the idea of this experiment and aided in finding the instruments and the materials; Biomet®, for providing the needles and cement for the experiment. Moreover, I am deeply grateful to everyone who participated in the different evaluations and, especially, Bas van den Berg, for our excellent co-operation.

Above all, I would like to thank three really special people: my parents, Rita and Ilias, and my boyfriend, Minos, for encouraging me and being always there for me. Special thanks to all my friends who supported me, and mostly to my “luck-provider”, Belén. Finally, this thesis is dedicated to my grandfather, Nicola.

The layout and sectioning of this thesis was inspired by the article ‘How to Write a Visualization Research Paper: A Starting Point’, written by Laramée [2011], while the advices of Tamara Munzner in her paper “Process and Pitfalls in Writing Information Visualization Research Papers” [2008] were also taken into consideration.

Contents

Preface	iii
Contents	iv
List of Figures & Tables	v
1 Introduction	1
1.1 Motivation	1
1.2 Research Questions	1
1.3 Research Approach	2
1.4 System Requirements	2
1.5 Contributions	3
1.6 Organization	3
2 Background	5
2.1 Computer Assisted Orthopedic Surgery	5
2.1.1 Computer Assisted Orthopedic Surgery: General Pipeline	5
2.1.2 Medical Imaging Modalities in Computer Assisted Orthopedic Surgery	6
2.1.3 Computer Assisted Orthopedic Surgery: Benefits and Drawbacks	6
2.2 Aseptic Loosening and Minimally Invasive Refixation	6
3 Related Work	9
3.1 Computer Assisted Orthopedic Surgery System	9
3.2 Uncertainty Visualization	11
4 Method	13
4.1 Overview	13
4.2 Pre-Operative Planning	14
4.3 Digitally Reconstructed Radiograph Simulation	16
4.4 Intra-Operative Guidance	18
4.5 Cement Filling Uncertainty Visualization	19
4.5.1 Decision making: Visualization Technique	20
4.5.2 Decision making: Visualization Colormap	22
4.5.3 Cement Filling vs. Uncertainty Visualization	23
4.6 Summary	24
5 Implementation	25
5.1 User Interface Build-Up	25
5.2 Datasets	25
5.3 Pre-Operative Planning Implementation	26
5.4 Digitally Reconstructed Radiograph Simulation Implementation	28
5.5 Intra-Operative Guidance Implementation	28
5.6 Cement Filling Uncertainty Visualization Implementation	29
5.7 Summary	30
6 Results	31
6.1 General Results	31
6.2 Performance	32
6.3 Evaluations	33
6.3.1 Colormap Determination Survey	33
6.3.2 Color-Deficiency Evaluation of Uncertainty Visualization	34
6.3.3 Graphics User Interface (GUI) Evaluation	34
6.3.3.1 Graphics User Interface Evaluation with ISO9241-11	34

6.3.3.2	Graphics User Interface Evaluation with the System Usability Score (SUS)	35
6.3.4	Cement Filling Uncertainty Evaluation	36
6.3.4.1	Quantitative Cement Filling Uncertainty Visualization Evaluation	36
6.3.4.2	Qualitative Cement Filling Uncertainty Visualization Evaluation	37
6.4	Domain Expert Review	38
6.4.1	Review on Pre-Operative Planning	39
6.4.2	Review on Digitally Reconstructed Radiograph Simulation	39
6.4.3	Review on Intra-Operative Guidance	39
6.4.4	Review on Cement Filling Uncertainty Visualization	40
6.4.5	Overall Review on HipRFX	40
6.5	Cadaver Study Evaluation	40
6.5	Limitations	43
6.6	Summary	43
7	Conclusions and Future Work	45
7.1	Conclusions	45
7.2	Future Work	46
	Bibliography	47
	Appendix A	51
	Glossary	55

List of Figures & Tables

Figure 1.1: Flow chart of our research approach.	2
Figure 2.1: Typical flow path of a CAOS system [Joskowicz 2001].	5
Figure 2.2: Aseptic loosening after total hip arthroplasty, with extensive osteolysis around the femoral component (shown with the arrows) and mechanical failure of the prosthesis, resulting in aseptic loosening [Wilkinson 2011].	7
Figure 2.3: Typical example of minimally invasive refixation, as held at the LUMC. (A) – Needles being hammered in the periprosthetic space. (B) – Cement injection. (C) – Intra-operative fluoroscopic guidance of the cement flow. (D) – Cross-sectional model of the hip during minimally invasive refixation.	7
Figure 3.1: Placement of needle into sacroiliac joint, using XperGuide, (A) – on a slice and (B) – on 3D volume [Racadio 2007].	9
Figure 3.2: Fixation of a patient with osteotomy at his calcaneus, with the use of two pedicle screws. (A) – 3D reconstruction of the screws on a 2D reconstruction of the coronal plane of the lower foot. (B) – 3D visualization of the same region. The calcaneus is depicted with green, the talus with red and the rest of the lower foot with blue [Dahlen 2001].	10
Figure 3.3: Tumor Formation Visualization. (A) – Polygonal model of tumor, without uncertainty information.	11
(B) – Polygonal model with pseudocolor, where the tumor geometry and the uncertainty information are conveyed. (C) – Point-based model [Grigoryan 2004].	11
Figure 3.4: Three frames of an uncertainty animation on a renal angiography, for a region suspected for stenosis [Lundström 2007].	12
Figure 4.1: Conceptual model	13
Figure 4.2: Workflow of the pre-operative planning.	14
Figure 4.3: Graphics User Interface and renderers. (A) – Additional Renderers, (B) – Main Renderer, (C) – Operation Panel	14
Figure 4.4: Two examples of multi-tissue visualizations. Color legend: (Blue) – Cortical Bone, (Cyan) – Trabecular Bone, (Dark Green) – Cement Target, (Light Green) – Old Cement, (Red) – Vessel to avoid, (Yellow) – Prosthesis, (White) – Bone.	15
Figure 4.5: Needles insertion procedure (in green we visualize once more the cement target)	15
Figure 4.6: Measurements. (A) – Distance measurement (in mms), (B) – Angle measurement (in degrees)	16
Figure 4.7: Digitally Reconstructed Radiograph simulation of a needle and cement target insertion (A), compared to a real fluoroscopic image (B).	16
Figure 4.8: An H&D curve with all the parameters that are used to describe it	17
Figure 4.9: Digitally Reconstructed Radiograph Simulation without overlays (A) and with overlays (B) to highlight specific structures, such as cement target (dark green), old cement (light green) and cortical bone (blue).	17
Figure 4.10: Workflow of the intra-operative guidance.	18
Figure 4.11: Stepwise intra-operative guidance workflow. (A) – Before the intervention, (B) – Optimal view for the insertion of a first needle, (C) – Optimal view for the insertion of a second needle, (D) – Optimal view for the insertion of a third needle, (E), (F), (G) – Cement Injection from different viewpoints, (H) – Model of a patient in a C-arm fluoroscope, to view the position of the fluoroscope for each of the previous cases, (I) – Operations Panel.	18
Figure 4.12: Difference Images Tool. (A) – Radiograph captured before the operation. (B) – Radiograph after the needle and cement target insertion. (C) – Deformed Annotation Grid for the difference image between (A) and (B). (D) – (Flickering) Overlaid difference image between (A) and (B).	19
Figure 4.13: Concept of cement filling uncertainty.	20
Figure 4.14: Related work, used as inspiration for our implementation. (A) – Value-by-alpha map to depict the standardized mortality ratio for cervical cancer, relative to the reliability score, for different cities in the US [Woodruff 2009]. (B) – Structure of a two-dimensional perceptually uniform isoluminant scale [Hemminger 1993]. (C) – The colormap that we employed in the visualization	21
Figure 4.15: (A) – Workflow of the cement filling uncertainty visualization. (B) – Workflow of the calculation of the cement filling and uncertainty (2D).	23
Figure 4.16: Cement Filling Uncertainty Visualization. (A) – Slice-based view of the spatial information of the volume on the data of the patient. (B) – Slice-based view of the uncertainty vs. filling information. (C) – Volume-based representation of the uncertainty vs. filling volume. (D) – Pie depicting the percentage of cement-filled space. (E) – Cement Uncertainty Distribution of the volume pixels.	23
Figure 5.1: An example of the user interface of HipRFX, while in use. (A) – Pre-Operative Planning Tab, (B) – Digitally Reconstructed Radiograph Simulation, (C) – Intra-Operative Guidance, (D) – Cement Filling Uncertainty Visualization.	25

Figure 5.2: Multi-Tissue Visualization Workflow. (A) – For the automatic bone volume rendering and skin surface rendering, (B) – For the manually segmented structures.	27
Figure 5.3: Difference Image Visualization Workflow.	29
Figure 5.4: Cement Filling Uncertainty Visualization Workflow.	29
Figure 6.1: Nested Model for the evaluation of the HipRFX system (adapted by [Munzner 2009], on the left). On the right, table showing the target level and also the employed method, for each evaluation.	31
Figure 6.2: Results from the implementation of our HipRFX system on different datasets. For each dataset (same row) we show the three most important tasks: multi-tissue visualization, simulation of the fluoroscopic images after the insertion of needles and cement injection, and the cement filling vs. uncertainty visualization (3D and 2D slices).	32
Figure 6.3: Options and preference results (pie chart indicating preference) of the evaluation concerning (A) the red-to-green colormap and (B) the blue-to-yellow colormap. Not all eight combinations were considered, only the four more sensible.	33
Figure 6.4: VisCheck testing of our cement uncertainty visualization. (A) – For blue-to-yellow colormap. (B) – For red-to-green colormap. Checks: (I) – Deuteranope Simulation, (II) – Daltonized Image, (III) – Deuteranope Simulation of Daltonized Image.	34
Figure 6.5: Boxplots for the evaluation results concerning the effectiveness, efficiency, satisfaction [ISO9241-11/1998] of the HipRFX interface, for each one of the tasks involved in the three first cases. The green lines refer to the median values, the grey lines to the min/max values and the red lines to the 1 st and 3 rd quartile. A legend for the tasks is also provided.	35
Figure 6.6: Graph depicting the System Usability Scale Score [Brooke 1996]. With blue we show the median value (72.5%), with grey the 80% confidence interval and with red and green, the min and max values, respectively.	36
Figure 6.7: Graph depicting the workflow for the quantitative evaluation of the cement filling uncertainty visualization.	36
Figure 6.8: Boxplot of the predicted values of the cement filling percentage for two demos and histogram for the proximity of the predictions to the true value.	37
Figure 6.9: Boxplot of the predicted values of the cement filling uncertainty percentage for two demos and histogram for the proximity of the predictions to the true value.	38
Figure 6.10: Graph depicting the workflow for the cadaver experiment.	40
Figure 6.11: CT scan of aseptic loosening simulation by creating periprosthetic lesions to the cadaver legs.	41
Figure 6.12: Pre-operative plan generation for one of the cadaver legs.	41
Figure 6.13: Cadaver Experiment setting and different stages. (A) – Prosthesis placement. (B) – Creation of periprosthetic lesions for simulating aseptic loosening. (C) – Needle insertion with the aid of the pre-operative plan generated by HipRFX, (D) – Cement injection monitored by fluoroscopy. The cadaver legs have been hidden, due to ethical implications.	42
Figure A.1: Distribution of the participants based on sex and experience with user interfaces.	51
Figure A.2: Adapted SUS-System Usability Score Scale (SUS: Digital Equipment Corporation ©, 1986)	51
Figure A.3: Histograms showing the probability distribution of the uncertainty for the 18 simulated cases that we tested the visualization tool. We depict with the red vertical reference line the mean value of the uncertainty and with the blue vertical reference line the value for the differentiation of the uncertain from the certain areas. Since it is an uncertainty distribution the value 0 corresponds to totally certain, while the value 1 to the totally uncertain. On the caption of every histogram, we provide the mean value and the clustering value U (mean + standard deviation).	52
Figure A.4: Scatterplot showing the linear relationship between the two Hard Dice Indices given by the equation $y=0,9984x$	53
Figure A.5: Scatterplot showing the linear relationship between the Rough Hard Dice and the Soft Scaled Dice Index given by the equation $y=0,9987x$	53
Figure A.6: Scatterplot showing the exponential relationship between the Scaled Soft Dice Index and the Cement filling percentage, as calculated from the system for each one of the simulations.	53
Figure A.7: Scatterplot showing the exponential relationship between the Scaled Soft Dice Index and the Cement filling, as well as with both Hard Dice Indices. The Refined Hard Index is mapped to the traffic-light color scale. The Rough Hard Index is mapped to the circles size.	54
Figure A.8: Boxplots of the four characteristics scores and the cumulative (average of the four characteristics) score of the uncertainty visualization. We present with the red lines the mean value, with the green lines the median and with the grey the minimum/maximum values. The first and third quartiles are also visible.	54
Figure A.9: Performance time reduction for the 5 subjects of the cadaver experiment, with the use of HipRFX	54
<hr/>	
Table 4.1: Different Technique Options for Uncertainty Visualization (in green, adapted from [Griethe 2005]) and Important Key Challenges and Required Features (in blue, adapted from [MacEarchen2005]).	20
Table 4.2: Comparison of colormap effectiveness (adapted by [Moreland 2009]).	22

Chapter 1

Introduction

In this chapter, we introduce the motivation for our research, as well as the primary research questions and our approach. This is followed by the system requirements for our solution and the contributions of our work.

1.1 Motivation

Annually, 1.5 million hips receive a prosthetic implant [Otten 2010]. Between 1995 and 2005, the annual number of hip replacements in the Netherlands increased from 13,785 to 20,715. It was estimated that by 2030, this number will rise up to 31,731 [Otten 2010]. Although orthopedic surgery is a mature practice, 5-10% of prostheses fail within 10-15 years, due to aseptic loosening. These patients have to go back to the operation room, for a revision.

At the Leiden University Medical Center, orthopedic surgeons adopted a new technique for the revision of failed hip prostheses: minimally invasive refixation by cement injection. During this procedure, needles are inserted into the periprosthetic space of the patient, guided by intra-operative computed tomography (CT). This means that until the needle is placed correctly, the patient might be scanned multiple times, increasing his radiation exposure. Then, polymethylmethacrylate (PMMA) cement is injected, while its flow is monitored by a c-arm fluoroscope [dePoorter 2008]. Although fluoroscopy provides cheap and real-time monitoring, with a low radiation dose, it gives lower image quality and no depth information. Both imaging modalities have disadvantages and their combined use in the refixation procedure is not optimal, yet.

Computer Assisted Surgery (CAS) is an active field of research. It has managed to improve the accuracy of surgical procedures, made minimally invasive surgery easier and gave the chance to surgeons to explore new concepts in surgery [Sugano 2003]. Additionally, it has facilitated training and education, with the aid of pre-operative planning, which allows surgeons to simulate and optimize surgical procedures [Sugano 2003]. Minimally invasive refixation procedures could benefit from a CAS system that would provide a better workflow. At the same time, the use of intra-operative computed tomography scans would be limited only to pre-operative stages, to reduce radiation exposure.

1.2 Research Questions

The main research questions that we aim to answer are the following:

- How can we develop a system that will improve the planning and guidance workflow of minimally invasive refixation procedures, by supplanting intra-operative CT to reduce radiation exposure? How can this system be compatible with already existing hardware (c-arm fluoroscopes)?
- How can we aid users to gain new post-operative understanding by visualizing the cement filling? How can we enrich this insight, with the visualization of the expected error or uncertainty of the cement filling data?

As we already mentioned in the Motivation part, surgeons performing minimally invasive refixation could employ a better system than the currently used approach, by avoiding intra-operative CT. The first challenge was to implement an accurate and complete system, HipRFX. This would provide a better workflow in the operational procedure. It would not require new hardware in the operation room and it would ensure compatibility with the already existing fluoroscope.

The second point is to provide new insight, by introducing uncertainty visualization in the final step of our system, for the assessment of the cement filling. Uncertainty is often overlooked, but it is an important influence on the data. It is also challenging, because it has to be visualized in a careful way, ensuring that it does not lead the user to any false conclusions.

1.3 Research Approach

Our HipRFX system facilitates and enhances minimally invasive refixation procedures step-by-step. Its workflow is depicted in Figure 1.1, below. In our approach, the patient is inserted in the CT scanner only once. Based on this dataset, the surgeon can build the pre-operative plan, by virtually inserting the needles and injecting the cement, into the periprosthetic space. Then, the system can simulate pseudo-fluoroscopic images, from our pre-operative plan. These will imitate in a realistic way the ideal view on the fluoroscopic monitor, during the surgical procedure. The surgeon can capture the simulated radiographs, in order to use them intra-operatively, in the form of two-dimensional steps. After the operation, the surgeon can perform the cement filling uncertainty visualization for the assessment of the surgical outcome, based on a single 2D radiograph. In this visualization, the uncertainty is situated in areas hidden by the prosthesis.

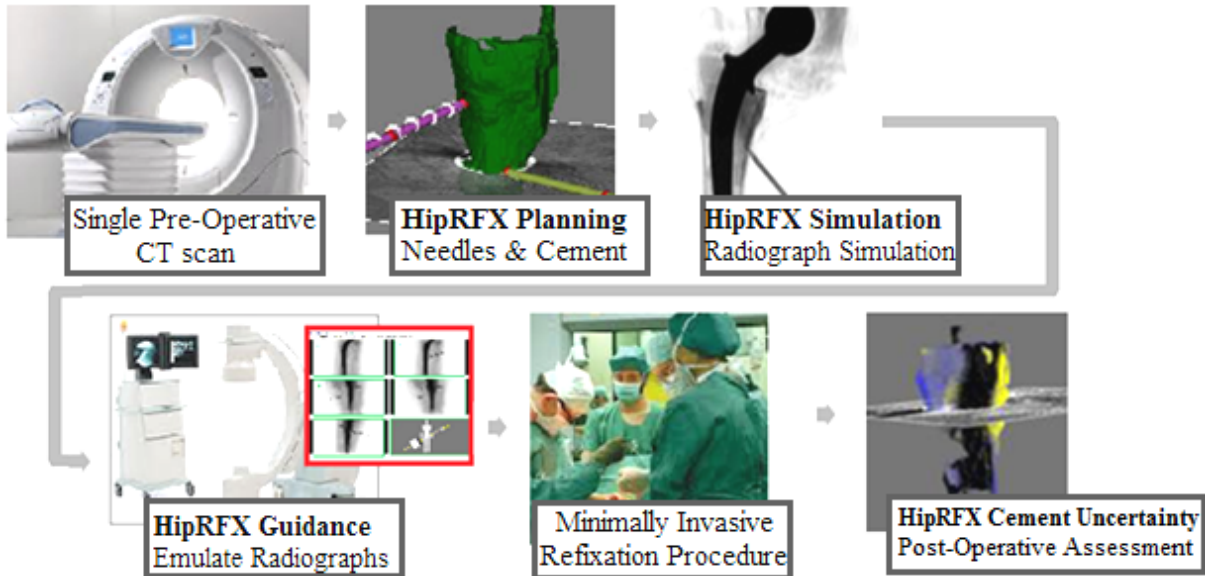


Figure 1.1: Flow chart of our research approach.

The HipRFX system was tested on real clinical CT datasets, which were all provided by the Leiden University Medical Center. Apart from that, we performed a domain expert review for feedback on the usefulness of specific features, on missing traits and on limitations of the system. Moreover, we tested the system in situ, experimenting on 5 cadaver subjects. Finally, we conducted a user interface design evaluation and four different evaluations concerning cement filling uncertainty visualization. These evaluations covered different aspects of our system and showed its potential, as it will be discussed in the following chapters.

1.4 System Requirements

The requirements for the successfulness of our systems are the following:

1. Datasets requirements:
 - The system should be able to deal with all possible types of datasets that the clinicians use.
 - The system should be able to handle datasets acquired by different machines, having, therefore, different resolutions and spacings.
2. Functional requirements:
 - The system should introduce a new workflow for minimally invasive cement refixation. Pre-operatively, it should require only a single CT scan, which will provide high quality three-dimensional information on the region of interest. Intra-operatively, it should not involve CT, but only fluoroscopy, for lower radiation exposure. Other new hardware should also be avoided, for cost reduction.
 - The system should be compatible with the traditional, cheap and widely available C-arm fluoroscopes. In this way, registration with expensive and bulky reflective tracking markers will be avoided. A fluoroscopy-based intra-operative approach ensures also real-time feedback. In our

approach, it will be combined with pre-operative CT, for achieving higher quality images and depth information.

- The system should opt for intuitive pre-operative planning and intra-operative guidance, based on the pre-operatively acquired CT and on radiographs simulated from this dataset. For post-operative assessment, we require a visualization of the periprosthetic space that was filled by cement. It is also important to show the uncertainty of the cement filling, in the areas, where the fluoroscopic view is hindered by the implant.
- The system should be independent from the surgeon experience. Different surgeons might also consider different intra-operative information important for the completion of the operation. Therefore, the workflow and, especially intra-operative guidance, involves a high degree of subjectivity. For that, the system should be flexible.

3. Visualization requirements:

- During pre-operative planning, the desired needle placement and cementing targets should be interactively visualized in space. The system needs to be able to visualize all the relevant anatomical information.
- During digitally reconstructed radiograph simulation, all the structures, along with the needles and the injected cement, should be realistically simulated.
- During intra-operative guidance, the three-dimensional plan should be illustrated with a series of two-dimensional stepwise information, including the needle(s), target site, and desired injected bone cement distribution.
- For the cement filling uncertainty visualization, we know that the uncertainty should not overshadow the data (or vice versa). The uncertainty information could, therefore, be an additional parameter to the filling data. It is desirable to use linked 2D and 3D views.

1.5 Contributions

Our main contribution is the implementation of HipRFX. It consists the first practical investigation of a complete system for assisting minimally invasive refixation procedures. This will aid orthopedic surgeons, step-by-step, in pre-operative planning, intra-operative guidance and post-operative assessment. Additionally, visualizing three-dimensional volumetric cement filling, based on a single 2D radiographic projection, entails a degree of uncertainty. This uncertainty is located, especially, in the areas, where the view is hindered by the prosthesis. Therefore, cement filling uncertainty visualization can provide new insight into the data, aiding the surgeon to assess the surgical outcome.

Our secondary contribution emerges from our manifold evaluation (domain expert review, cadaver experiment, user interface evaluation, color-map determination and assessment, simulated test-cases and qualitative evaluation for the cement filling uncertainty visualization). These evaluations showed how well the different components of our system work. Additionally, the results of our evaluations can be used in further research, or in other related developments.

1.6 Organization

The rest of the paper is organized as follows. In Section 2 and 3, respectively, the medical background and previous work related to the topic is presented. Those two sections are a summarized version of the literature study, conducted at the beginning of this project, entitled “Image based planning of orthopedic surgery”. Section 4 presents the method used for the implementation of our tool, which is described subsequently in Section 5. In Section 6 we present the results obtained from our evaluations. Finally, Section 7 includes conclusions and directions for future work.

Chapter 2

Background

In this chapter we include some background information on computer assisted orthopedic surgery, its general pipeline, the medical imaging modalities that it employs and the benefits from its use. In the problem domain, we describe aseptic loosening and minimally invasive refixation.

2.1 Computer Assisted Orthopedic Surgery

Computer Assisted Orthopedic Surgery (CAOS) does not have a single definition in literature [Carr 2010, Stiehl 2010, Ellis 2005], mainly due to its broad variety of applications. In the present work, this term could be described as the combined use of computer-integrated technologies – such as medical imaging technology or robotics, mathematical algorithms, surgical tools and clinical methods [Jaramaz 2004(2)] – in orthopedic surgical procedures. CAOS systems aim at improving the surgeon’s perception of the surgical field, his skills or dexterity and the outcome of the operation [Kowal 2007].

2.1.1 Computer Assisted Orthopedic Surgery: General Pipeline

The process of CAOS systems differs, depending on the application [Jaramaz 2004(2)]. However, there is a general pipeline that consists of three phases: pre-operative planning, intra-operative guidance and post-operative assessment. This pipeline is outlined in Figure 2.1. Usually, the procedure can be virtually performed in the pre-operative planning environment. This yields information about what can be expected during surgery. In order to do so, medical images of the patient, usually CT, MRI or radiographs, are acquired before the operation. These images are converted into computational models, with information regarding the shape and the position of anatomical landmarks of the patient [Simon 1998, Joskowicz 2001]. In the second phase, intra-operative guidance, the images of the patient and the pre-operative plan are brought to the operating room and registered to the patient [Joskowicz 2001]. After the registration, the plan or the model may require an update. Then, the operation is executed. In the third and last phase (post-operative assessment) the information acquired during the first two phases is combined with further images or tests to assess the outcome of the surgical operation [Joskowicz 2001].

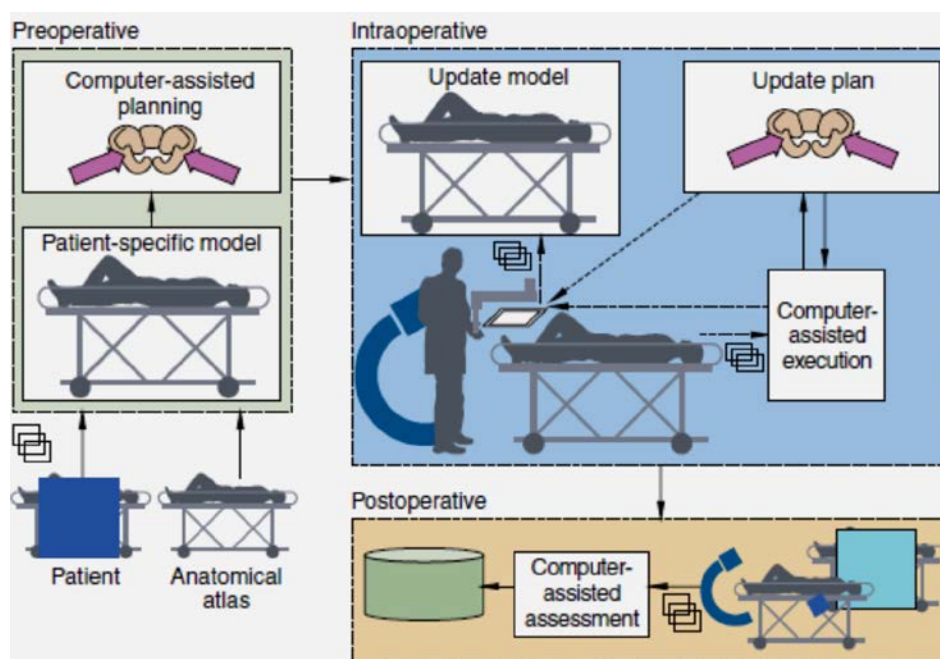


Figure 2.1: Typical flow path of a CAOS system [Joskowicz 2001].

2.1.2 Medical Imaging Modalities in Computer Assisted Orthopedic Surgery

One of the major drivers, for the development of CAOS systems, is the development and improvement of imaging modalities [Robb 1996]. According to the paper of Nobuhiko Sugano [2003], three types of approaches are used: volumetric image-based, fluoroscopy-based and imageless.

The first type uses volumetric images, most commonly CT, because of its high resolution and high contrast between the bone and the surrounding soft tissues [Sugano 2003]. It is also a widely available imaging modality [Langlotz 2002] that gives three-dimensional information and high quality images. It does not require any calibration and is often used as a “canned reality” [Langlotz 2004]. However, the radiation exposure for the patient and the medical staff [Hodgson 2008, Taylor 2001] is a major drawback. Other modalities employed less often in orthopedic surgery are X-rays, MRI, ultrasounds and nuclear imaging.

The second type employs intra-operative fluoroscopic images. These are less expensive and are used to construct an intra-operative map that does not require registration [Sugano 2003]. By using fluoroscopy, the surgeon can monitor quickly and in real-time, without extra radiation [Sugano 2003, Racadio 2007]. However, the two-dimensional image quality is lower [Hodgson 2008, Langlotz 2002]. In different operational procedures, also in minimally invasive refixation, both CT and fluoroscopy are used [Taylor 2001, Jaramaz 2004, Leschka 2011, Racadio 2007]. Although this combination is reliable in needle interventions, for its high accuracy [Leschka 2011], it is not optimal for minimally invasive refixation, because of the respective disadvantages of the two modalities.

The last type (imageless approach) uses intra-operative kinetic or morphometric information on the target, instead of pre-operative or intra-operative images [Sugano 2003]. In the present work, we are not going to discuss this type further.

2.1.3 Computer Assisted Orthopedic Surgery: Benefits and Drawbacks

The introduction of computer assisted surgery in orthopedics has brought significant benefits, mainly due to planning. First of all, planning can ensure higher accuracy and reliability, as it enables surgeons to avoid eventual complications or problems [Braak 2010, Cimerman 2007, Eggli 1998, Sariali 2009]. Equipment needs [Knight 1992, Ma 2010], or technical difficulties that may rise in the OR [Knight 1992] can also be addressed correctly. Moreover, it forces the surgeon to inspect the radiographs thoroughly, increasing the chance of foreseeing all the intra-operative anatomical difficulties. It has been reported [Eggli 1998] that more than 80% of these difficulties could be handled beforehand, with a pre-operative plan. It has also been noticed that pre-operative planning familiarizes the surgeon with the patient's anatomy, prior to the surgical procedure [Knight 1992], for easier decision-making [Eggli 1998, Franco 2010, Sugano 1998]. Besides, the fact that the surgeon is able to plan the exact procedure saves a lot of time, during the operation [Franco 2010, Hodgson 2008, Stiehl 2010]. In addition to that, some systems are suitable also for less experienced surgeons, due to their repeatability and reproducibility [Glinkowski 2008, Wade 1998]. Another use of pre-operative planning emerges post-operatively, when the surgical outcome should be checked, in comparison to the plan [Dahlen 2001].

Despite the benefits of CAS systems, the number of operations aided by these systems is small, compared to the entire number of the orthopedic surgical procedures [Cimerman 2007]. This is mainly due to the costly hardware [Schlenzka 2000], their learning curve [Citak 2008] and the difficulty to design and perform clinical trials to prove their benefits [Cimerman 2007]. Often, the surgeon skips pre-operative planning, due to lack of time [Aliotti 2004]. Additionally, some papers imply that CAS systems are safe and suitable only for experienced surgeons [Schlenzka 2000, Fichtinger 2005], while others recommend them only to beginners [Carl 1997]. There are also concerns regarding the radiation dose, to which both the patient and the surgeon are exposed [Sariali 2009] and regarding pitfalls of the imaging modalities or the registration [Braak 2010, Aliotti 2004, Schlenzka 2000, Simon 1998]. Therefore, when designing a new system, all the above mentioned should be taken into consideration.

2.2 Aseptic Loosening and Minimally Invasive Refixation

Diseases, such as osteoarthritis or rheumatoid arthritis, destroy human joints in an aggressive manner, leading to mobility restrictions and severe pain. The remedy for that is to replace the affected joint surgically, with an artificial one. Due to the increasing prevalence of musculoskeletal diseases [Woolf 2003, Otten 2010], significant pressure has been added on health care, for providing effective and durable treatments. However,

there is still a percentage of prosthesis failure (5-10%), because of aseptic loosening [Otten 2010]. Figure 2.2, below, depicts an example of aseptic loosening, with extensive osteolysis, in the areas indicated by the arrows. During this process, wear particles are formed and the cement between the prosthesis and the bone starts cracking. The response of the human body to the released particles is an inflammation and formation of fibrous tissue. So, the prosthesis will start moving inside the bone, leading to the deterioration of the bone quality and eventually to painful consequences for the patient [Abu 2007]. At this point, a revision procedure is required.



Figure 2.2: Aseptic loosening after total hip arthroplasty, with extensive osteolysis around the femoral component (shown with the arrows) and mechanical failure of the prosthesis, resulting in aseptic loosening [Wilkinson 2011].

A revision approach, performed at the Leiden University Medical Center, is minimally invasive refixation [dePoorter 2008]. During this operation, the prosthesis is not replaced or removed from the patient's body. Instead, needles are introduced in the space between the prosthesis and the bone (periprosthetic space), using a hammer. The placement of the needles is guided, by intra-operative CT scans. This means that the patients may be inserted to the CT scanner multiple times, until the needle is placed correctly. When the needle reaches the desired interface position, a C-arm is brought over the patient, to control the flow of the new polymethylmethacrylate (PMMA) cement. This cement is injected into the periprosthetic space, under high pressure, with a dedicated tool. The injection is monitored in real-time, on the fluoroscope screen, until the periprosthetic space is filled. When cement threatens to leak into the joint space or into the soft tissues, the needles are removed [dePoorter 2008]. Real-time feedback is important for cement injection, because the cement hardens, within approximately 10 minutes. In Figure 2.3, below, we show the steps of a minimally invasive refixation procedure, as performed at the LUMC.

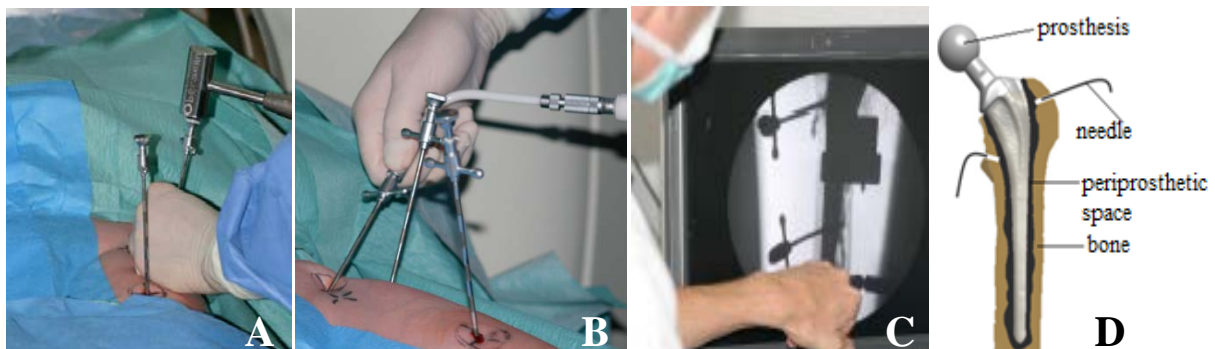


Figure 2.3: Typical example of minimally invasive refixation, as held at the LUMC. (A) – Needles being hammered in the periprosthetic space. (B) – Cement injection. (C) – Intra-operative fluoroscopic guidance of the cement flow. (D) – Cross-sectional model of the hip during minimally invasive refixation.

Chapter 3

Related Work

Minimally invasive refixation by cement injection would benefit from a system that could offer better planning and guidance workflow. In literature, there are papers concerning computer assisted orthopedic surgery, but we are not aware of previous work that presents a complete system for minimally invasive refixation. The same stands for previous work, concerning cement filling uncertainty visualization. In this chapter, we summarize important previous work related to computer assisted orthopedic surgery systems and to uncertainty visualization.

3.1 Computer Assisted Orthopedic Surgery Systems

The papers of Racadio [2007] and Braak [2010] present two similar needle intervention methods that use the same software: XperGuide. These methods use fluoroscopic images, co-registered with a 3D cone beam CT dataset, on which the needle trajectory is planned. The user draws a path from the target to the skin in a proposed access route, avoiding vital anatomic structures. Then, the calculated trajectory, which provides easiest access to the target and minimal trauma on the patient, is projected on the real-time fluoroscopy image. XperGuide combines the advantages of CT and fluoroscopy into one technology, allowing rapid (real-time), interactive two-dimensional and three-dimensional visualization, as well as easy and accurate access to the operation target [Racadio 2007, Braak 2010]. However, the application focuses only on the calculation of the optimal needle trajectory. It is not specifically applicable to cement injection, where more complex radio-opaque regions are involved. It does not include also any concept of uncertainty. Additionally, this technique requires a dedicated XperCT system, while our system is compatible with the traditional, cheap and widely available C-arm fluoroscopes. In Figure 3.1, below, the XperGuide system is presented for the case of a 16-year old girl with a trauma, due to an accident.

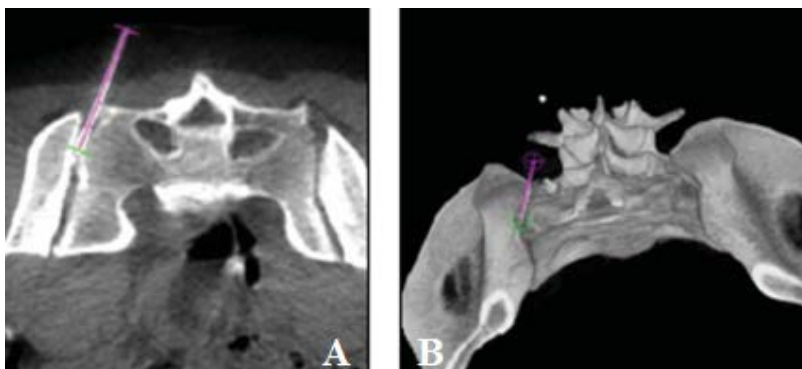


Figure 3.1: Placement of needle into sacroiliac joint, using XperGuide, (A) – on a slice and (B) – on 3D volume [Racadio2007].

Another area of research concerns brain tumor biopsy planning [Herghelegiu 2012]. The Biopsy Planner allows identifying, visualizing, analyzing and validating a biopsy needle trajectory, minimizing the risks for the patient, without eliminating the interaction with the surgeon. This is achieved through 2D and 3D visualizations, as well as dedicated views to warn the surgeon, in case there is a blood vessel in the proximity of the needle. In breast tumor biopsy, there are also similar techniques to define the entrance and the target points of the needle insertion [Vancamberg 2011, Alterovitz 2009]. However, as we already mentioned, in orthopedic planning for minimally invasive refixation by cement injection, not only the needle insertion is important, but also the cement injection and the cement filling uncertainty.

In orthopedics, RoboDoc was the first robot-assisted surgical system for planning and guidance. It was firstly used on a human in 1992 and it included a pre-operative planner, known as OrthoDoc, for the preparation of bone for uncemented femoral implants [Picard 2004]. It used CT data that were loaded in OrthoDoc to construct models of the femur, by interpolation between the slices. Then, the surgeon selected from an implant database, the style and the size of the correct template implant. The output of the pre-operative planning was a data file,

specifying the geometry and the position of the implant, as set by the surgeon, in the CT coordinate system [Kazanides 1998]. The main difference with our system is that RoboDoc is a robot-assisted surgical system for the correct determination of a hip implant. Our HipRFX is assisted by technology that already exists in the OR, in order to facilitate and enhance the revision procedure of the failed prosthesis.

A similar planning technique for determining the correct hip prosthesis, using three-dimensional templates, involves the HIP-PLAN software [Sariali 2009]. This system enables the determination of all the anatomical landmarks or measurements, needed to simulate the insertion of the implant with 3D templates. A color coding, representing the density of the bone, is employed for the determination of the correct position and the stability of the implant. Although this system demonstrates that 3D planning is superior to 2D planning [Sariali 2009], there is still a concern about the radiation dose that the patient was exposed to, during the multiple CT scans. In order to minimize those concerns, in our approach, the patient is scanned only once. Afterwards, the procedure is only fluoroscopy-based. Additionally, with HipRFX, the CT scan is performed pre-operatively, so the procedure does not need to be performed in a CT room.

Another example of pre-operative orthopedic surgery planning is 3D-Software Voxim [Dahlen 2001]. With this software, the slices are firstly reconstructed in all planes. Afterwards, the procedure differs depending on the data type. For CT datasets, the desired bony structure is segmented from the surrounding environment through threshold value segmentation, while for MRIs the segmentation must be performed manually. Then, different segments are delineated as different structures, using different colors [Suero 2010]. The system enables also other tasks: volume rendering for the 3D representation of the bony structures, distance and angle measurements, clipping, insertions of scalable CAD objects, such as screws and pedicles, and a simulator for osteotomies [Dahlen 2001]. In Figure 3.2, below, an application of 3D-Voxim, to a lower foot osteotomy, is depicted. Although this system is capable of running on a conventional computer, without requiring additional hardware, performance time was a major drawback. This can discourage surgeons to use it, no matter the precious insight into the fracture [Dahlen 2001]. Therefore, one main objective for our HipRFX was to achieve interactive, real-time performance.

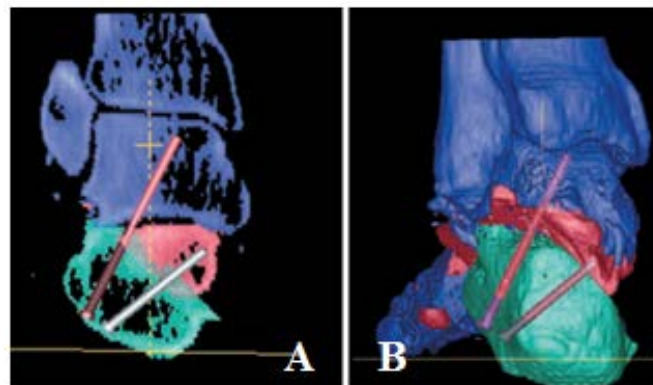


Figure 3.2: Fixation of a patient with osteotomy at his calcaneus, with the use of two pedicle screws. (A) – 3D reconstruction of the screws on a 2D reconstruction of the coronal plane of the lower foot. (B) – 3D visualization of the same region. The calcaneus is depicted with green, the talus with red and the rest of the lower foot with blue [Dahlen 2001].

The system used at the Kingston General Hospital [Ellis 2005] is employed for surgical plans, simulations of surgical procedures and assistance of the surgeon during the planning phase. The effects of different interventional procedures (such as bone shortening, lengthening and realignment procedures, including visualization of the fixation devices used to stabilize the bone fragments) can be simulated on decimated iso-surface models from CT scans. This system is compatible with a custom surgical planning and simulation package. It is applicable to different surgical operation types and has a nice workflow. However, it requires optical marker-based registration, between the patient anatomy and the CT scans, to guide surgeons intra-operatively. In our case, we preferred to use the advantages of intra-operative fluoroscopy, instead of the expensive, bulky, complex and time consuming tracking with reflective markers. In this way, the procedure is cheaper, easier and quicker, using technology already integrated in the OR.

Systems that include simulators are also popular in literature. DiGioia et al, in their paper [2000], describe an image-guided surgical navigation system, HipNav, in order to measure and guide the placement of implants in total hip replacement surgery. The system incorporates a 3D pre-operative planner with a range of motion (ROM) simulator, for preselected leg-motion paths. It is based on CT scans and 3D models of the femur and the pelvis, allowing the surgeon to determine the size, position and orientation of the implant [DiGioia 2000,

Jaramaz 2007]. A practical technique for the calculation and visualization of the shoulder ROM, with the use of motion envelopes was presented in the paper of Krekel et al. [2006]. This software, Articulis, enables the exploration of a shoulder replacement planning in real-time. For every change made by the surgeon during the pre-operative planning, the resulting ROM and its effects can be interactively predicted and visualized with motion envelopes. The VIRTOPS software system [Handels 2000] enables pre-operative planning and simulation of different pelvis and hip operations, such as operations of bone tumors, using multimodal image information (CT and MRI). After the pre-processing steps (registration between bone segmentation, using intensity threshold in the CT data, and manual bone tumors segmentations, in the MRI data), the surgeon can use 3D bone models to determine the shape and geometry of the prosthesis, as well as, to plan the position of the implant and the screws. However, in our case, we are not visualizing ROMs and we considered that such a simulator will not add more value to the software. Therefore, the only simulation that we include is where we simulate the view on the fluoroscopic monitor, based on our pre-operative plan.

3.2 Uncertainty Visualization

All kinds of measurements can be related to uncertainty [Grigoryan 2004], introduced during all the steps of the visualization pipeline [Griethe 2005, Lodha 1996]. However, this has been a highly overlooked subject in the past [Lodha 1996] and there is, still, no unanimous opinion on its definition. According to the NIST standards, “data uncertainty includes concepts, such as statistical variation or spread, error or inaccuracy, and minimum-maximum ranges” [Lodha 1996]. A clearer definition is provided by Griethe et al [2004], as “a composition of different concepts, such as error (outlier or deviation from a true value), imprecision (resolution of a value compared to the needed resolution), subjectivity (degree of subjective influence in the data) and non-specificity (lack of distinction for objects)”.

In this part, we discuss significant previous work related to uncertainty visualization, taken into account for our later implementation of the cement filling uncertainty visualization. We do not refer explicitly to their advantages and disadvantages, here. This will be done extensively in the Method chapter, where we explain our choice on the approach we decided to follow.

In the paper of Lodha et al. [1996], six methods for visualizing uncertainty in fluid flow visualizations are presented. These methods consist of utilization of uncertainty glyphs, envelopes, animations, priority sequencing, twirling baton displays of trace viewpoints and rakes. All those methods were tested on datasets and proved to be valuable for people interested in decision-making with missing or imperfect flow data. Also the paper of Botchen [2006] presents a flexible, interactive and compatible texture-based flow visualization technique for the uncertainties on the real-world measured data. This is performed either by a generic texture filtering process to improve the perception of uncertainty affected regions, or by a user-adjusted color coding of uncertainty [Botchen 2006].

The paper of Grigoryan et al. [2004] is related to the employment of point-based surfaces that show the uncertainty of a tumor surface. The surfaces are rendered as a collection of points and each point is displaced from its original location along the surface normal, proportionally to the uncertainty, as it can be seen in Figure 3.3 below. Combined with pseudo-coloring and transparency, this method can be time-efficient enough, to be interactive, effective, intuitive, non-distracting, and up-to-six-dimensional. However, this approach might be misleading, in case the conveyed information is sensitive to spatial deformation.

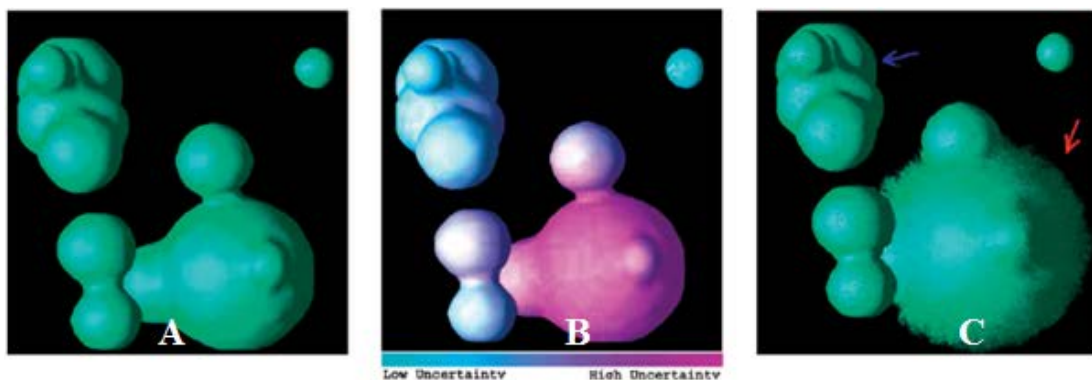


Figure 3.3: Tumor Formation Visualization. (A) – Polygonal model of tumor, without uncertainty information. (B) – Polygonal model with pseudocolor, where the tumor geometry and the uncertainty information are conveyed. (C) – Point-based model [Grigoryan 2004].

Rhodes et al. present in their paper [2003] a technique where the uncertainty is incorporated in surface visualization by using color or texture. Color is an easy and effective attribute. It can be used as an additional parameter, without adding much distraction. On the other hand, texture can make the surface color available for the visualization of an additional variable. Papers that include similar concepts are encountered often. Twiddy et al. [1994], propose to handle missing data similarly to the restoration of paintings, by using some neutral and non-distracting shades of grey. Davis et al. [1997] employ an approach, where different shades or different levels of hue represent different levels of uncertainty. Also, Djurcilov et al. [2001] use volume rendered images to depict regions of uncertainty in the data are presented. This is done either in-line, by incorporating uncertainty directly into volume rendering using grids (for one-dimensional data) and transfer functions (for two-dimensional data); or post-process, by adding speckles, holes, noise and texture to uncertain areas.

Two medical applications of uncertainty visualization can be found in the papers of Lundström [2007] and Drapikowski [2008]. In the first one, tissue classification uncertainty is addressed with the use of animation methods to depict uncertainty in the rendering, with the use of transfer functions. Regions that are certain will remain static, while uncertain structures will change with time in an animation cycle. This was, yet, documented to cause visual fatigue [Lundström 2007]. Figure 3.4 is an example from their paper, where they present an example of this uncertainty animation. The second paper presents a method for depicting uncertainty of surface-based models from fragments of CT or MRI data. This uncertainty relates to errors in the geometry of the models, which are presented with the combined use of a color scale, to show the quality, and a ribbon, to show the quantity proportional to uncertainty [Drapikowski 2008].



Figure 3.4: Three frames of an uncertainty animation on a renal angiography, for a region suspected for stenosis [Lundström 2007].

There are also papers proposing the use of uncertainty glyphs [Wittenbrink 1996], or distorted annotation grids [Cedilnik 2000] to show the uncertainty along with the data. Pang et al. [1997] give an interesting overview of the existing and likely uncertainty visualization techniques. They introduce new uncertainty visualization methods, such as adding glyphs, adding geometry, modifying attributes, modifying geometry, animation, sonification and psycho-visual approaches. Additionally, the paper of Newman [2004] provides an effectiveness study on eight uncertainty techniques (transparency, colormapping, ball glyphs, arrow glyphs, cylinder glyphs, multi-point glyphs, and aliasing) with interesting results.

All the previously mentioned methods were taken into consideration for the implementation of our cement filling uncertainty visualization. However, uncertainty visualization is a complicated issue. It depends on the data type and on the already employed data visualization. Also, many methods, visualizing data with uncertainty, distort the data and emphasize areas with uncertain values, distracting the user. Ideally, uncertainty information should not conceal or obscure the underlying data [Cedilnik 2000, Griethe 2005]. Therefore, some of the mentioned techniques were not applicable to our case, while others proved to be poor. We will discuss the process of our decision making in the following Method chapter.

Chapter 4

Method

The method that we propose as an answer to our research questions is HipRFX. It is a complete system for facilitating and enhancing the revision procedure of a failed hip prosthesis. HipRFX assists orthopedic surgeons, during all the steps of minimally invasive refixation procedures. The main objective of the system is to diminish the radiation exposure, due to multiple CT scanning, while being compatible with the widely available C-arm fluoroscopes. With this fluoroscopy-based approach, we also manage to achieve real time performance, avoiding reflective markers for registration. We also introduce the idea of visualizing the cement filling uncertainty, which is a new concept. In this chapter, the system is described in a brief overview, followed by a more detailed description of the different stages of the method. The section is concluded with a short summary.

4.1 Overview

In our approach, the patient is inserted in the CT scanner only once. Based on the acquired data, the surgeon can build thoroughly the pre-operative plan. He can virtually insert the needles and inject the cement into the periprosthetic space, while visualizing all the important structures in the femoral region. Subsequently, the system can simulate pseudo-fluoroscopic images from the pre-operative plan. These digitally reconstructed radiograph (DRR) simulations imitate in a realistic way how the pre-operative plan would ideally look on the fluoroscopic monitor, during the surgical procedure. At this stage, the surgeon can capture simulated images, in order to use them intra-operatively, in the form of two-dimensional steps. Intra-operative guidance requires emulating the simulated images on the fluoroscopic monitor. After the completion of the operation, the surgeon can use a fluoroscopic image to perform the cement filling uncertainty visualization. In this way he can assess the outcome of the surgery, by detecting cement areas that were probably inadequately filled.

In Figure 4.1 below, an overview diagram of the conceptual model of the method is presented, showing the four stages of the workflow: pre-operative planning, digitally reconstructed radiograph simulation, intra-operative guidance and cement filling uncertainty visualization.

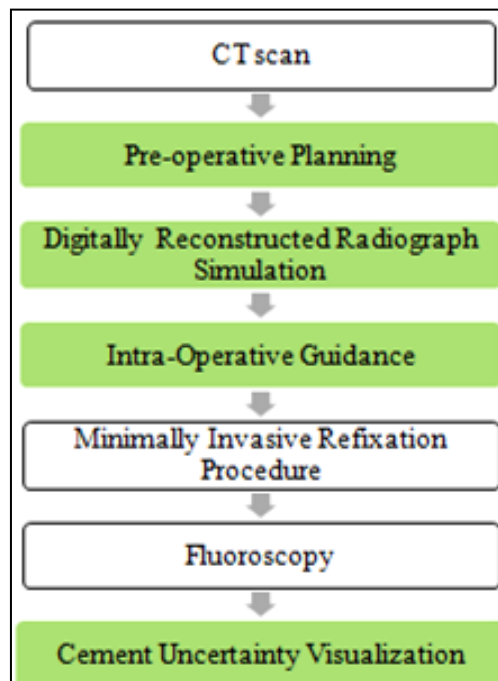


Figure 4.1: Conceptual model

4.2 Pre-Operative Planning

Pre-operative planning is the first stage of the HipRFX system. During this part, the surgeon establishes the operating target and performs a detailed planning of the operating procedure. Figure 4.2, below, shows the workflow of this stage. In green, we show the mandatory steps and in blue, the optional steps of the workflow. The green lines show the links between different components.

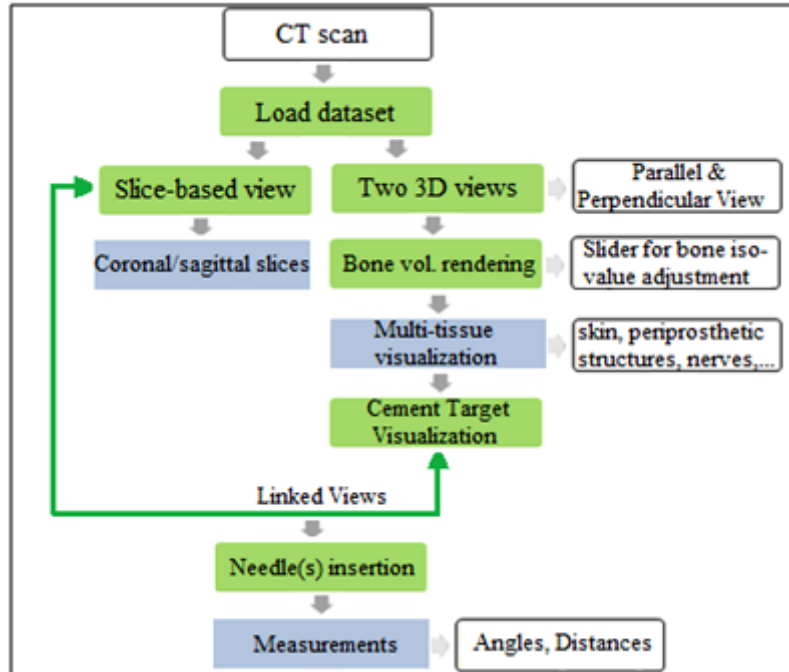


Figure 4.2: Workflow of the pre-operative planning.

The pre-operative planning starts by loading the pre-operatively acquired CT dataset. The main renderer, which is the middle, grey panel (B) in Figure 4.3, offers a slice-based representation of the data. The user can optionally inspect the sagittal or the coronal slices, in addition to the axial. He can also see specific structures with reference to the slice-based dataset, by importing them to the main renderer. The two 3D renderers on the left (A), dynamically show views respectively perpendicular and parallel to the last inserted needle. Their role is to enable the easier 3D manipulation of the needle, on the 2D screen, or to be used as “storage” windows, where all the loaded structures are visualized. The user can import structures from these renderers to the main one. We also use a red linear marker, as a linkage between the slice-based view and each one of the side renderers. This shows where the specific slice is located, with reference to the structures that are visible in the side renderers. The operation panel, in Figure 4.3 (C), contains all the necessary elements for the operations.

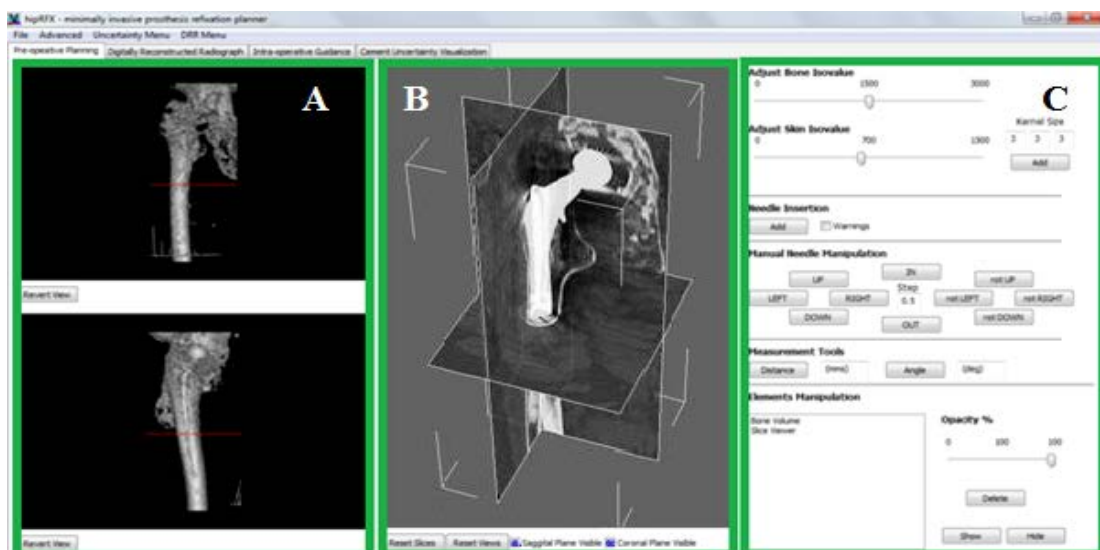


Figure 4.3: Graphics User Interface and renderers. (A) – Additional Renderers, (B) – Main Renderer, (C) – Operation Panel

After the user has loaded the patient CT dataset, a volume rendering of the bone is performed, automatically. However, the bone isovalue can be adjusted, with a slider, so that the rendering matches the requirements of the task. The skin surface can also be rendered and its isovalue is adjustable, too. The surgeon can optionally load a segmentation file, containing the periprosthetic structures (fibrous tissue, cortical and trabecular bone, old cement and prosthesis), as well as structures that should not be punctured during the procedure. These are segmented at a pre-processing stage, before the plan is performed. The most important structure is the cement target, which is the part of the periprosthetic space that should be ideally filled with cement. The opacity of all those structures can be altered with a slider, to be able to see behind intersecting areas.

In Figure 4.4, below, two examples of the multi-tissue visualization are presented. Every color corresponds to a different structure. For the first one (A), the cement target (green) is visualized in respect to the bony structure. In the second (B), a more complex, multi-tissue visualization is presented. Fibrous tissue was omitted from (B), since it overlaps with the cement target, while skin can be also visualized. The opacities of the structures have been altered.

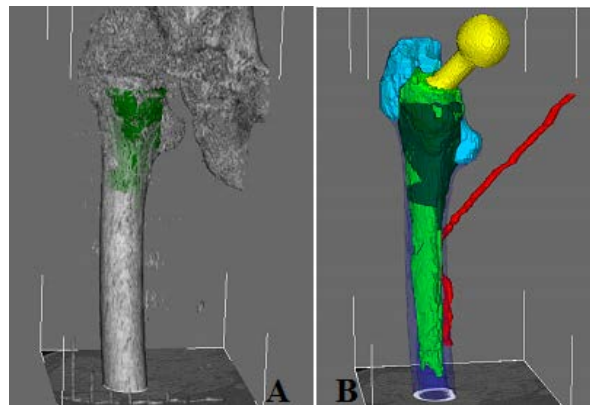


Figure 4.4: Two examples of multi-tissue visualizations. Color legend: (Blue) – Cortical Bone, (Cyan) – Trabecular Bone, (Dark Green) – Cement Target, (Light Green) – Old Cement, (Red) – Vessel to avoid, (Yellow) – Prosthesis, (White) – Bone.

The next step after the cement target visualization is to insert the needle(s) in the most appropriate locations. This is done by a simple picking event, triggered by the mouse. The system requires two points for the needle insertion: the target point, which is the position of the tip of the needle, and the end point, which is the position that gives the direction of the needle. The surgeon can, then, manipulate the needles, in two ways: either with the mouse, or through the operations panel, by setting a step for the automatic rotation or translation of each needle. Since the needle is a cylindrical object, five degrees-of-freedom were required (three translations and two rotations). In case the user has loaded a structure, such as a nerve or a vessel that must not be punctured, there is a warning option. When the needle approaches the structure, within a certain safety margin, the user is warned.

In Figure 4.5, below, we present an example of two inserted needles. Here, the cement target, which was created based on the fibrous tissue, was loaded. Then, two needles were placed in positions that will allow achieving the best result, as defined by the user. The red dots are the insertion points of the needles. The purple needle has a ruler, which is marked every 5mms for aiding the user to determine easily the depth of insertion. When the cement target or the needles are loaded, they are automatically visible on the DRR simulated image, which will be presented in the following section.

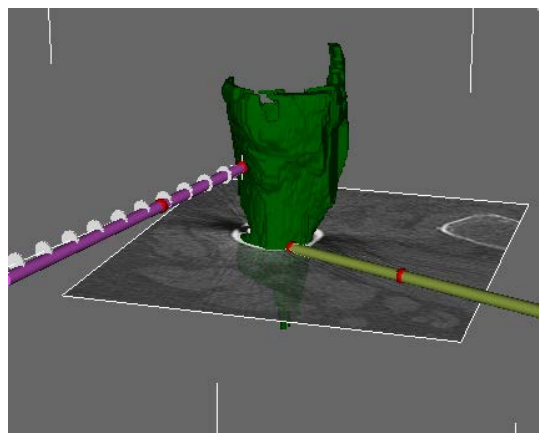


Figure 4.5: Needles insertion procedure (in green we visualize once more the cement target)

Finally, it is useful for the physicians to be able to perform measurements on the slices or on the volumes. These measurements include distances and angles. Therefore, we implemented a tool that allows the user to select two or three points, to calculate respectively the distance or the angle between them. In Figure 4.6, below, a distance and an angle (of the hip neck on the shaft) measurement are shown.

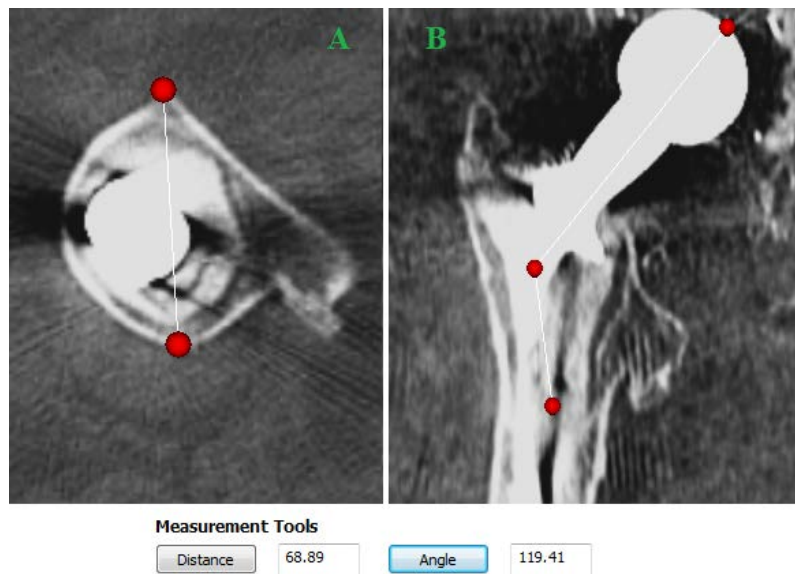


Figure 4.6: Measurements. (A) – Distance measurement (in mms), (B) – Angle measurement (in degrees)

4.3 Digitally Reconstructed Radiograph Simulation

Digitally Reconstructed Radiograph (DRR) Simulation is the second stage of the HipRFX system. During this part, the surgeon can simulate fluoroscopic images, using the data of the previously performed plan, where he has inserted needles and injected the cement target. Therefore, in this step the user can simulate the ideal appearance of his pre-operative planning on the fluoroscopic monitor in the OR. He can also see the effect of different changes on the simulated radiographs, while he performs the pre-operative plan. In Figure 4.7, an example of a simulation (A) is presented next to a real fluoroscopic image (B). These simulated fluoroscopic images will be used in the next stage of the system, the Intra-Operative Guidance.

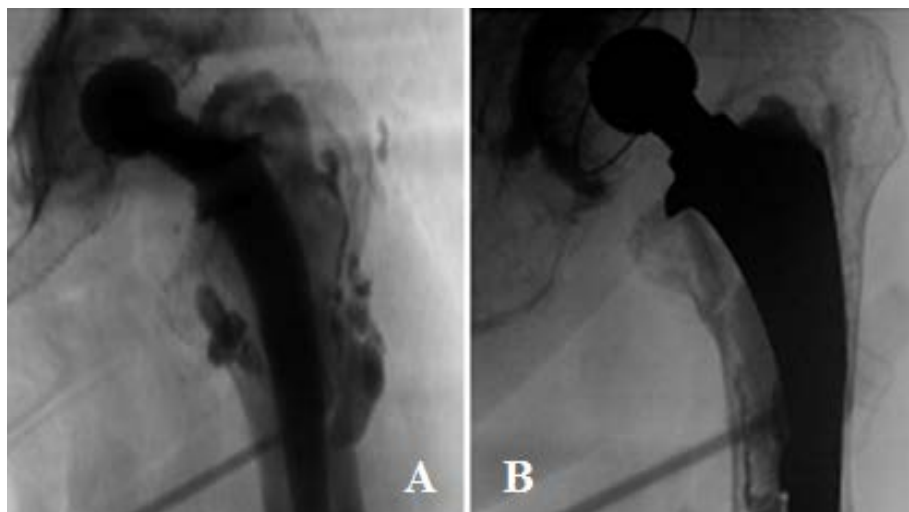


Figure 4.7: Digitally Reconstructed Radiograph simulation of a needle and cement target insertion (A), compared to a real fluoroscopic image (B).

This simulation is done in real-time and is interactive. This means that the surgeon can look through the object from every possible angle, while the image is reciprocally coupled with a model of a patient in a C-arm fluoroscope. Therefore, the user can manipulate either the image, or the model and see the effects of the changes in real-time on the other. This synchronization makes clearer and easier to determine which radiograph is simulated and from which view.

The digitally reconstructed radiograph simulation part was mostly implemented by Bas van den Berg for his M.Sc. project “Optimally generating CT-based simulated fluoroscopy for guiding percutaneous cement injection”. For this, he created a modified version of a volume raycaster. This includes an altered raycast composite function that calculates and renders the absorption of the ray passing by the volume, instead of the whole CT volume data. This composite transfer function relates the Hounsfield units of the CT dataset, augmented by needles or cement target, to the opacity values used in the ray caster. This is how the grey-scale values result on the simulated fluoroscopic screen. The transfer function is an approximation of the so-called H&D (Hurter and Driffield) curve, shown in Figure 4.8, below.

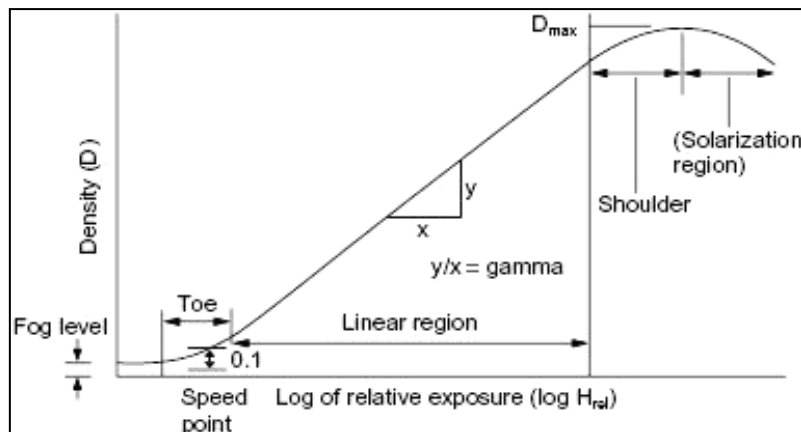


Figure 4.8: An H&D curve with all the parameters that are used to describe it.¹

A typical H&D curve is S-shaped, with a low exposure/low density toe, a linear portion and a high exposure/high density shoulder. The density never goes to zero, because of the so-called base fog optical density, even in absence of exposure [Prince 2006]. In our case, only the linear part of the curve is taken into account. The other parts are constant and the fog level is ignored. The controllable parameters are the gamma, toe position and latitude of the H&D curve. The gamma is the slope of the linear region of the curve. The latitude is the range of exposures (the range of Hounsfield units) for which the H&D curve is linear. Two modes are available, X-ray and fluoroscopy, employing two different color transfer functions.

Moreover, different volume masks with different colors can be superimposed on the different structures. By supplying a mask, it is possible to highlight some areas of interest in the radiograph. In order to do so, the composite function keeps track if the ray passes through the mask and assigns colors to it, instead of grayscale values. These so-called overlays can be turned on and off, while the user can also alter their opacities, in order to see any underlying structures. Figure 4.9 depicts a simulated radiograph without overlays (A) and with overlays (B). The color scheme followed here is the same as in the pre-operative planning for each structure, in the multi-tissue visualization.

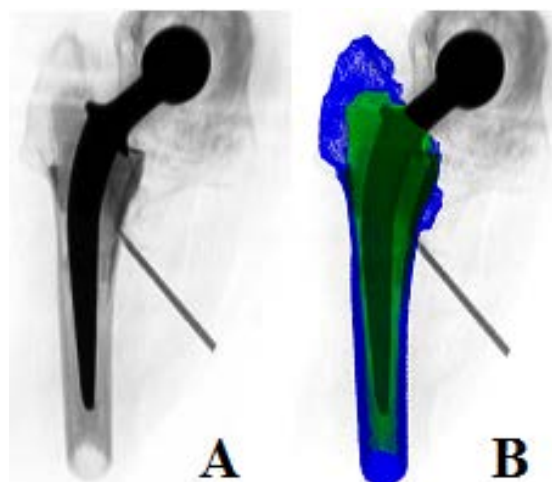


Figure 4.9: Digitally Reconstructed Radiograph Simulation without overlays (A) and with overlays (B) to highlight specific structures, such as cement target (dark green), old cement (light green) and cortical bone (blue).

¹ www.answers.com/topic/sensitometry-and-film-speed

4.4 Intra-Operative Guidance

Intra-operative guidance is the third stage of the HipRFX system. During this part, the surgeon can use the pre-operative plan and the simulated radiographs for real-time surgical guidance, by employing in-situ anatomical and functional information. The surgeon will match the real images on the C-arm monitor to the simulated radiographs, aided by the stored virtual c-arm configuration. In Figure 4.10, below, we show an overview of the workflow of the intra-operative guidance. In blue, we show the optional steps of the workflow. The green lines show the links between different components.

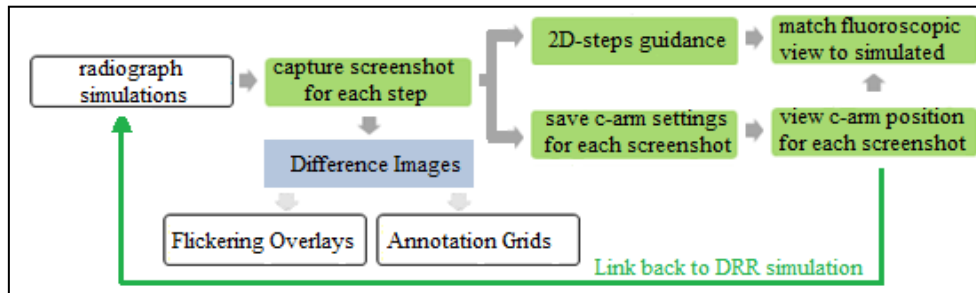


Figure 4.10: Workflow of the intra-operative guidance.

The main idea behind this stage is that the surgeon can capture screenshots during the pre-operative planning phase and, especially, during the digital reconstruction radiograph simulation. Then, he can use them as a visual feedback, in the form of two-dimensional steps in the OR. In other words, the surgeon will emulate the ideal simulated radiographs. With this step-by-step guidance with 2D images, the surgeon manages to retain all the important information, while not being distracted, as it would occur in the case of an animation.

In Figure 4.11, below, an example of our intra-operative guidance approach is provided. We simulated some steps to be followed, such as the appearance of the area of interest before the intervention (A), the insertion of three needles (B), (C), (D) and the injection of the cement, shown from different viewpoints (E), (F), (G). For this example, we use simple simulated radiographs, without any overlays. A model of a patient in a C-arm (H) is employed, to show the position of the fluoroscope for each viewpoint. In this example, the model shows the viewpoint of (E).

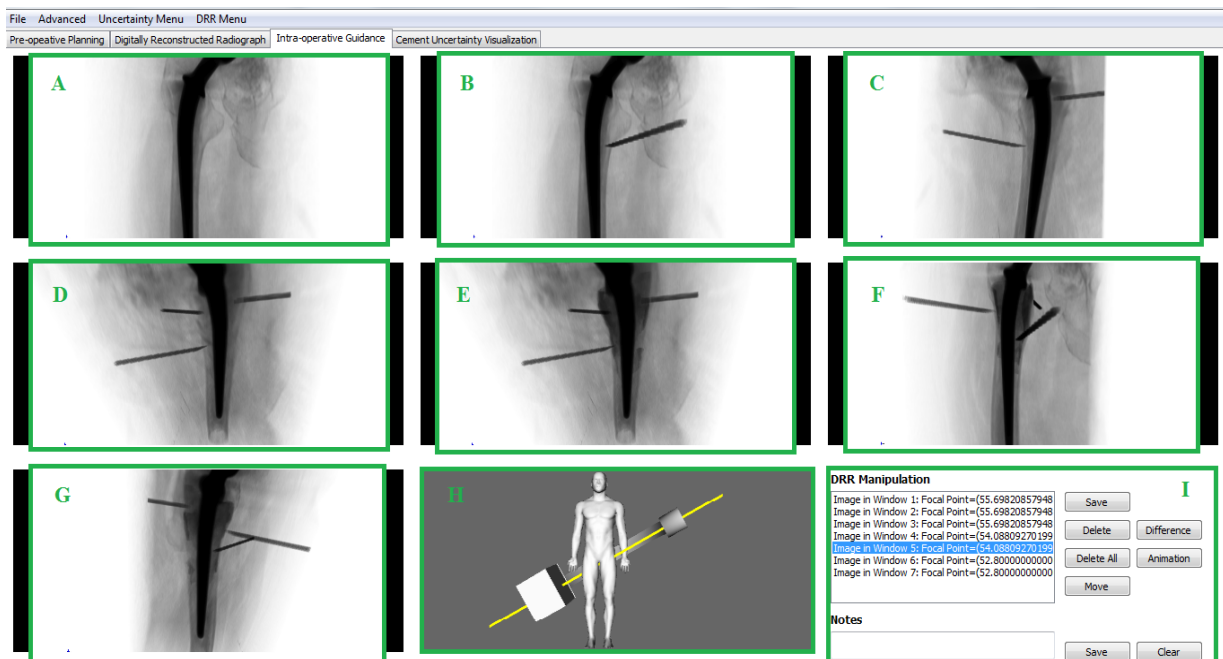


Figure 4.11: Stepwise intra-operative guidance workflow. (A) – Before the intervention, (B), (C), (D) – Optimal view for the insertion of the needles, (E), (F), (G) – Cement Injection from different viewpoints, (H) – Model of a patient in a C-arm fluoroscope, to view the position of the fluoroscope for each of the previous cases, (I) – Operations Panel.

As we already mentioned, a model of a patient in a C-arm fluoroscope is employed for viewing the stored position of the fluoroscope for every simulated image that we have captured in our guidance interface. This

implementation enables with a simple click on each captured radiograph (or on the images list in the operations panel) to view in real-time and interactively the placement of the fluoroscope. Additionally, the user can be easily linked back to the previous step and make eventual corrections, since the fluoroscope in the guidance tab is coupled to the fluoroscope in the DRR tab.

An additional tool enables to highlight differences between two images. We have implemented two approaches for that. There are also other approaches, but these will be investigated in the future. The first one is an animated (flickering) overlay, which blinks periodically, to show the different structures between two radiographs. The second one is a static annotation grid, the opacity of which is proportional to the magnitude of the difference image. The difference image, in the form of an overlay, results as a simple subtraction of one radiograph from another, while the annotation grids were inspired by the paper of Cedilnik et al. [2000].

The conceptual idea, behind the use of the annotation difference grids, was to allow the surgeon to see the underlying structure with minimal distraction and concealment. Also, the flickering overlays can provoke visual fatigue to the user and cannot be shown on static modalities, such as printouts. However, for radiographs with small differences, we observed that the annotations were losing information located in between the grid spacing. Therefore, the user will be responsible for deciding, which one is better to use, in every case. In Figure 4.12 below, we show an example of a difference image, between a radiograph captured before the intervention (A) and after the needle and cement insertion (B), visualized both with deformed annotation grids (C) and with flickering overlays (D).

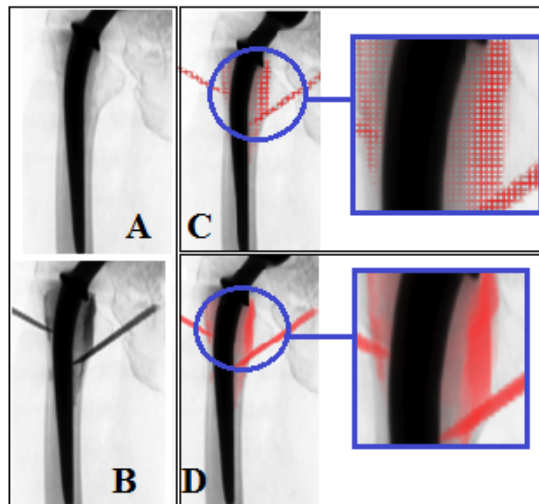


Figure 4.12: Difference Images Tool. (A) – Radiograph captured before the operation. (B) – Radiograph after the needle and cement target insertion. (C) – Deformed Annotation Grid for the difference image between (A) and (B). (D) – (Flickering) Overlaid difference image between (A) and (B).

4.5 Cement Filling Uncertainty Visualization

Post-operatively, surgeons need a tool for assessing the outcome of the minimally invasive refixation procedure. The last stage of HipRFX allows them to see the areas of the periprosthetic space that they have actually managed to fill, based on back-projection from a single two-dimensional radiograph. However, in a 2D radiograph, there are areas where the user cannot be certain about the cement filling. Although it is important to be aware of the uncertainty information and its influence on the data [Grigoryan 2004, Botchen 2006], most of the visualization work done up to now, has overlooked this concept [Lodha 1996]. Still, this negligence can lead to wrong conclusions and bias of the evaluation process [Botchen 2006]. In order to avoid that, we enhance the cement filling visualization with information about uncertain areas.

In our case, these uncertain areas emerge, because the metal implant is a radio-opaque structure. Therefore, the areas of the periprosthetic space in front of and behind the prosthesis are hidden in the radiograph. In these parts, the cement filling (shape and amount) cannot be discerned. Based on the definition of Griethe [2005] that we already mentioned in the Related Work section, we can describe our cement filling uncertainty, as a non-specificity case. It is obvious that the cement filling uncertainty depends on the acquisition angle of the 2D fluoroscopic image.

Our uncertainty concept is also shown in Figure 4.13. With green, we denote the areas, within which we can discern the cement filling. Also, the cement filling in position (1) is more radio-opaque than position (2), which

means that the amount of cement in (1) is higher. However, in front of and behind the prosthesis, we are uncertain about the filling. We show only two of the possible examples of cement filling, included within the red and yellow lines. For these areas, we will calculate and visualize the uncertainty.

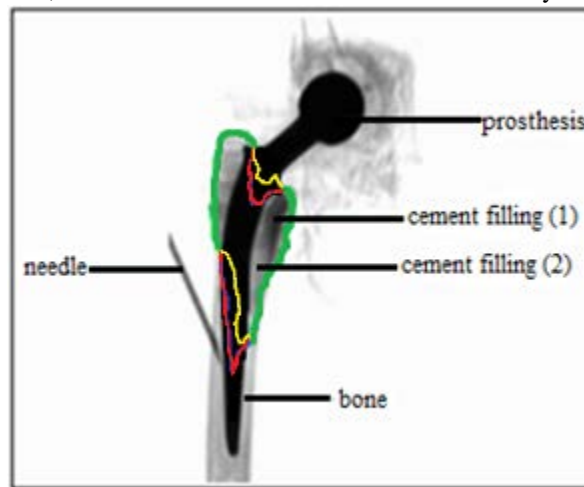


Figure 4.13: Concept of cement filling uncertainty.

4.5.1 Decision making: Visualization Technique

Since we want to visualize two variables, certainty vs. cement filling, we need to employ a feasible and intuitive way of showing them both, without interfering with each other. Especially, the uncertainty should not overshadow the cement filling data [Cedilnik 2000]. At the same time, our visualization tool should provide information concerning the shape, the cement filling and the uncertainty of the filling.

The papers of MacEachren [2005] and Griethe [2005] aided decision making, on the employment of a specific method for the uncertainty visualization. MacEachren et al [2005] underline seven key challenges or features in uncertainty visualization that should be taken into consideration, when deciding upon the method to be employed. Those points are presented in Table 4.1 (with blue). This table shows also all the possible technique options (in green), for the uncertainty visualization implementation, based on the outline provided by Griethe [2005].

Table 4.1: Different Technique Options for Uncertainty Visualization (in green, adapted from [Griethe 2005]) and Important Key Challenges and Required Features (in blue, adapted from [MacEarchen2005]).

Free graphical variables	Additional graphical objects	Animation	Interactive Representation	Acoustic or Haptic Feedback	Key Challenges and Required Features
<ul style="list-style-type: none"> • color • size • position • angle • focus • clarity • fuzziness • transparency • edge crispness 	<ul style="list-style-type: none"> • difference images • uncertainty glyphs • labels • isosurfaces with different thickness • overlay grid with varying thickness, sharpness or transparency 	<ul style="list-style-type: none"> • speed • duration • blinking • blur • ROM • order • oscillation 	<ul style="list-style-type: none"> • mouse interaction 	<ul style="list-style-type: none"> • acoustic, e.g. pitch, volume or rhythm • haptic senses, e.g. touch or vibration 	<ul style="list-style-type: none"> • Understanding uncertainty and relationships to information needs • Understanding influence of uncertainty in decision making • Understanding uncertainty role in exploratory analysis • Methods for capturing and encoding uncertainty • Methods for depicting multiple kinds of uncertainty • Methods and tools for uncertainty interaction • Assessing the usability and utility of uncertainty visualization

Based on the table above, we decided to exclude animation, interactive representation and acoustic/haptic feedback options. First of all, interactive representation requires a lot of interaction with the interface. If the surgeon decided to use the uncertainty visualization inside the operation room, it would require a sterile mouse. This approach might make the visualization distracting, as well. Also, the quality of this representation cannot be assured, when used on conventional computers, with conventional screens. The datasets that are used are large. So, the computations would require a powerful machine and, probably, bigger screens to provide adequate resolution, not to mention a certain level of familiarization of the doctor with computers and the system. The animation option was also excluded for the same reasons, but also because it is known for causing visual fatigue to the user [Lundström 2007]. Additionally, manual manipulation of the visualized structures is preferred, since the structures to be presented are complicated and require subjective and user-defined viewing. Acoustic or haptic feedback was not considered a plausible and adequate choice for our application. This may also require additional hardware.

Therefore, our options were restricted to using free graphical objects or adding graphical objects to visualize an additional dimension for the cement filling uncertainty. However, the complexity and the size of the patient datasets would be an obstacle for employing additional graphics. We should ensure that the main data (i.e. the cement filling) are not overshadowed. By using additional graphics objects, such as glyphs or isosurfaces, we would face the chance of making a visualization that would distract the user’s attention from the main purpose of the tool. The visual overload of uncertainty visualization with glyphs or other objects could not be guaranteed [Newman 2004]. Finally, the representation within the already existing geometry of the anatomical structures is more explicit for the doctor. Thus, we decided to use a combination of color attributes (hue and luminance) to communicate both filling and uncertainty, on the volume of the periprosthetic target space. We preferred to avoid transparency. Its combination with color could lead to equivocal conclusions. For example, thin, incompletely filled areas and uncertain areas would look similar. Also, we wanted to avoid any kind of solution that would interfere with the geometry of the periprosthetic space, such as transparency and size or shape distortion. This is also proposed by Cedilnik [2000].

We decided to use a two-dimensional colormap varying in color and in luminance, where we match one axis to the filling and the other to the uncertainty. This idea was inspired by two papers: Woodruff et al. [2009] and Hemminger [1993]. In the first paper, they present a scheme that varies in color and alpha channel value. An application of that is shown in Figure 4.14 (A). The second paper presents a perceptually uniform luminance scale to encode one dimension, while each step of the luminance scale corresponds to a set of isoluminant hue steps for the other dimension. The concept of this paper is depicted in the sketch in Figure 4.14 (B). Our idea consists of using a bi-variant and isoluminant colormap, as we present in Figure 4.14 (C). In this scheme, every row has the same luminance, but varies in hue, while every column has the same hue, but different luminance. The hue contains the blue-to-yellow isoluminant scale, based on the perceptually linear colour scales published by Haim Levkowitz² [1992]. Also ColorBrewer³ has been consulted. The color choice is explained in the following section.

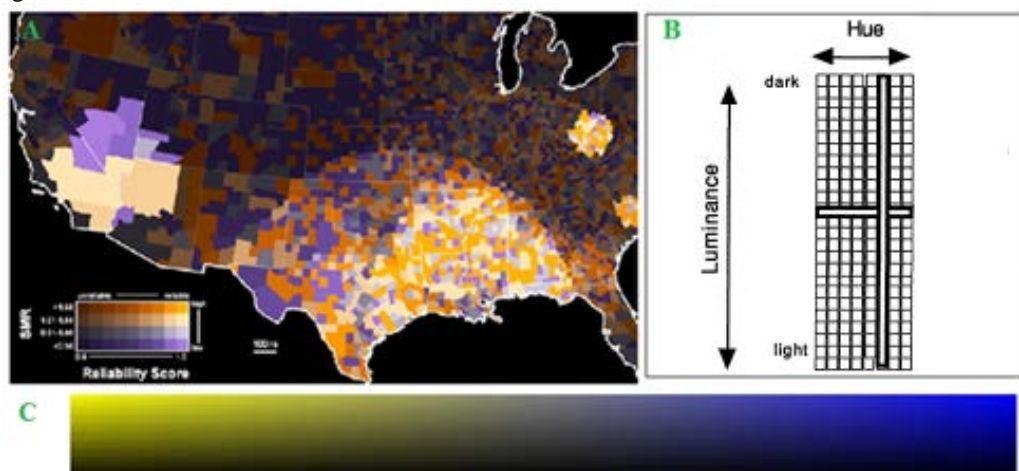


Figure 4.14: Related work, used as inspiration for our implementation. (A) – Value-by-alpha map to depict the standardized mortality ratio for cervical cancer, relative to the reliability score, for different cities in the US [Woodruff 2009]. (B) – Structure of a two-dimensional perceptually uniform isoluminant scale [Hemminger 1993]. (C) – The colormap that we employed in the visualization.

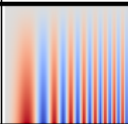
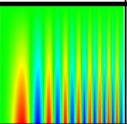
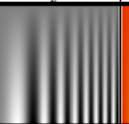
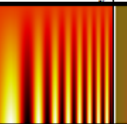
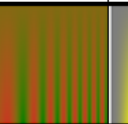
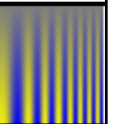
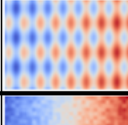
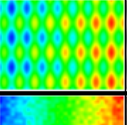
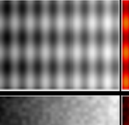
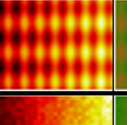
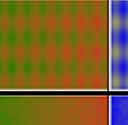
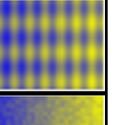
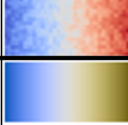
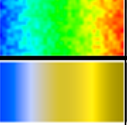
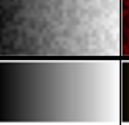
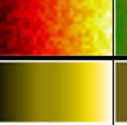
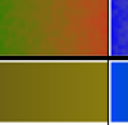
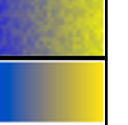

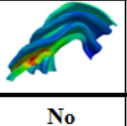

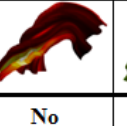


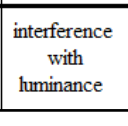
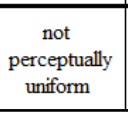
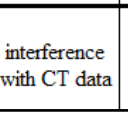
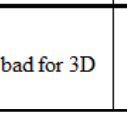
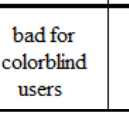
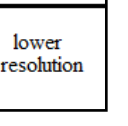
² <http://www.cs.uml.edu/~haim/ColorCenter/>

³ <http://www.colorbrewer.org/>

4.5.2 Decision making: Visualization Colormap

At this point two questions arose: the suitable correspondence of the two axes to each of the two variables and, mostly, the colors that we should employ. For the adequate colormap choice, we referred to the paper of Moreland [2009]. In this paper, different colormaps (cool-to-warm, rainbow, grayscale, heated body, red-to-green isoluminant and blue-to-yellow) are evaluated based on characteristics, such as performance with a spatial contrast sensitivity function, a low-frequency sensitivity function, high-frequency noise, with deuteranope color-deficient vision and 3D shading. This comparison of the colormaps effectiveness is presented in Table 4.2, below.

Table 4.2: Comparison of colormap effectiveness (adapted by [Moreland 2009]).

	Cool-Warm	Rainbow	Greyscale	Heated-body	Red-Green	Blue-Yellow
Contrast Sensitivity						
Low-f Sensitivity						
High-f Noise						
Color-Deficiency						
3D Shading						
Isoluminant	No	No	No	No	Yes	Can become
Main Reason Against Use	interference with luminance	not perceptually uniform	interference with CT data	bad for 3D	bad for colorblind users	lower resolution

The grayscale would cause confusion, because of the scale used for the CT dataset. The rainbow colormap was rejected as non-perceptually uniform. This is also opted by Borland [2007] who stressed that rainbow colormaps have no inherent ordering (especially with green) and colors that are much different to humans are close to each other. The cool-to-warm colormap was eliminated, due to the middle white value, which would be interfering with the luminance. Finally, the heated-body colormap performs poorly with three-dimensional representations and the red-to-green is not suitable for colorblind users. Also, the paper of Rheingans [1999], presents more colormaps, such as the census bureau-two variable map and the complementary display parameters map. These were discarded, as not intuitively applicable to our cases. Based on all that, we decided to use the blue-to-yellow colormap, in an isoluminant form, as also suggested by Bergman et al [2000].

For the axis-variable correspondence, in the paper of Rhodes et al. [2003], the uncertainty is mapped to the hue and the luminance is used to represent the shape of the structure. However, since our primarily important variable is the cement filling, we decided to employ the opposite mapping (hue to filling and luminance to uncertainty). Another reason for this choice is that the hue changes are perceived easier by the human eye [Rhodes 2003, Rheingans 1999]. In this way, the hue will provide more accurately distinguishable levels [Rheingans 1999] for our primary data. We also decided to map blue to empty and yellow to full. Despite the isoluminance of the colormap, yellow can be perceived as brighter and, therefore, will have a more positive association.

However, our colormap had two implications. Firstly, a legend is needed [Rheingans 1999], in order not to impose a memorization of the colormap. Secondly, our colormap complies with only three out of four principles of Trumbo [1981, Rheingans 1999]. These are: order (ordered colors to show data levels), separation (significantly different levels mapped to perceivably different colors) and rows/columns (preservation of univariate information in every row and column). It violates, though, the diagonal principle (colors can be classified in three classes: near the minor diagonal, above and below). According to Rheingans [1999], this is not a problem, if the goal of the visualization is to represent values of one variable (filling) across differing values of the other variable (uncertainty). Still, in order to ensure that this choice is the most suitable, we decided to

perform a wide survey, which confirmed our initial idea. We will discuss thoroughly this survey in the Results section.

4.5.3 Cement Filling vs. Uncertainty Visualization

The cement filling uncertainty visualization shows which parts of the periprosthetic space have been filled, as well as the certainty about this filling. This information results from the back-projection of a single radiograph, acquired post-operatively. This idea is depicted in Figure 4.15 (A), below.

Figure 4.15 (B) shows the concept behind the 2D calculation of the cement filling and uncertainty. The calculation algorithm was implemented by Bas van den Berg, for his M.Sc. project. The 3D calculations are performed from back-projection of the 2D calculations, which result as follows:

- The cement uncertainty is calculated for the areas in front of and behind the prosthesis (Figure 4.15 (B))
- The cement filling is calculated relatively to the ideal case, where the periprosthetic space is fully filled (Figure 4.15 (B)). Here, the fluoroscopic projection of an image with injected cement results as the multiplication of the attenuation values of the image without cement, by the attenuation value of the cement alone.

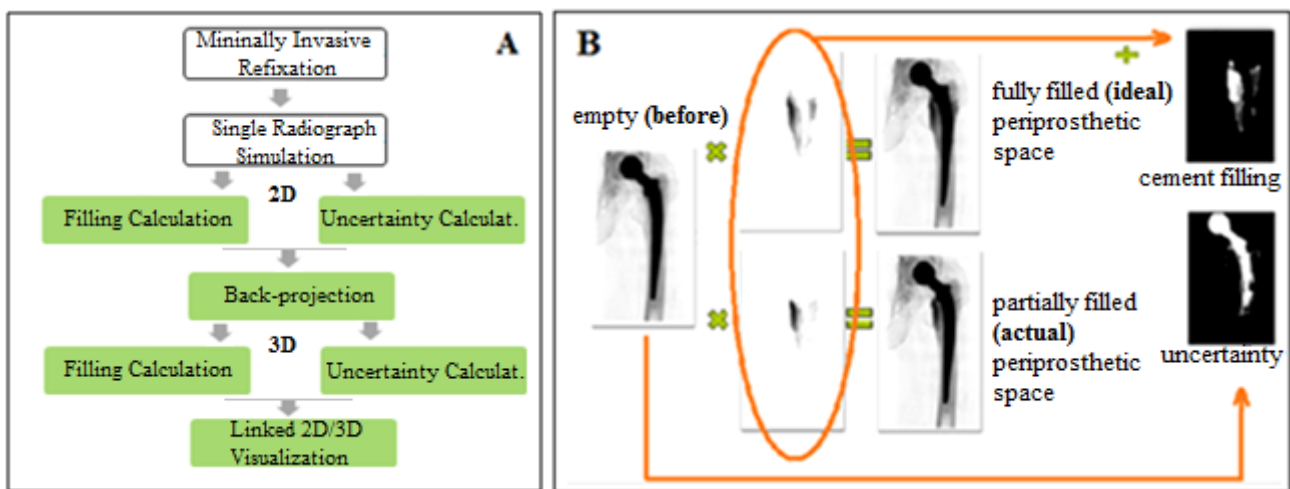


Figure 4.15: (A) – Workflow of the cement filling uncertainty visualization. (B) – Workflow of the calculation of the cement filling and uncertainty (2D).

The cement filling uncertainty visualization is performed both two-dimensionally and three-dimensionally, to take full advantage of the views, at the same time. To minimize mental effort, we propose to link and synchronize the viewers. Figure 4.16 shows an example of cement filling uncertainty visualization.

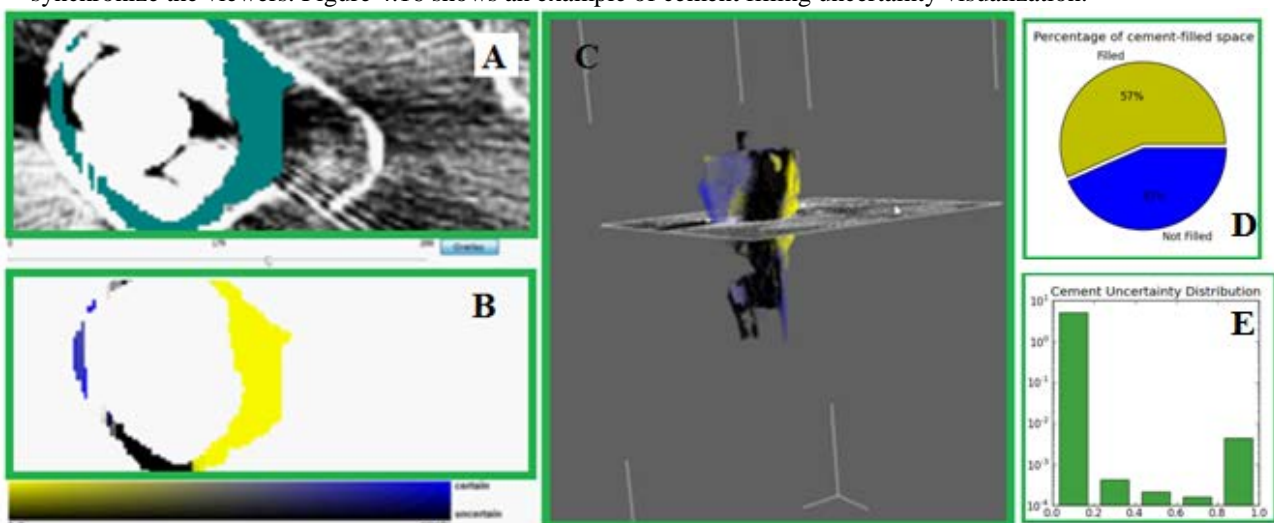


Figure 4.16: Cement Filling Uncertainty Visualization. (A) – Slice-based view of the spatial information of the volume on the data of the patient. (B) – Slice-based view of the uncertainty vs. filling information. (C) – Volume-based representation of the uncertainty vs. filling volume. (D) – Pie depicting the percentage of cement-filled space. (E) – Cement Uncertainty Distribution of the volume pixels.

On the left, the top renderer (A) provides optional two-dimensional spatial information of the periprosthetic space overlaid on the CT dataset. This overlay does not contain any information about the filling or the uncertainty, just information about where this volume is located. It is optional and it can be turned on and off.

The bottom renderer (B) contains a two-dimensional view of the axial slices of the volume in (C). In the right renderer (C), the user can see the three-dimensional volume with all the information regarding the uncertainty and the cement filling. This renderer contains a slice-based view of the initial patient dataset, so that the user can see the uncertainty vs. filling volume, with respect to the CT acquisitions. The role of the two-dimensional and three-dimensional representations is to complement each other, since human depth perception on screens is limited. We remind that the hue has been mapped to filling (blue to empty and yellow to full). The luminance has been mapped to the uncertainty, with darker colors depicting less certain values.

As a final step in our visualization, we present some statistics, concerning our uncertainty and filling calculations. These are, also, shown on Figure 4.16, above. They show the percentage of cement-filled space, in the form of a simple pie (D) and the cement filling uncertainty distribution on the image pixels, in the form of a histogram (E). Note that, in the histogram, the 0 value corresponds to total certainty, while 1 corresponds to total uncertainty. In the filling pie chart, we use colors, corresponding to those of the visualization.

4.6 Summary

In this chapter, we presented our HipRFX system for minimally invasive refixation by cement injection. Our approach consists of four steps:

- **Pre-operative Planning:** The user meticulously performs the pre-operative plan, by loading the cement target (the part, which we ideally want to fill, based on the fibrotic tissue interface) and inserting the needles to the adequate positions. He can also visualize all the structures and tissues of the region of interest.
- **Digitally Reconstructed Radiograph Simulation:** The user can simulate radiographs from the pre-operative plan, that show how the plan would ideally look on the fluoroscopic monitor in the OR.
- **Intra-operative Guidance:** The user can capture simulated radiograph screenshots, which he will use as step-by-step guidance, during the operation. Here, he can also see the placement of the fluoroscope for every step and link back to the previous DRR step.
- **Cement Filling Uncertainty Visualization:** The user can visualize with the use of a single fluoroscopic image, which parts of the periprosthetic target space were actually filled by cement and how the acquisition angle of this radiograph affects the filling certainty.

Chapter 5

Implementation

We implemented the HipRFX system in DeVIDE⁴, making extended use of the Visualization ToolKit (VTK)⁵ and wxPython⁶. DeVIDE is a “cross-platform software framework for the rapid prototyping, testing and deployment of visualization and image processing algorithms” [Botha 2008]. VTK was used for rendering and for implementing the visualization algorithms, while wxPython was used for creating a graphical user interface for our system. The following sections include a description of how the conceptual ideas, described in the Method section, were implemented. The chapter is concluded with a small summary.

5.1 User Interface Build-Up

In order to implement the full HipRFX system, we created a new DeVIDE module in Python, employing VTK for its visualization functionality. Our final version of the User Interface consists of four designated tabs: pre-operative planning, digitally reconstructed radiograph simulation, intra-operative guidance and cement filling uncertainty visualization. Each one of the tabs includes 1 to 3 renderers, depending on the requirements of the task and also an operation panel with buttons and other elements. In Figure 5.1, below, we show an example of the HipRFX tabs, while in use.

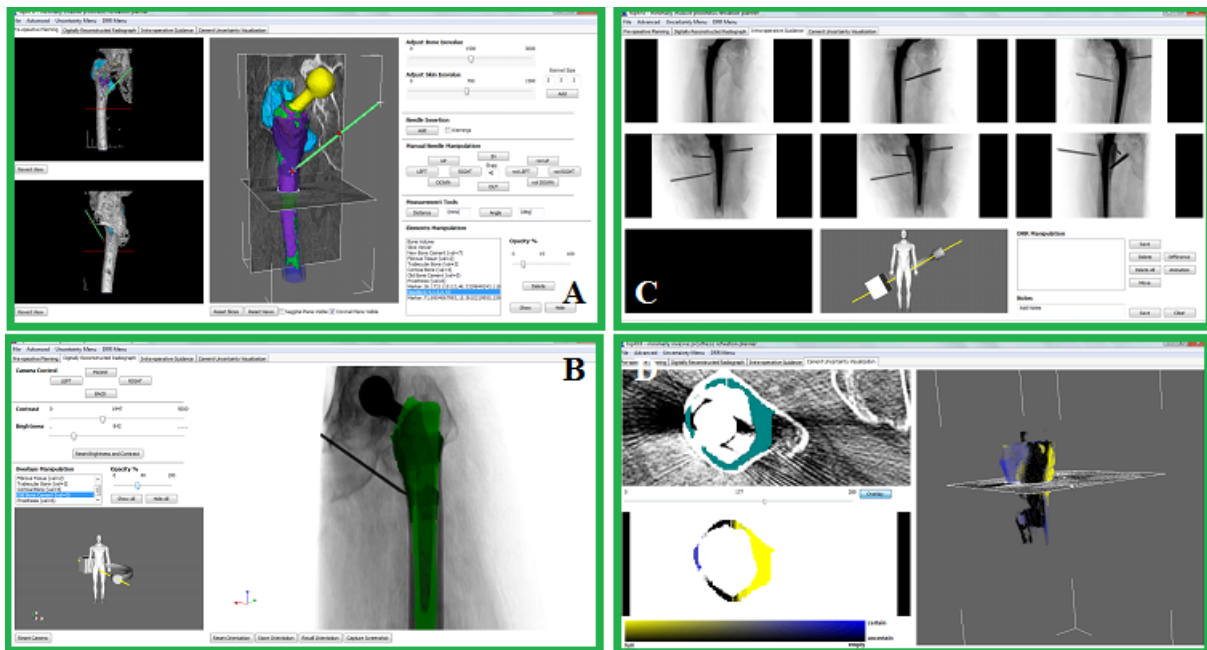


Figure 5.1: An example of the user interface of HipRFX, while in use. (A) – Pre-Operative Planning Tab, (B) – Digitally Reconstructed Radiograph Simulation, (C) – Intra-Operative Guidance, (D) – Cement Uncertainty Visualization.

5.2 Datasets

In the Method section, we already mentioned different datasets, all based on CT acquisitions. In CT scans, the absorption of the tissue is recorded, while the source (consisting of a beam of X-rays) and a one-dimensional array of detectors are rotated around the patient’s body. In this way, one-dimensional projections, recorded at different orientations of the body, are acquired [Elson 2010]. After all the parallel slices are acquired, a three-dimensional image can be created by mathematical reconstruction [Jaramaz 2004]. Computed tomography scans have high spatial resolution, little geometric distortion and a good signal to noise ratio [Taylor 2001], but

⁴ DeVIDE: Delft Visualisation and Image processing Development Environment (graphics.tudelft.nl/Projects/DeVIDE)

⁵ Visualization ToolKit (www.vtk.org)

⁶ wxPython (www.wxpython.org)

they require a higher exposure dose [Hodgson 2008]. In this section, we summarize all the datasets that were employed in our system. All datasets are in the same coordinate system as the original CT dataset.

Main datasets: All the used datasets were real clinical examples of patients suffering from aseptic femoral prosthesis loosening, due to periprosthetic osteolysis. The main datasets are real computed tomography (CT) datasets of the affected hip region of the patient. These datasets were used for the bone volume rendering and the skin surface rendering in the pre-operative planning. They were also used for the fluoroscopic image simulation and the cement filling uncertainty visualization.

Cement target datasets: The cement will be injected where the patient's fibrous interface tissue is located. Therefore, this is a binary dataset, containing the fibrous tissue segmented from the CT dataset of the patient. The segmentation must be performed beforehand, by a trained person, using some available software. The value 1 corresponds to our structure, while 0 delineates the areas outside the region of interest.

Structures to avoid datasets: The vulnerable structures, which should not be punctured during the operation, are contained in a binary dataset segmented from the CT dataset of the patient. This segmentation is similar to that of the cement target.

Segmentation files for multi-tissue visualization: This is a multi-tissue segmentation of the different periprosthetic structures. Every structure corresponds to a specific value, such as 1 for the intramedullary canal, 2 for the fibrous interface tissue, 3 for the trabecular (cancellous) bone, 4 for the cortical bone, 5 for the old cement and 6 for the prosthesis. Finally, 0 corresponds to areas outside the region of interest. We based our segmentations on the paper of Malan et al. [2012].

5.3 Pre-operative Planning Implementation

In the Method chapter, we mentioned our conceptual ideas concerning the pre-operative planning. It is important, though, to justify explicitly all the choices that we made and, also, the way we implemented them. For each one of the following issues, we refer to figures of the previous chapter.

Optimal viewports and linked renderers: In the planning tab, we employ three renderers, as it was shown in Figure 4.3. This is also visible in Figure 5.1 (A). As we already mentioned, the central renderer holds the main dataset in a slice-based representation, making use of an already existing module of DeVIDE, CMSliceViewer. This module was incorporated in the user interface and used in conjunction with VTK to render the slice view and the volume data. Moreover, we provide the user with two additional renderers, to facilitate the three-dimensional manipulation of the needle with the mouse. Depth perception might be limited on a screen [Tory 2004] and it has been documented that the two useful viewing perspectives are the one along the needle axis and the one perpendicular to it [Racadio 2007]. These viewports are calculated, based on the orientation of the last inserted needle. They also have a marker, linked to the current slice of the slice viewer, to show the position of the slice, relative to the anatomical structures.

Three-dimensional representation to enforce two-dimensional visualization: Although the surgeon is used to two-dimensional slice-based data, the 3D inspection of the dataset can provide a better spatial content for the needle insertion. Surgeons are experienced in mentally visualizing the physiological structures. Yet, a three-dimensional representation would give a better view of non-anatomical structures not present in the patient dataset, such as needles or new cement. Finally, it is important to see all the slices, not only along the axis of the scanning acquisition, but also for the other two planes (sagittal and coronal). The sagittal and coronal slices are extracted automatically from the dataset, based on some predefined matrices. Then they are presented in a 3-orthogonal slice viewer. This was depicted in Figure 4.3 and, also, in Figure 5.1 (A).

Multi-tissue visualization and cement target insertion: The multi-tissue visualization workflow is shown in Figure 5.2, below. When the patient dataset is loaded, the bony structures are automatically rendered, with the use of a volume ray cast function (`vtkVolumeRayCastCompositeFunction`). This function performs compositing along the ray, according to the properties stored in the `vtkVolumeProperty` for the volume. In this property, a `vtkColorTransferFunction` function is used to map the volume to an RGB color value. Also, a `vtkPiecewiseFunction` is employed, for defining which isovalues (Hounsfield values) will be visible or not in the rendering. This is controlled by the bone isovalue slider in the operation panel. After that, the skin surface can be also rendered. This is performed with the use of the skin isovalue slider, which controls the value of the threshold (`vtkThreshold`), in order to isolate the skin from the rest of the dataset. The thresholded data is, then, passed by a three-dimensional closing filter (`vtkImageContinuousDilate3D` and `vtkImageContinuousErode3D`) with a user-defined 3D kernel for filling small holes. Afterwards, a `vtkImageGaussianSmooth` filter with a voxel-based radius of 1.5 and a standard deviation of 2 will be employed to reduce noise. Finally, a `vtkContour` is

applied to render the skin surface. For the vulnerable structures (like vessels or nerves), for the periprosthetic structures and for the cement target, things are less complicated. Those structures are already segmented manually, by a trained human or semi-automatically with some software. So, `vtkContour` is applied to render them. The opacity of all those structures can be altered with a slider, so that the user can be able to discern all the overlapping areas.

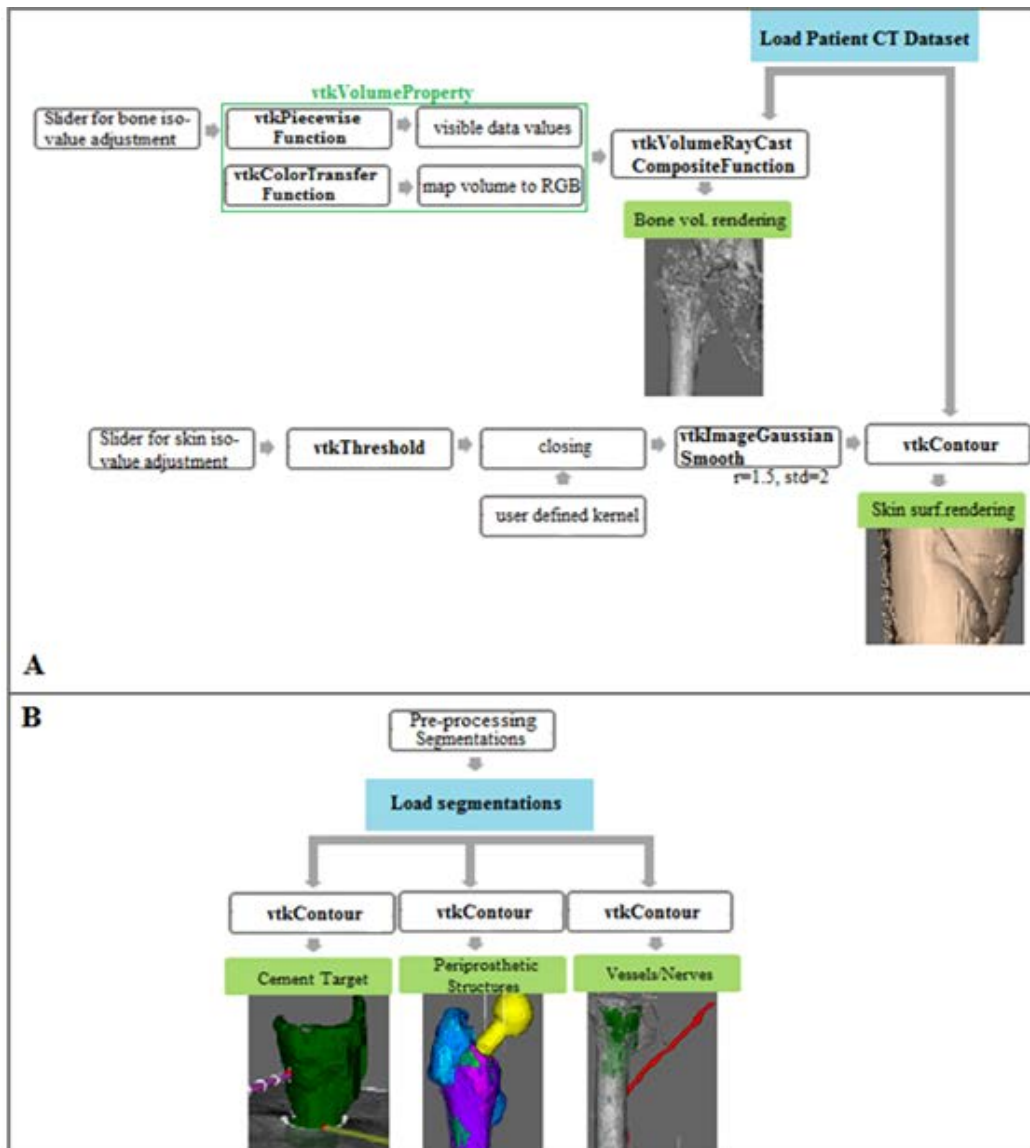


Figure 5.2: Multi-Tissue Visualization Workflow. (A) – For the automatic bone volume rendering and skin surface rendering, (B) – For the manually segmented structures.

Needle insertion: For the needle insertion, we decided to use an already existing feature of the CMSliceViewer, which is the ability to pick points on a slice with a simple left-button-triggered mouse event. This can be seen in Figure 4.5, or Figure 5.1 (A). The idea is to pick two points (a “target” and an “end” point), in order to provide the system with the position and the orientation information for the placement of the needle. The two points are captured with a key-press event, using the space key. Then, the needle is inserted by pressing the add-button. A ruler (`vtkDistanceWidget`) appears along the needle axis, to mark how deeply it was positioned. The needle was designed in Blender⁷, an “open source, cross platform suite of tools for 3D creation”, based on the model that is actually used in the procedure.

Needle manipulation & optional warnings for surrounding vulnerable tissues: The needle orientation and position can be altered, either by dragging-and-dropping the rendered graphical object; or automatically, with the use of transformations on the needle actor. In the first case, we employ a VTK interactor that switches between

⁷ www.blender.org

two modes, trackball camera and trackball actor. This enables the manipulation of the viewpoint of the scene and the interaction with independent objects in it. In the second case, a user-defined step is used to translate (in mms) or rotate (in degrees) the needle, for all five DoFs. An additional optional tool warns the user, if the needle approaches a specific vulnerable structure. In order to do that, we create a bounding box around the needle of 5x5x5 mms and we clip it from the binary data of the vulnerable structure. Afterwards, we check the scalar range inside this extent. If the range does not include the value 1, which is the value of the vulnerable structure, then there is no eventual intersection danger with the structure. Else, the user is warned.

Measurement tools: By exploiting again the picking feature of the CMSliceViewer, we can pick points on the slice, where we need to perform a distance or angle measurement. In this way, the user can select two or three points, respectively, to calculate the distance or the angle between them. Here, we make use of formulas, known from analytic geometry. We have showed the measurement tools in Figure 4.6.

5.4 Digitally Reconstructed Radiograph Simulation Implementation

As we already mentioned in the Method section, the digitally reconstructed radiograph simulation part was mostly implemented by Bas van den Berg for his M.Sc. project. For this module, he created a modified version of the VTK volume raycaster that calculates the ray absorption by the volume and renders it, instead of the whole CT volume data. This can be seen in Figure 4.7 and also in Figure 5.1 (B). It uses a composite transfer function, related to the linear part of an H&D curve and its characteristics. It is also possible to highlight some areas of interest, by assigning colors to the ray, instead of grayscale values. An example of that was presented in Figure 4.9. The bi-directional linkage between the C-arm model and the simulated fluoroscopic images was employed to show the position to the fluoroscope relatively to the patient. It was performed by binding the camera attributes in the simulation render, to the fluoroscope model actor orientation.

5.5 Intra-Operative Guidance Implementation

During the intra-operative guidance, the surgeon uses captured images from the pre-operative planning, along with the simulated fluoroscopic images. Then, he uses them as guidelines during the operation, with minimal distraction and maximum visual feedback. This concept can be seen in Figure 5.1 (C).

Stepwise two-dimensional intra-operative guidance: In order to capture each one of the images to be used in the guidance, we make use of a `vtkWindowToImageFilter`. This produces a two-dimensional screencast image of the rendered window view. Then, each of these images is brought into the first empty render window in the intra-operative guidance tab, along with annotated information, concerning the position of the fluoroscope. Just before the operation, the surgeon can either print those images, or directly display the system interface on a screen, if he wants to retain the fluoroscope configuration.

Fluoroscope placement information and linkage to DRR: As we already mentioned, the intra-operative guidance tab interface holds a model of a patient in a C-arm fluoroscope. Also, each one of the screenshots has annotated information on the fluoroscope positioning. Therefore, the user can click on each image to get the respective positioning of the fluoroscope model, which is coupled to the DRR fluoroscope-settings panel. For that, the orientation/position of the interactive fluoroscope CAD model is automatically manipulated.

Difference images implementation: The workflow, for the difference image visualization, is shown in Figure 5.3, below. The difference image, between two images, is calculated by the absolute value of the subtraction of those images. For that, we use two `vtkImageMathematics` filters. The first operation is set to subtraction, while the second one to absolute value. As we already described in the Method section, we have two options for visualizing difference images: optionally flickering overlays or static deformed annotation grids. There is a trade-off of qualities, when choosing between them, regarding the visual fatigue, information loss and the ability to show the underlying structure with minimal distraction. For the overlays approach, we use an animation of the image difference overlay. This is created with the use of a `vtkLookupTable`, to map the scalar difference values to red-green-blue-alpha transparency, and a `vtkImageMapToColors`, to map the image through this lookup table. For the second approach of the annotation grids, we create a two-dimensional `vtkImageGridSource` with a small spacing (3x3pixels) and we multiply it by the stencil (`vtkImageStencil`) of the difference image. In this way, we keep the values of the difference image on the grid and we can display it in a static way. It is obvious, though, that we lose the information in between the spacing of the grid. The annotation grids were inspired by the paper of Cedilnik et al. [2000].

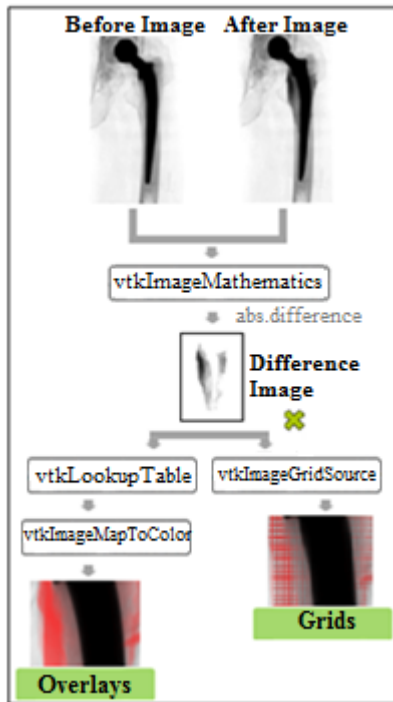


Figure 5.3: Difference Image Visualization Workflow.

5.6 Cement Filling Uncertainty Visualization Implementation

In the cement filling uncertainty visualization tool of our HipRFX, we define and visualize the cement filling, enhanced with information about uncertain areas. Those areas emerge, due to the fact that the cement filling of the parts in front and behind the prosthesis cannot be discerned in a two-dimensional radiograph. We showed in Figure 4.16, but also in Figure 5.1(D), an example of this visualization.

The volumetric data resulting from the calculation of the uncertainty and the filling are visualized, both in two and in three dimensions. The workflow of this visualization is shown in Figure 5.4, below. In the two-dimensional visualization, we use a `vtkColorTransferFunction` to build a `vtkLookupTable`, with an alpha value equal to 1 and a hue that ranges from blue to yellow. This is used to depict the empty to full range. We also employ a `vtkPiecewiseFunction`, to build a second `vtkLookupTable`, with a varying alpha value (0 to 1) for a black hue. This will depict the certain to uncertain range. After mapping the filling and uncertainty values, we render the filling on the slice viewer, making use of the `CMSliceViewer`, and we overlay the uncertainty. Regarding the three-dimensional visualization, we render the volume of the filling and the volume of the uncertainty, using a `vtkVolumeTextureMapper3D`, for each. The `vtkProperty` attributes of these two volumes are set as in the two-dimensional case. Finally, we employ a library, `matplotlib`, to plot a pie chart for the cement filling percentage and a histogram pixel distribution for the cement filling uncertainty.

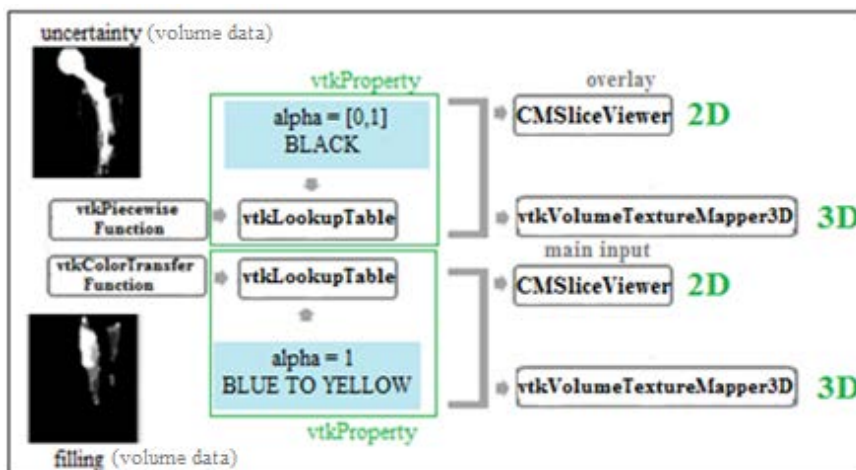


Figure 5.4: Cement Filling Uncertainty Visualization Workflow.

5.7 Summary

In this chapter we justified all the choices that we made during the implementation of the four stages of the HipRFX.

- In the planning stage, a volume ray cast function was used for the bony structures. The other important structures (cement, vulnerable structures, bone segmentations, skin) were rendered using contouring, based on thresholds defined in Hounsfield Units.
- In the digital reconstructed radiograph simulation, the employed visualization was implemented using a modified version of the VTK volume ray-caster, created by Bas van den Berg.
- In the intra-operative guidance, the difference of two simulated radiographs is calculated by subtracting those two images. For the overlay approach a lookup table was employed. The deformed annotation grid approach was implemented with the use of a thick grid with variable opacity, proportional to the magnitude of the difference at each point.
- In the cement filling uncertainty visualization, we preferred again to employ both 3D and 2D visualization to enhance the perception of the surgeon. We created overlays on the CT data slices, by using color transfer functions, to visualize the cement filling and uncertainty. Using the same colors, with the use of piecewise functions, we render this same information, as a 3D volume.

Chapter 6

Results

After the implementation of HipRFX, we aimed at answering two main questions about it: “Is it right?” and “Can it be better?”. In order to evaluate our work, we used the following methods:

- Tests on real patient CT datasets, provided by Leiden University Medical Center
- A user interface evaluation, in a group of 25 subjects.
- Four evaluations specifically targeted to the cement filling uncertainty visualization:
 - An extensive survey, with 80 participants, for the colormap determination
 - An assessment for color-deficient users
 - A quantitative evaluation of the performance of the cement filling uncertainty visualization, with 18 simulated cases
 - A qualitative evaluation of the cement filling uncertainty visualization, where we documented the opinion of a group of 25 people, on the characteristics of this visualization.
- A domain expert review, where a clinical expert evaluated the system. This provided feedback on the usefulness of specific features, on missing traits and on limitations of the system.
- An in situ experiment, on 5 cadaveric leg subjects.

We based our evaluations on the nested model proposed by Munzner [2009], which comprises of four levels. This model provides “prescriptive guidance for determining appropriate evaluation approaches (immediate and downstream), by identifying threats to validity unique to each level” [Munzner 2009]. This approach helped us formulate all the topics that needed to be answered, during the evaluations. The nested model, in Figure 6.1 (left), shows the four levels of the evaluation, along with the main threat for each level and the validation solutions. The target level of each evaluation, along with the employed method, is shown in Figure 6.1 (right).

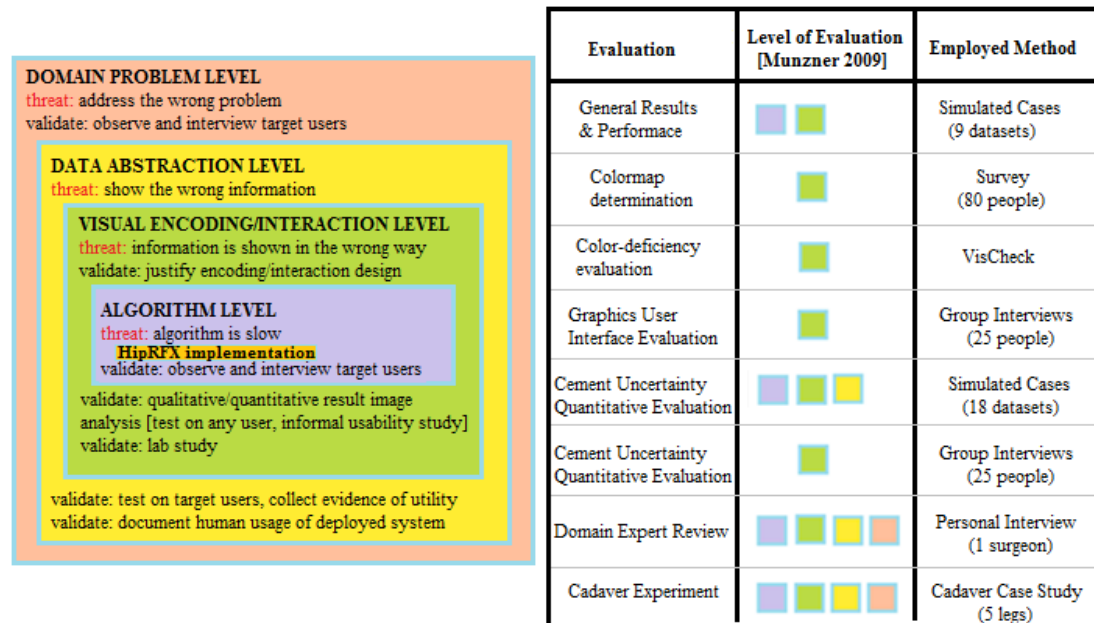


Figure 6.1: Nested Model for the evaluation of the HipRFX system (adapted by [Munzner 2009], on the left). On the right, table showing the target level and also the employed method, for each evaluation.

6.1 General Results

In the present section, we demonstrate some more examples of our method. The HipRFX system was tested on 9 real CT datasets of patients, suffering from aseptic loosening, due to periprosthetic osteolysis. The dimensions of the datasets varied from 155x124x271 to 512x512x323 and their spacing from 0.332x0.332x1 to 0.512x0.521x2.

The smaller datasets were cropped versions of full resolution sets, without down-sampling. In Figure 6.2, below, we present the application of our method to three different cases, for the three most important tasks (multi-tissue visualization, simulation of the fluoroscopic images after needle insertion and cement injection, volume and slice-based cement filling uncertainty visualization).

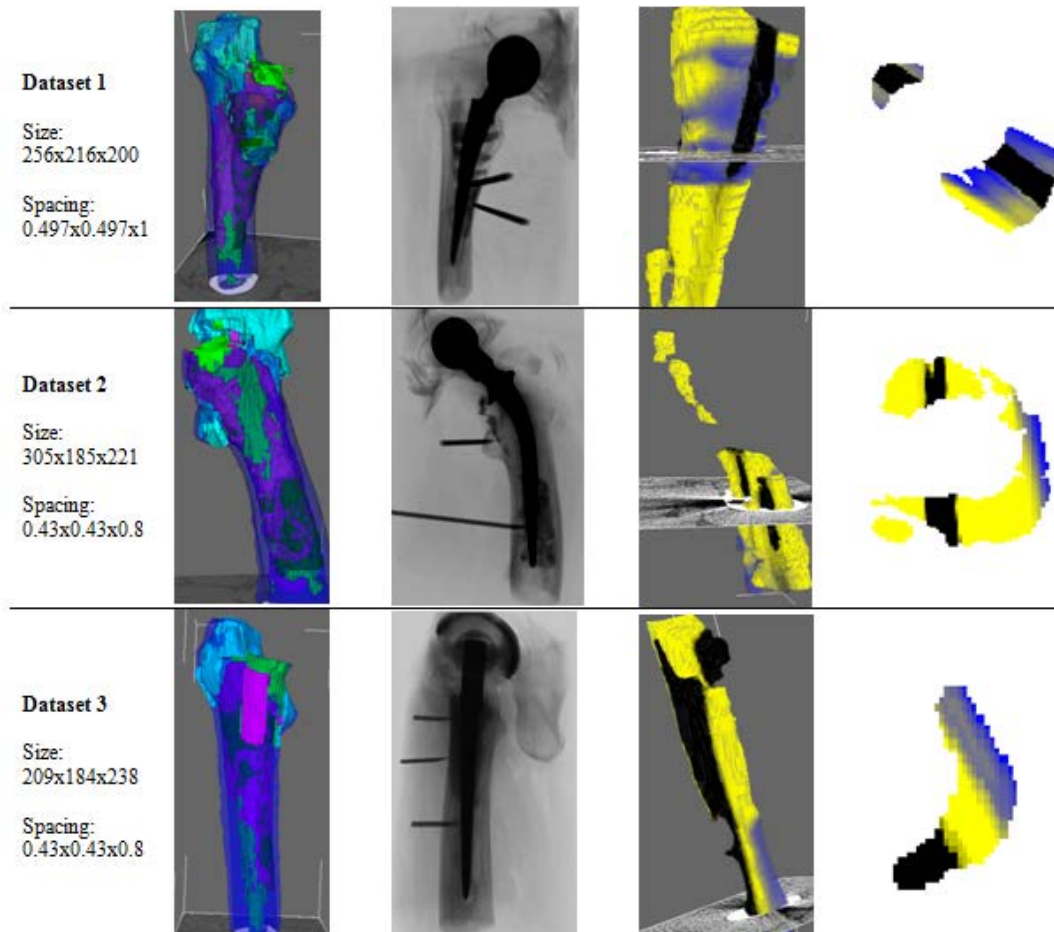


Figure 6.2: Results from the implementation of our HipRFX system on different datasets. For each dataset (same row) we show the three most important tasks: multi-tissue visualization, simulation of the fluoroscopic images after the insertion of needles and cement injection, and the cement filling vs. uncertainty visualization (3D and 2D slices).

Our system gives comparable results, no matter the dataset sizing, or spacing and, regardless the specific anatomical characteristics of each patient, or the specific details, or characteristics of the procedure. At this point, we can make the following remarks:

- The multi-tissue visualization is highly dependent on the segmentation pre-processing step. It is, basically, the rendering of these segmented structures. In case the segmentation is not accurate, also our multi-tissue visualization will be sub-optimal.
- The radiograph simulation was performed in real-time. By changing the value of the brightness and the contrast, we can achieve a realistic simulation of fluoroscopic images. Both needles and cement are visualized realistically.
- The computation time for the uncertainty visualization of those datasets, varied from 40 seconds to 1 minute. Cement filling uncertainty visualization will be discussed more in the following sections.

6.2 Performance

The HipRFX system was tested on CT datasets from real patients. Although the testing was performed offline, we can approximate that the real time of the planning procedure is around 45 minutes. This does not take into consideration the pre-processing stages and it depends on the experience of the user with computers and the system. The calculation and visualization of the cement filling and uncertainty takes 40-90 seconds, depending on the employed computer and dataset size. Some operations, such as the multi-tissue visualization and the cement filling uncertainty visualization, are slower, when larger datasets are used. According to the clinical

experts, the employed time is reasonable, both for the planning procedure and for the cement filling uncertainty visualization. Therefore, the performance of our system is good, in terms of speed. It is expected that with some experience, the planning time will reduce to an even more acceptable level. Also, on faster hardware, the computation time may become less noticeable, even when working with bigger datasets.

6.3 Evaluations

In this section, we present five methods that we followed for the evaluation of our HipRFX system.

6.3.1 Colormap Determination Survey

We performed a survey for determining the suitable correspondence of the two colormap axes (hue, luminance) to each of the two variables (cement uncertainty, cement filling). Before this survey, we thought of mapping the color hue to the main data, which is the cement filling, and the luminance to the secondary information, which is the cement uncertainty. Yet, we needed to confirm it, as a suitable option.

We showed a list of options to 80 non-colorblind people, aged between 23 and 55 years old. Firstly, we provided them with four options, concerning a bivariate isoluminant colormap, going from red to green and from high to low luminance. After, we provided them with the same four options, changing the colormap, to range from blue to yellow. In both cases, they had to indicate the most intuitive. The options and preference results of the red to green colormap survey are depicted in Figure 6.3 (A), below. These four options are only half of the eight possible combinations for the colormap, because the rest (for example, red equals to full and green to empty) did not make sense. Figure 6.3 (B) presents the options and results of the blue to yellow colormap survey. In this case, we mapped blue to either empty or uncertain, because yellow can have a more positive association than blue, as we already mentioned.

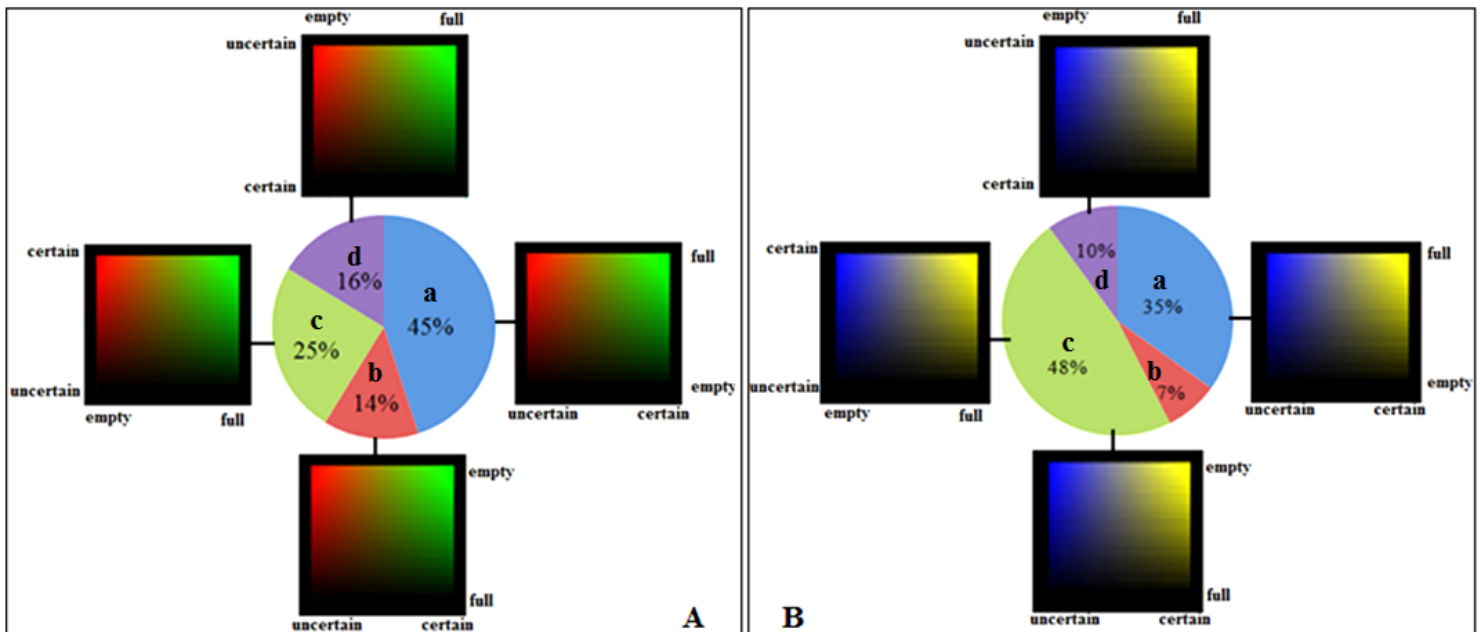


Figure 6.3: Options and preference results (pie chart indicating preference) of the evaluation concerning (A) the red-to-green colormap and (B) the blue-to-yellow colormap. Not all eight combinations were considered, only the four more sensible.

For the blue-to-yellow colormap case, our initial hypothesis, concerning the axis-variable correspondence (option c), was verified. Yet, for the red-to-green colormap, the most intuitive choice is to map the hue to the certainty and the luminance to the filling (option a). This is related to the conventional connotation of red to negative feelings and green to positive ones [Rheingans 1999], due to other applications of the colormap (such as traffic lights, gaming). Additionally, the fact that the hue is a more explicit feature than the luminance may also have affected the perception of the subjects. In both cases, options (b) and (d) were less popular. In those cases, a filled cement area or a certain area for option, respectively, is black and, therefore, indistinguishable. However, this was more obvious for the blue-to-yellow colormap. Still, a non-trivial percentage opted for them, probably viewers who are used to media that map the highest value to black (e.g. higher amounts of ink) [Rheingans 1999].

6.3.2 Color-Deficiency Evaluation of Uncertainty Visualization

An important reason, for which we preferred to use the blue-to-yellow colormap, is its suitability for people with color-deficient vision. We wanted to reinforce this, by using VisCheck⁸, “a computer simulation of the entire process of human vision” that manages to show how color-blind people see our visualization. The results from VisCheck are presented in Figure 6.4, below. We include a VisCheck test of a red-to-green colormap, as well.

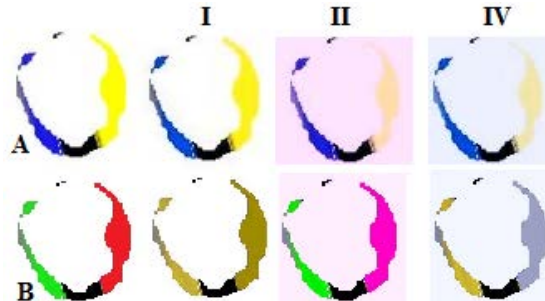


Figure 6.4: VisCheck testing of our cement filling uncertainty visualization. (A) – For blue-to-yellow colormap. (B) – For red-to-green colormap. Checks: (I) – Deuteranope Simulation, (II) – Daltonized Image, (III) – Deuteranope Simulation of Daltonized Image.

6.3.3 Graphics User Interface (GUI) Evaluation

The User Interface design involves subjective principles, such as ergonomics and psychology. Therefore, it is important to evaluate it, to ensure that the system can be operated effectively. For this, we decided to employ two methods. The first method uses ISO9241 international standard, and especially, Part 11: Guidance on Usability [ISO9241-11/1998]. The second method uses the System Usability Score [Brooke 1996].

The target group of this evaluation included 25 engineers and designers (11 females and 14 males), with a medium to high experience with user interfaces. In Appendix A (Figure A.1), we show the distribution of the participants, based on their experience with user interfaces. We decided to perform small group interviews of three to five people, instead of single subject surveys, mainly, due to time restrictions. During those sessions, we described and manipulated the system. Then, the interviewees rated the system in terms of usability, according to the two methods mentioned before. They were not allowed to discuss their choices with the group, to avoid biasing their opinions.

6.3.3.1 GUI Evaluation with ISO9241-11

ISO9241-11 explains how to evaluate the usability of a system. Here, usability is defined as “the extent to which a product can be used by specified users to achieve specified goals with effectiveness, efficiency and satisfaction in a specified context of use” [ISO9241-11/1998]. The effectiveness is related to the accuracy and completeness of a goal [Bevan 2001, ISO9241-11/1998]. The efficiency measures the mental or physical effort, time, materials or financial cost that a goal requires [Bevan 2001, ISO9241-11/1998]. In order to measure the usability of the GUI, we defined the most important goals of the system. These would be rated for their effectiveness, efficiency and satisfaction, by our target group, in a simple 0-10 scale:

1. In pre-operative planning:
 - A. needle insertion and manipulation
 - B. multi-tissue visualization
 - C. cement insertion
2. In digitally reconstructed radiograph simulation:
 - D. simulation of fluoroscopic images with needles and cement
 - E. enhancement of fluoroscopic images with overlays
3. In intra-operative guidance:
 - F. stepwise guidance concept
 - G. link to DRR and fluoro-settings
 - H. difference images to show details
4. In cement filling uncertainty visualization:
 - I. cement filling uncertainty vs. filling visualization
 - J. filling/uncertainty statistics
 - K. 3D volume to enhance 2D view.

⁸ <http://www.vischeck.com/>

In Figure 6.5 below, we show the results of the evaluation for the effectiveness, the efficiency and the satisfaction, for each one of the tasks of the HipRFX system. The green line of the boxplots stands for the median. The first and third quartiles are depicted with red, while the minimum and maximum values are given in grey. All the values are included within the whiskers and we do not depict the outliers separately, in order to give a full aspect of the range of values.

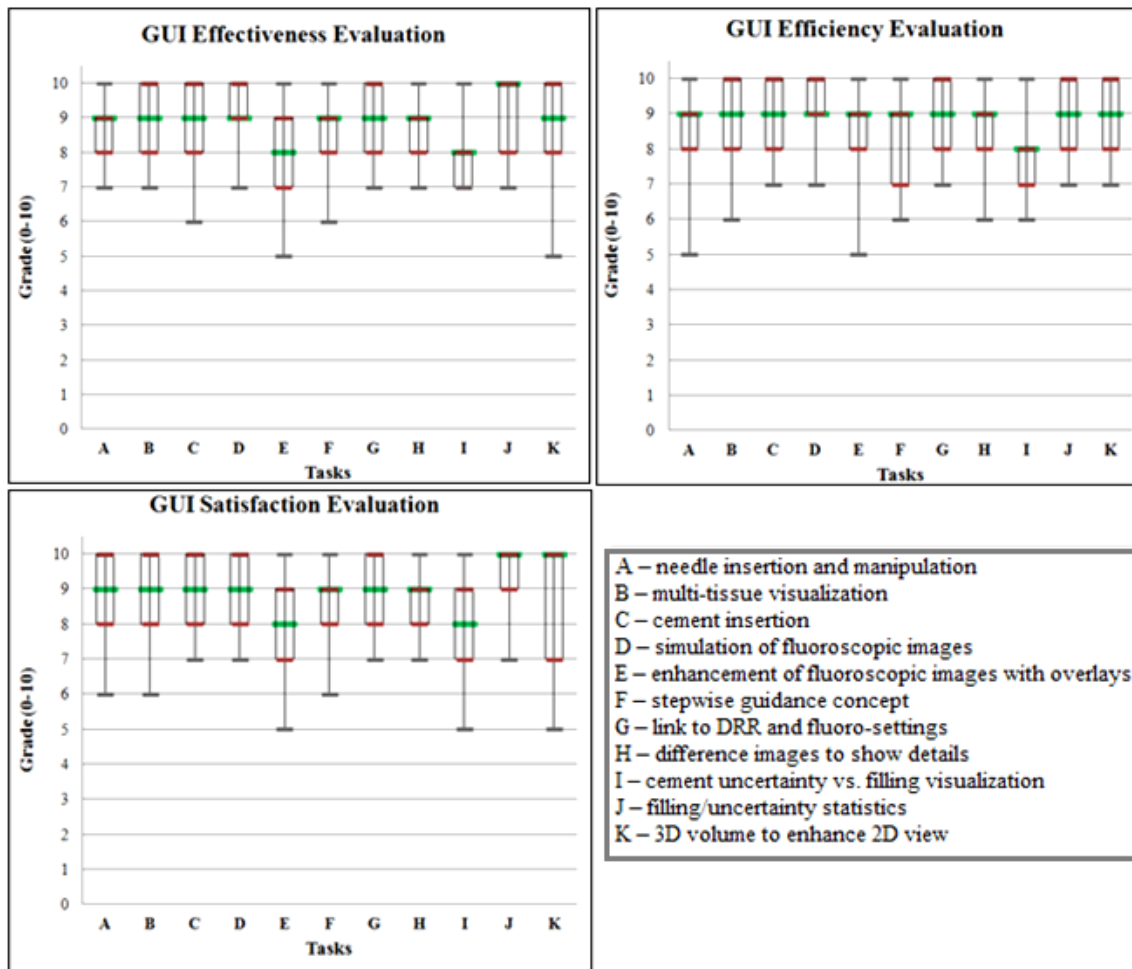


Figure 6.5: Boxplots for the evaluation results concerning the effectiveness, efficiency, satisfaction [ISO9241-11/1998] of the HipRFX interface, for each one of the tasks involved in the three first cases. The green lines refer to the median values, the grey lines to the min/max values and the red lines to the 1st and 3rd quartile. A legend for the tasks is also provided.

The usability (effectiveness, efficiency, satisfaction) of the system is evaluated to be generally high, by our target group. Yet, two specific tasks (E – enhancement of fluoroscopic images with overlays, I – cement uncertainty vs. filling visualization) are a bit lower. For those two tasks, the concept is harder to understand. So, the reviewers might not have been totally able to evaluate its completeness and accuracy, or be more satisfied. However, the efficiency is affected, only in the case of the uncertainty visualization. This requires, indeed, more time (around one minute) for the calculation of the uncertainty and the visualization of the two variables, especially in 3D. The efficiency of the stepwise guidance also presents a low value, but still a high median. This is probably, because the manual effort or time expenditure were considered high by the reviewers. Additionally, the satisfaction from the 3D volume shows some low values, as well, but again a high median. That is related to the preferences of some reviewers towards the slice-based representation, as we will see in the following sections.

6.3.3.2 GUI Evaluation with the System Usability Score (SUS)

The second approach that we followed was the System Usability Score (SUS: Digital Equipment Corporation ©, 1986). It is a simple, reliable, low-cost Likert scale, containing 10 ready-made statements about the usability of a system [Brooke 1996]. We include the SUS scale in Appendix A (Figure A.2). Figure 6.6, below, presents the results of this evaluation. The mean score is 72.2% and is depicted in the graph with the blue reference line. We also show the minimum (50%) and the maximum value (92.5%) with red and green, respectively. The grey reference lines show the 80% confidence interval.

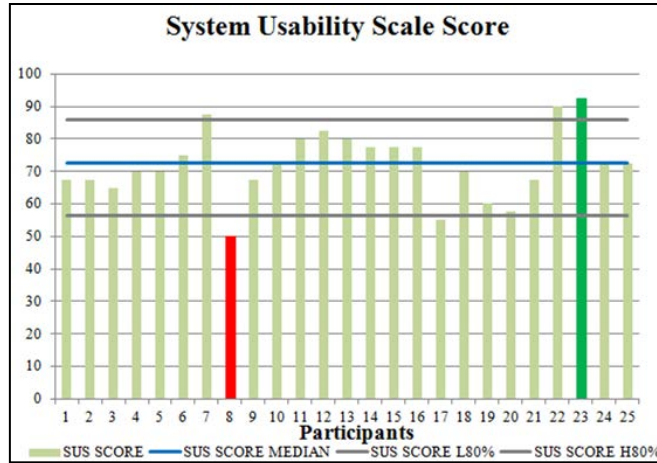


Figure 6.6: Graph depicting the System Usability Scale Score [Brooke 1996]. With blue we show the mean value (72.2%), with grey the 80% confidence interval and with red and green, the min and max values, respectively.

This score proved to be a bit lower, relatively to the ISO9241-11 results, but it is still satisfactory. However, it should be taken into account that the SUS scale is a ready-made scale. So, some of its statements may have not been totally applicable to our case. Lastly, some reviewers reported that they found it hard to grade in a 1 to 5 scale, while they had fewer problems with a 0-10 range.

6.3.4 Cement Filling Uncertainty Visualization Evaluation

The next step in our evaluations assesses the cement filling uncertainty visualization tools in two ways: The qualitative assessment is related to the quality of the visualization, in terms of its characteristics. The quantitative assessment is related to the performance of the tool for simulated cases.

6.3.4.1 Quantitative Cement Filling Uncertainty Visualization Evaluation

In this evaluation, we simulated 18 different cases of cement filling and uncertainty patterns, all from real patient datasets. For each case, we created the 3D cement filling pattern and we simulated a radiograph. Then, we computed the filling and uncertainty, from this simulated radiograph only. We followed the method, depicted in Figure 6.7, below.

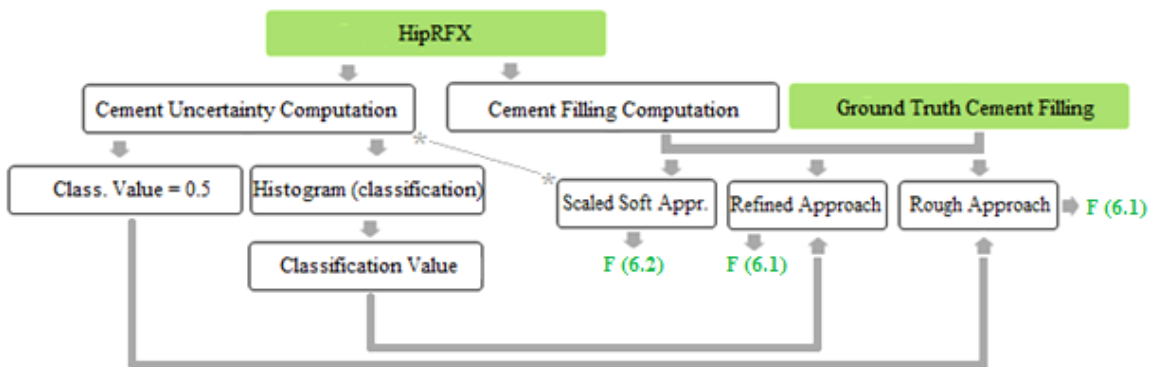


Figure 6.7: Graph depicting the workflow for the quantitative evaluation of the cement uncertainty visualization.

Firstly, HipRFX computed the filling and the uncertainty, as we explained in section 4.5.3. For the uncertainty data, it is important to differentiate between the values representing certainty and the ones representing uncertainty. Thus, we followed two approaches: the rough and the refined. In the rough approach, we considered 0.5 to be the value that differentiates certain (0 to 0.5) from uncertain values (0.5 to 1). In the refined approach, we found a more accurate value for this binary classification, from a histogram of the uncertainty distribution. The results of these histogram classifications for our 18 cases can be found in Appendix A (Figure A.3). For the filling data, we had to measure the proximity of the HipRFX filling computation to the actual filling. Here, we involved the Dice coefficient, a similarity measure to show the spatial overlap between two sets [Babaola 2008]. It ranges between 0 (no overlap) and 1 (total agreement) and is given by formula (6.1), below. In this formula, A is our binary ground truth (only the voxels that have a value above 0.5 for the rough approach, or the clustering value for the refined approach) and B is the filling. The ground truth was manually delineated and provided by François Malan, while the filling was computed by HipRFX.

$$D = \frac{2 \cdot |A \cap B|}{|A| + |B|} \quad (6.1)$$

where $|A \cap B| = \sum_{i=0}^N (A_i \cdot B_i)$, $|A| = \sum_{i=0}^N A_i$ and $|B| = \sum_{i=0}^N B_i$

However, in these two approaches, we did not take into consideration the false positives and false negatives. In order to do so, we employ a third approach, the scaled soft Dice evaluation, which is more robust, in eliminating eventual false positives and false negatives. For this approach, the ground truth A and the filling B were scaled by the uncertainty, as shown in formula (6.2), below. In this formula, A is our binary ground truth (all the voxels) and B is the filling, while we denote with c the per-voxel certainty value.

$$D = \frac{2 \cdot \sum_{i=0}^N (A_i \cdot B_i \cdot c_i)}{\sum_{i=0}^N (A_i \cdot c_i) + \sum_{i=0}^N (B_i \cdot c_i)} \quad (6.2)$$

The three Dice indices that we calculated are linearly correlated. In Appendix A, we show their linear relationships (Figure A.4, A.5), which implies that their behaviors will be identical. Also, the filling percentage (as calculated by HipRFX) and the dice indices correlate positively, and this relationship can be described by a monotonic exponential function (Figure A.6, Appendix A). From this evaluation, it results that, as long as there is a large degree of cement filling, the dice indices are high. So, the computed filling is similar to the actual filling. However, for a filling percentage lower than 50%, the dice indices do not behave well. To sum up, for the simulated data, we believe that if the filling is higher than approximately 50%, the filling calculated from the back-projection will match the ground truth. Therefore, our cement filling vs. uncertainty calculation will work in a satisfactory manner.

6.3.4.2 Qualitative Cement Filling Uncertainty Visualization Evaluation

For this evaluation, we employed the same 25 people, as in the Graphics User Interface evaluation, also in small groups of three to five people. During this interview, we showed two demos of different cement filling uncertainty visualization cases. The tasks of this interview were:

1. To determine the percentage of the filled and the certain periprosthetic space, in both cases
2. To note the preference, concerning the 2D or 3D cement filling uncertainty visualization
3. To grade four important characteristics of the visualization [Newman 2004], in a Likert (1-5) scale:
 - degree of difficulty to identify the data
 - degree of difficulty to identify the uncertainty
 - visual overload
 - level of brightness/contrast.

For the first task, we show the results in Figures 6.8 and 6.9, below. We present the predictions of the interviewees, along with their proximity to the true value. In the boxplots, we depict the true value with a red line, while the median of the predictions is shown in green. The minimum and maximum values, as well as the first and third quartiles are also visible. In the proximity histograms, we consider deviations till 5% satisfactory.

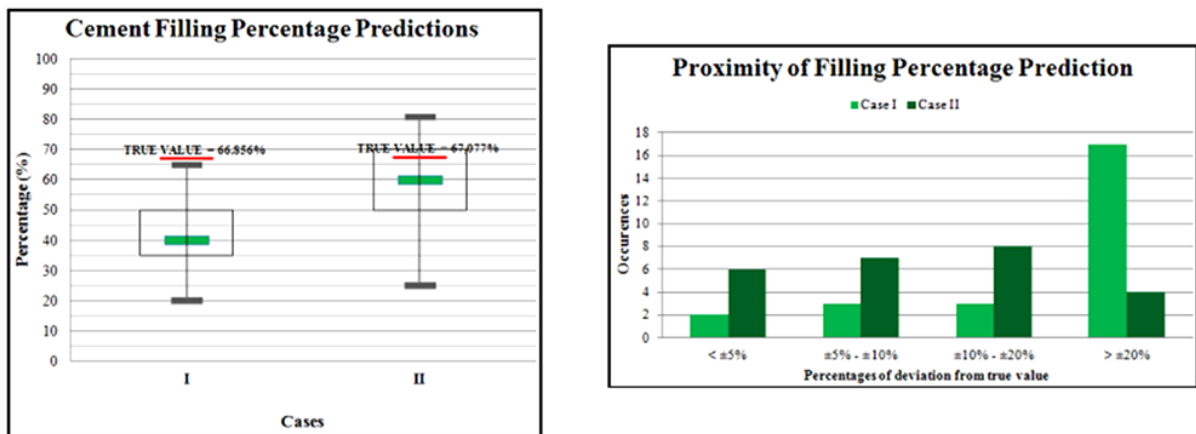


Figure 6.8: Boxplot of the predicted values of the cement filling percentage for two demos and histogram for the proximity of the predictions to the true value.

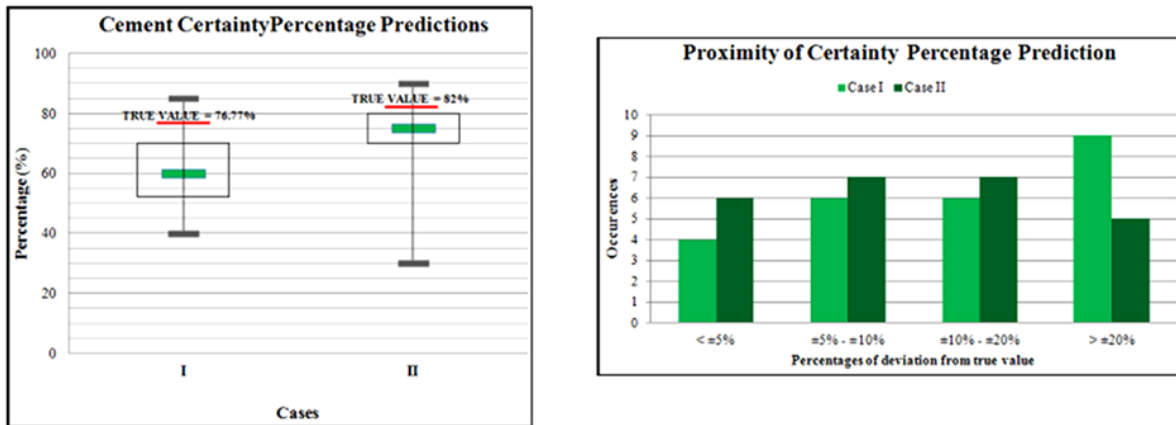


Figure 6.9: Boxplot of the predicted values of the cement uncertainty percentage for two demos and histogram for the proximity of the predictions to the true value.

The predictions for the first demo are worse than for the second demo, both for the filling and the uncertainty. This is more probably, due to the “training” that the first demo provided. Beforehand, we were aware of this, but we preferred not to change the order of the demonstrations, to keep the same conditions, for all the group interviews. Additionally, the graphs show that it was easier to determine the percentage of the certain space than the percentage of the filled space. A probable reason for that is that the uncertain space has an easier shape (a stripe behind and one in front of the prosthesis) than filled space, which has the intricate geometry of the fibrotic interface tissue. Knowing that human vision and perception for determining volumes is limited, we expected these bad results. Therefore, the statistics tool for the filling and the uncertainty, included in the cement filling uncertainty visualization stage of HipRFX, is a useful feature.

For the second task, the majority of participants (72%, 18 people) expressed their preference for the 3D visualization. The 2D visualization was mostly preferred by males (5/7), but their performance was equal, regardless their preferences. Also, male participants performed, in general, better than women (5% closer to true values). However, the two women that preferred the 2D visualization demonstrated better results than the ones preferring the volume representation.

For the third task, the ability to identify the data and the uncertainty was critical, in order to make sure that none of the two is overshadowed by the other. The visual overload could interfere with the user’s perception and the correct use of brightness/contrast would improve visibility and enhance insight [Newman 2004]. We present the ratings for these four characteristics, in Figure A.8 (Appendix A). All the characteristics and the overall visualization presented high mean scores. So, both the data and the uncertainty are conveyed, without obstructing each other, while the contrast is also helping towards this direction. The only characteristic with a lower score is the visual overload. However, the interviewees had no previous experience with concepts like uncertainty visualization, nor were familiar with the operational procedure and anatomy. Hence, some structures could interfere with their comprehension. Overall, our visualization tool can display uncertain data, without overshadowing the main filling data in an insightful and suitable manner.

6.4 Domain Expert Review

During domain expert reviews, we can request the opinion of people directly involved in using a tool, for immediate feedback, regarding the fulfillment of their needs and requirements [Lam 2011, Plaisant 2004]. We can document useful features and detect missing traits or limitations, to improve our implementation [Lam 2011]. At the same time, we can see how it works in its natural environment, in realistic settings [Plaisant 2004].

We performed our case study review with Prof. Dr. Rob G.H.H. Nelissen, the surgeon that performs minimally invasive refixation procedures at the Leiden University Medical Center. As the case, we simulated the visual environment of a minimally invasive refixation procedure, in all its phases. Our main goal was to verify if our tool has achieved its design requirements by answering the question: “Does the HipRFX system provide a better surgical environment for minimally invasive refixation procedure? What are its useful aspects? Which are its limitations?”

We split the system into simpler tasks, which we demonstrated to the surgeon. This was done, due to time restrictions and the surgeon’s lack of previous experience with our tool. During the demonstration, we presented

each task with a short subjective introduction about how it works. After that, he observed or interacted with HipRFX and evaluated our system. At the end, we provided the surgeon with the same Likert scale as in the qualitative evaluation of the cement filling uncertainty visualization, to evaluate its four important characteristics (data and uncertainty identification, visual overload and brightness/contrast). In the following subsections, we present the remarks of the surgeon, on every task. We also refer to figures from previous chapters for each one of them.

6.4.1 Review on Pre-Operative Planning

According to Prof. Nelissen, the workflow of this step is intuitive and includes useful tools that can assist surgeons in planning. Learning to work with all these tools might it take time, but they add value to the standard procedure. Additionally, as the doctor stated, some features can be used in other operational procedures, which makes it easier for our system to expand its use in other practices.

- Use of three renderers, with linked slice viewers and multiple slices (Figure 4.3): The concept of having three windows in our interface to provide a better view point was a sensible choice. The surgeon also confirmed that the slice viewer, in the main renderer, is intuitive. The manipulation of the slice viewer (zooming, panning, window/level and slicing) and the ability to see the additional sagittal and coronal slices were verified to be useful. The linkage between the three windows was indicated to be practical.
- Needle insertion and manipulation (Figure 4.5): The needle insertion is performed intuitively, while its manipulation (manual and fine-grained) is helpful and easy. It is good that we enable the user to see the target and the end points for the needle placement, especially in the case where they lie on different slices or planes. Also, the feature for warnings (for vessels or nerves in the area) adds value to the procedure. Additionally, Dr. Nelissen suggested enabling the insertion of more objects, such as pegs or screws.
- Cement insertion (Figure 4.5): The cement insertion is performed satisfactorily. It is useful that we can simulate realistically cement in the radiographs, but the surgeon proposed including a warning for the user that this does not consist an exact representation of the structure.
- Multi-tissue visualization and manipulation (Figure 4.4): The ability to visualize all the different structures of the region of interest is practical for the clinicians. Prof. Nelissen would use it often, especially because during the operation, these structures are covered with blood and it is difficult to discern them. He indicated that this is useful also in revision surgery, for removing the old fibrotic tissue and the old cement.
- Measurement tools (Figure 4.6): The doctor confirmed that this is a handy feature for orthopedic applications in general, but it is not fully applicable in minimally invasive re-fixation.

6.4.2 Review on Digitally Reconstructed Radiograph Simulation

According to the doctor, digital reconstructed radiographs manage to simulate in a realistic way the view on the fluoroscope. Additionally, it is important that this is done interactively and in real-time.

- Simulation of fluoroscopic images (Figure 4.7): The resulting fluoroscopic images are realistically simulated. The needles and the injected cement are easily detected, due to their realistic appearance. According to the surgeon, our guidance approach can be pragmatic. For an expert surgeon, it is feasible not to use any additional hardware for matching the views (registration), since accuracy, in terms of mms, is not required.
- Enhancement of fluoroscopic images with overlays (Figure 4.9): Dr. Nelissen estimated that it looks pleasant and provides visual feedback concerning the structures in the area. Still, in reality, this feature would be seldom used. The main reason for that is that the surgeons are not used to see colors, overlaid on grey-scale fluoroscopic images. It could be used, though, in a low contrast case.
- C-arm manipulation: The reciprocal manipulation of the C-arm is a valuable trait for the surgeon. It enables to see, in real-time, the changes on the simulated image, when changing the position of the fluoroscope, or vice versa. Moreover, it can give a rough guideline about the fluoroscope position, so that the surgeon does not spend much time on achieving it, only on optimizing it, if needed.

6.4.3 Review on Intra-Operative Guidance

The feedback that the surgeon provided for this step is valuable for the improvement of the system. He estimates that some parts are intricate, but the system could be used, even in its current form.

- Guidance with the form of steps (Figure 4.11): The surgeon believes that the acquisition of the in-between radiographic steps is not totally necessary. For him, it is better to acquire the final simulated fluoroscopic image and also images from the pre-operative plan. This step of the surgical procedure is subjective and

relates to the experience and practice of each surgeon. So, it is good that we allow the user to capture screenshots, both from the radiograph simulation and the planning.

- Linking back to DRR and fluoroscopic settings: The concept of this feature adds value to the intra-operative guidance step. The surgeon opted, though, for avoiding clicking on the acquired images to see the position of the fluoroscope, due to sterility reasons. It would be better to show the fluoroscope position in one of the lower corners of the respective step image.
- Difference image to show details (Figure 4.12): Prof. Nelissen expressed the opinion that surgeons are experienced in detecting changes on the fluoroscopic images, but they might still need this tool for showing small, inconceivable differences. He showed a preference for the overlay approach.

6.4.4 Review on Cement Filling Uncertainty Visualization

The surgeon found our work on cement filling uncertainty visualization helpful. Also, it was important that it was time-efficient, with a computation time of around one minute.

- Colormap choice (Figures 4.14 and 4.16): The surgeon himself is not color-blind. However, he found our choice, on the use of colors for this visualization, sensible and insightful.
- Filling vs. Uncertainty Visualization (Figure 4.16): In contrast to the non-clinical experts that reviewed our visualization tool, the surgeon found it easy to understand our concept. His feedback was to combine two or more fluoroscopic views, to reduce the uncertain areas in the cement visualization. His grading for the four characteristics of the visualization showed that the filling and the uncertainty information are conveyed in an insightful way, without overshadowing each other. Also, the calculation time (1 min) was not discouraging.
- Filling Pie and Uncertainty Distribution (Figure 4.16): According to Dr. Nelissen, the filling pie plot is helpful and intuitive. The uncertainty distribution histogram was considered confusing, though. He would prefer a second pie plot, instead.
- Three-dimensional volume to enhance slice-based two-dimensional representation (Figure 4.16): According to the surgeon, both views are important. In a real situation, he believes that both of them would be useful and that he would combine them to have a full aspect of the visualized filling and uncertainty information. Also, the synchronization of the three slice-viewers made the visualization less tiring for the doctor.

6.4.5 Overall Review on HipRFX

The surgeon agreed that a better system than the current approach is needed. For him, intra-operative CT scanning should be avoided, if at all possible, both due to the radiation exposure and due to costs. He believes that HipRFX can actually work in practice, since it has all the necessary components. There are no major limitations that would hinder the adoption of the HipRFX system. He estimates that, with small adjustments or enhancements, it would perform well in the procedure. For the doctor, it is important that the system is time-efficient. It is also necessary to minimize interaction with the program, intra-operatively, due to sterility issues.

6.5 Cadaver Study Evaluation

Our previously described evaluations showed that our system can, theoretically, work satisfactorily in the operation room. In order to check if HipRFX can also work in practice, we performed an in situ experiment, on 5 cadaveric leg subjects. Our cadaver experiment workflow is depicted in Figure 6.10, below.

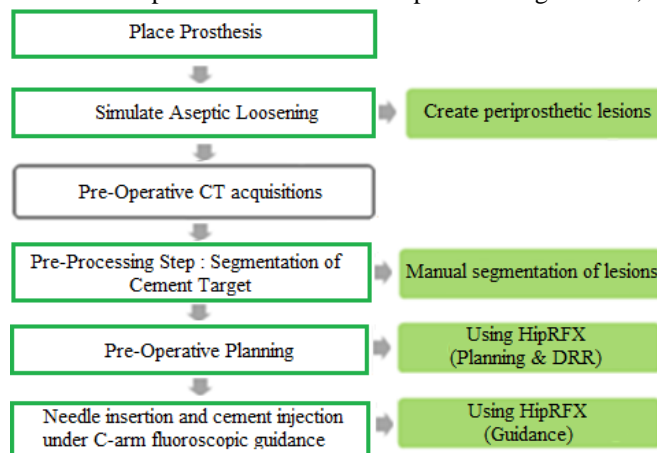


Figure 6.10: Graph depicting the workflow for the cadaver experiment.

In our experiment, we used 5 exarticulated cadaver leg segments. These segments included the whole femoral region, from the superior to the inferior epiphysis. Two surgeons, Dr H.J.L. van der Heide and Dr Marc Nieuwenhuijse, placed a polished Stryker Exeter™ stem to each one of them, without removing the soft tissues around the bone. The prosthesis had to be made removable for two reasons: firstly, to facilitate the subsequent simulation of aseptic loosening and, secondly, because we had access to two implants, only. Our two implants were sized 3 and 4 (with an offset of 44 mms). This phase can be seen in Figure 6.13 (A).

The next step of our experiment was to simulate aseptic loosening. For that, we had to create periprosthetic lesions to the cadaver legs. We sawed the femoral bones in half, below the lesser trochanter, and we drilled holes, up to 5 cm deep, on each side of the sawing, using a dremel tool. For each subject, a pre-operative CT scan was performed. In Figure 6.11, we show a CT scan (in a 3-orthogonal slice viewer), where the cut and the periprosthetic lesions are visible. This phase of the experiment can be also seen in Figure 6.13 (B).

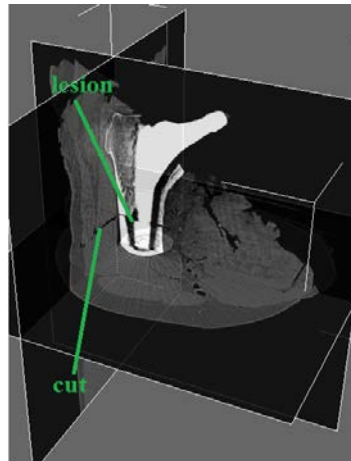


Figure 6.11: CT scan showing aseptic loosening simulation by creating periprosthetic lesions to the cadaver legs.

After that, we performed a manual segmentation of the periprosthetic lesions, representing the target areas that we intended to fill with cement. For that, we used MITK⁹, a “free open-source software system for the development of interactive medical image processing”. In order to minimize the subjectivity of the manual segmentations, as much as possible, they were performed by two users. An example of this segmentation is visible in Figure 6.12, below, shown as the green cement target.

Then, HipRFX was employed to perform the pre-operative plan. The needles were virtually inserted in the periprosthetic space and the cement was virtually injected. Also, we simulated and captured radiographs, for the intra-operative guidance. For every inserted needle or for the cement injection, we generated screenshots from different fluoroscopic acquisition angles. In Figure 6.12, we present an example of pre-operative planning for one of the cadaver legs.

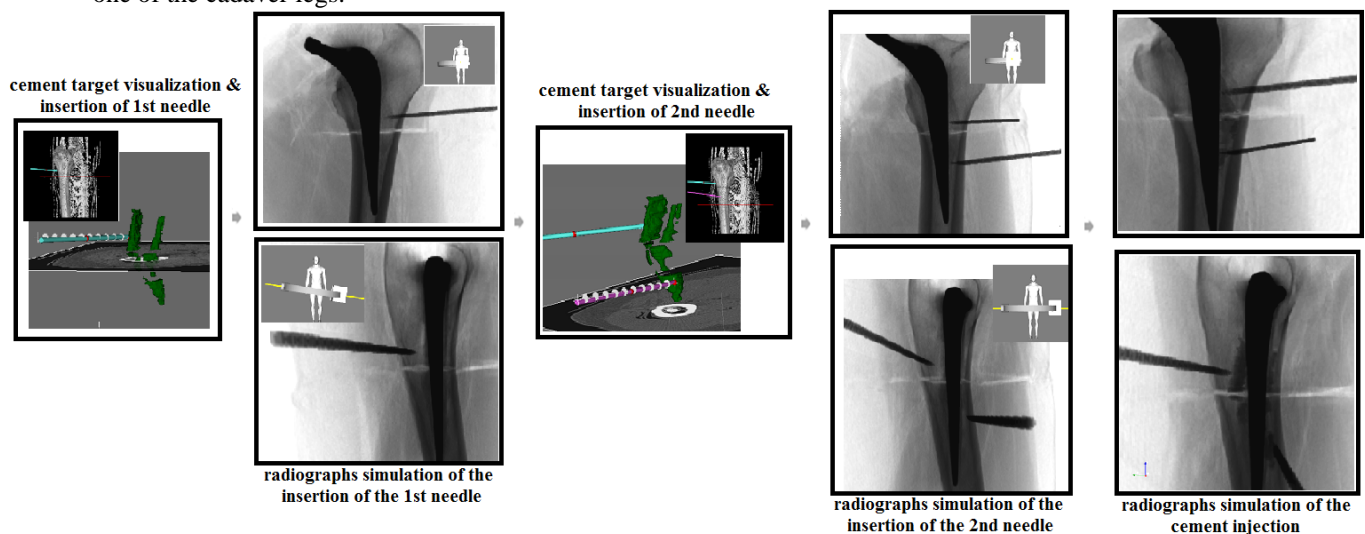


Figure 6.12: Pre-operative plan generation for one of the cadaver legs.

⁹ <http://www.mitk.org/>

Intra-operatively, the surgeon used the previously mentioned plan to execute the operation. For that, we used a tablet, where we had stored all the high-resolution simulated radiographs and screenshots from the planning. The surgeon consulted them, in order to determine the positioning of the fluoroscope, together with the radiographer and, subsequently, to insert the needles. The needles were inserted with the use of a hammer, but if the cortex was too thick, a needle with a drill was used first. In four cases, two needles were inserted, while in the other case, only one needle was required. After that, the PMMA cement was prepared and injected into the periprosthetic lesions, under high pressure. The cement flow was monitored by the fluoroscope, in real-time. The injection continued, until the periprosthetic space was filled or until the cement threatened to leak out, in the soft tissue. At the end, the surgeon consulted the screenshots with the simulated cement, in order to determine whether everything went as planned. In order to focus on the HipRFX workflow evaluation only, we decided not to perform cement filling uncertainty calculation and visualization, for the time being. This part will be included in a paper that will be written, as a continuation of this project. Figure 6.13, below, depicts the different stages of our experiment. The needles (VerteShark Access Biomet® needles, 11Gx15cm), the cement (Biomet® Bone Cement V) and the cementing systems (Optivac® Procedure Set) were all provided by Biomet®. The C-arm was a BV Pulsara model, by Philips.



Figure 6.13: Cadaver Experiment setting and different stages. (A) – Prosthesis placement. (B) – Creation of periprosthetic lesions for simulating aseptic loosening. (C) – Needle insertion with the aid of the pre-operative plan generated by HipRFX, (D) – Cement injection monitored by fluoroscopy. The cadaver legs have been hidden, due to ethical implications. (Photos reproduced with permission from the LUMC Anatomy Department)

This experiment showed that the surgeons can benefit from using HipRFX in the workflow of minimally invasive refixation procedures. First of all, the procedure was faster than with the existing technique. According to Prof. Nelissen, the needle insertion and cement injection takes usually one hour. The duration of the procedures for our five subjects was between 39 minutes, for the first, and 15 minutes, for the last. Since this experiment was conducted on cadavers, there were no safety issues for the subjects and, therefore, some things could have been performed faster. We tried, though, to keep the experiment settings, as realistic as possible. So, the time reduction from the first to the last subject (and also compared to the duration of the currently used technique) is interesting. In Appendix A, Figure A.9 shows a graph of this time reduction.

Moreover, the cadaver experiment proved that our approach, where CT is used only pre-operatively and avoided intra-operatively, can work in practice. The pre-operative CT scan allows the surgeon to position needles with greater certainty, than in the case of only fluoroscopy-based cement injection. At the same time, by avoiding intra-operative CT, the radiation exposure is minimized. Yet, the simulated radiographs, enhanced with the annotated information on the fluoroscope positioning, provide enough information, intra-operatively. The fluoroscopic settings information enable the surgeon to position the c-arm adequately. Also, the needles are

simulated realistically enough to be positioned accurately, in an easy and fast manner. The virtual cement injection is sufficient for confirming, whether the final image on the fluoroscopic monitor looks as it should.

We have not calculated the exact filling percentage that the surgeon achieved, because as we already mentioned this experiment focused mainly in answering whether HipRFX can be used in practice. However, according to the surgeon, the outcome of all five cases was successful and the periprosthetic lesions were filled adequately. Future work will focus on calculating the exact filling percentage and also on performing a cement filling uncertainty visualization, to verify how it performs, with real cement filling cases.

6.6 Limitations

The previously described evaluations confirm that our system is promising. However, they exposed also some limitations.

- We were not able to include more than one user in our evaluation, because we wanted to perform our domain expert study only with doctors, who are actually performing this surgical procedure. We are aware that this could entail limitations or bias, but at this stage of investigation we consider one evaluator to be enough.
- The pre-processing segmentation procedure is not flawless. There are errors in the exact representation of structures. We could, therefore, examine how our system will deal with these errors, but we are not researching improvements to the segmentation workflow, in the present work.
- The interaction with the system should be minimized, during the operation, for sterility reasons.
- In the cement filling uncertainty visualization, the uncertain areas of the periprosthetic space are large. We have used only one radiograph for the calculation of the uncertainty, showing parts hidden by the prosthesis. To address that, more simulated fluoroscopic images with different acquisition angles can be used.
- There are more types of uncertainty, present in all steps of the visualization pipeline. However, at the moment, we address only uncertainty, due to non-specificity.
- Clinical familiarity with the existing technique might be limiting for the adoption of our method.

6.7 Summary

The previous evaluations and case studies gave us valuable information on the strong points of our implementation. Also, they provided suggestions about parts of our system that have potential for further improvement. We summarize here, the feedback from the conducted evaluations.

- The colormap determination survey allowed us to decide on the suitable colormap for our cement filling uncertainty visualization. It also gave us insight on the importance of the proper use of colors.
- The color-deficiency assessment, using VisCheck, ensured that the implemented visualization is suitable also for color-blind users.
- The Graphics User Interface allowed us to be confident about the usability of our system. It should be mentioned that this evaluation had some coinciding points with the domain expert review, even if this target group was not familiar with the surgical procedure.
- The quantitative evaluation of the cement filling uncertainty visualization showed that our tool is satisfactory. The cement filling, calculated by HipRFX from back-projection, matched the ground truth for 18 simulated cases, for filling percentages higher than 50%.
- The qualitative evaluation of the cement filling uncertainty visualization provided with evidence that the employed visualization manages to display uncertain data without overshadowing the main filling data, in an insightful and suitable manner.
- The domain expert review offered valuable feedback, directly from an eventual user of HipRFX, concerning its usefulness, its limitations and potential for improvement. Prof. Nelissen confirmed that minimally invasive refixation could benefit from our system. On his opinion, HipRFX can work in practice, since it has all the necessary components and is time-efficient.
- The cadaver experiments proved that our approach can work, in practice, supplanting intra-operative CT, since the surgeon can acquire all the required information from the pre-operative CT scans of the patient. Needles and cement can be inserted sufficiently with the use of digitally reconstructed radiographs that simulate in a realistic way intra-operative fluoroscopy. Shorter intra-operative times were also documented. The surgeon confirmed that the procedure was successful, but future work is needed to measure the exact filling percentage of cement filling that was achieved.

Chapter 7

Conclusions and Future Work

In this final chapter, we reflect on the results of our work and draw some conclusions. We provide also an overview of our contributions and, finally, some ideas for future work.

7.1 Conclusions

HipRFX was implemented to provide a more efficient and effective workflow for minimally invasive refixation. It was designed to avoid intra-operative computed tomography and to follow a fluoroscopic-based procedure. With HipRFX, the patient is scanned once, before the operation. This CT acquisition is used to build the pre-operative plan for the simulation of radiographs that will be employed in intra-operative guidance. As post-operative assessment, we proposed cement filling uncertainty visualization.

Our system was evaluated, using the nested model proposed by Munzner [2009], as we described in the introduction of the Results chapter and showed in Figure 6.1. This was used for addressing all the important questions that emerged, after our implementation, based on the threats for every level. The main points, from the inner to the outer level, are:

- In the algorithm design level, the threat for our method would be to be slow. The surgeon confirmed that our system is fast and interactive enough. It offers real-time visual feedback in all stages, while the cement filling uncertainty visualization duration is small. This was also proved during our quantitative evaluation and the cadaver experiments.
- In the visual encoding and interaction domain, the risk would be to show information in the wrong way. We proved that the design and visualization choices of our system are suitable. This was verified by the surgeon who agreed that our system offers good insight to the data. Also, it was experienced, during the cadaver study. The qualitative cement filling uncertainty and the user interface evaluation, as well as the colormap-related evaluations, were also performed for this purpose. They ensured the suitability of our choices, as well.
- In the data abstraction level, the problem would be to show the wrong information. According to the clinical expert, our system contains all the necessary steps to assist minimally invasive refixation procedures and to offer new insight to the cement filling visualization. The results of the evaluation on the simulated cases, but also the cadaver experiment results, validate the opinion of the doctor. Additionally, we ensured that our approach can supplant intra-operative CT, since the surgeon can acquire all the required information from the pre-operative scans. So, our method can work in practice.
- In the domain level, the danger would be to address the wrong problem. Based on the surgeon's opinion and the cadaver experiments, we are able to confirm that the surgeons would appreciate a better system. In this case, HipRFX would allow them a more efficient and effective workflow, while avoiding intra-operative computed tomography scans. With our system, the surgeon can, indeed, acquire all the required information from the pre-operative CT scans of the patient. Also, needles and cement can be inserted sufficiently with the use of digitally reconstructed radiographs that simulate in a realistic way intra-operative fluoroscopy.

To sum up, with the implementation of our HipRFX system, we managed to contribute from three different aspects:

- We introduced a novel integrated system for planning and guiding minimally invasive refixation. It was the first time that a technical approach for the improvement of the workflow of this procedure is presented in literature. This new workflow proved to be better than only fluoroscopic based procedures, while it does not require additional intra-operative CT scanning, or new hardware.
- We introduced cement filling uncertainty visualization, as a means of post-operative assessment, based on preoperative information. It allows the surgeon to see the achieved cement filling of the periprosthetic space, enhanced with information about the uncertain areas. To our knowledge, this is a novel domain.
- Our evaluations covered several aspects of our HipRFX system. They showed that it is adequate in creating a plan that can be subsequently executed in realistically simulated clinical settings. In future, our approach may also be adapted for clinical use on patients undergoing minimally invasive hip prosthesis revision.

7.2 Future Work

The performed evaluations and experiments offered a full aspect of the limitations and the eventual improvements of our HipRFX. Following that direction, we can foresee future work that would add value to our implemented system. It is true that up to now, none of the existing CAOS methods has managed to become a state-of-the-art in the broad medical community. The main reason for that is that they did not manage to prove long-term results [Langlotz 2004] and they could not dissolve the concerns about computer malfunctions, personnel training, need of extra time and cost [Callaghan 2006]. Therefore, it would be interesting to see the long-term results from the performance of HipRFX, once it is refined and ready for clinical use.

As we already mentioned, our first concern will be to continue the cadaver experiment. In this second phase we will calculate the exact filling percentage that the surgeon achieved. We will perform, based on that, a cement filling uncertainty visualization, to verify how it behaves, also in real cement filling cases.

Future work includes also creating a better and more detailed hip model for the pre-operative planning. At the moment, the planning procedure of HipRFX relies mostly on the manual segmentation, performed during the pre-processing stage. Errors on that stage will induce errors in our system. Apart from accuracy in the segmentation, we should also aim at segmenting more structures, for providing a more detailed plan.

We should also enhance our uncertainty visualization in two ways: Firstly, the uncertainty should be calculated using more than one simulated fluoroscopic images, with different acquisition angles, to diminish the uncertain areas. Secondly, it would be interesting to enhance our visualization, with more sources of uncertainty, such as errors, imprecision or variations that are introduced in all the steps of the visualization pipeline.

Based on the feedback that we received from our clinical expert, our system can be applicable also in other clinical approaches. Therefore, we could generalize our system to make it usable also in other surgical procedures. However, this would require a refinement of the requirements and the goals of the system.

A simplified web version of the HipRFX system could enable the surgeons to view their already performed plan or the cement filling uncertainty, for post-operative assessment, from any computer with internet access, within the hospital. It would also be important to make our system feasible, without the installment of additional software, or the need of a specialized workstation.

At the moment, the matching of the viewport of the simulated images to the fluoroscope placement is performed roughly, by the eye. According to the surgeon, this is enough for an experienced user, who can position the fluoroscope approximately and, then, optimize it. However, HipRFX should provide more information, on the alignment procedure.

Finally, the educational value of our system includes surgical training. In this way, both surgeons and students can practice surgical procedures in a virtual environment, to be prepared for different anatomical or surgical simulated cases.

Bibliography

- Abu 2007** Aseptic loosening of total joint replacements: mechanisms underlying osteolysis and potential therapies. Abu-Amer, Y., Darwech, I., Clohisy, J.C. *Arthritis Res Ther.* 2007; 9(Suppl 1): S6.
- Aliotti 2004** Numerical Vision for the Medical Planning in Orthopaedic Surgery. Aliotti, A., Laget, B., Favier, E. *IEEE International Conference on Industrial Technology (ICIT)*, 2004.
- Alterovitz 2009** Sensorless motion planning for medical needle insertion in deformable tissues. Alterovitz R., Goldberg K.Y., Pouliot J., Hsu L.C. *Trans. Info. Tech. Biomed.* 13 (January 2009), 217-225.
- Babaola 2008** Comparison and Evaluation of Segmentation Techniques for Subcortical Structures in Brain MRI. Babaola, K.O., Patenaude, B., Aljabar, P., Schnabel, J., Kennedy, D., Crum, W., Smith, S., Cootes, T.F., Jenkinson, M., Rueckert, D. *11th International Conference on Medical Image Computing and Computer Assisted Intervention (MICCAI)*, New York City, September 2008.
- Bergman 2000** A rule-Based tool for assisting colormap selections. Bergman, L.D., Rogowitz, B.E., Treinish, L.A. *Proc. IEEE Symp. Information Visualization.* pp.85-89. 2000
- Bevan 2001** International Standards for HCI and Usability. Bevan N. *International Journal of Human Computer Studies*, 55(4), 533-552. 2001
- Borland 2007** Rainbow Colormap (Still) Considered Harmful. Borland D., Taylor R.M. *IEEE Comput Graph IEEE Computer Society, Los Alamitos, CA, USA* 27:14-17, 2007
- Botchen 2006** Interactive Visualization of Uncertainty in Flow-Fields using Texture-Based Techniques. Botchen, R.P., Weiskopf D., Ertl T. *12th International Symposium of Flow Visualization* 2006, Göttingen, Germany
- Botha 2008** Hybrid scheduling in the DeVIDE dataflow visualisation environment. Botha, C.P., Post, F.H. *Proceedings of Simulation and Visualization (H. Hauser, S. Strassburger, and H. Theisel, eds.)*, pp. 309--322, SCS Publishing House Erlangen, February 2008.
- Braak 2010** Real-Time 3D Fluoroscopy Guidance During Needle Interventions: Technique, Accuracy, and Feasibility. Braak, S. J., van Strijen, M.J.L., van Leersum, M., van Es, H.W., van Heeswijk, J.P.M. *American Roentgen Ray Society, AJR*:194, May 2010
- Brooke 1996** SUS: a "quick and dirty" usability scale. Brooke, J. . In P. W. Jordan, B. Thomas, B. A. Weerdmeester, & A. L. McClelland. *Usability Evaluation in Industry*. London: Taylor and Francis. 1996.
- Callaghan 2006** Computer-Assisted Surgery: A Wine Before its Time: In the Affirmative. Callaghan, J.J., Liu, S.S. and Warth, L.C. *The Journal of Arthroplasty*, 2006.
- Carl 1997** In vitro simulation: early results of stereotaxy for pedicle screw placement. Carl, A., Khanuja, H.S., Sachs, B.L., Gatto, C.A., vom Lehn, J., Vosburgh, K., Schenck, J., Lorensen, W., Rohling, K., Disler, D. *Spine* 22 :1160–1164, 1997
- Carr 2010** Orthopaedic Surgery: Current Trends and Recent Innovations (chapter 70). Carr, A., Gwilym, S. [book auth.] H. Derbas, A.Darzi T.Athanasiou. *Key Topics in Surgical Research and Methodology*. s.l. : Springer, 2010.
- Cedilnik 2000** Procedural Annotation of Uncertain Information. Cedilnik A., Rheingans P. *Proceedings of IEEE Visualization.* (2000), 77-83.
- Cimerman 2007** Preoperative planning in pelvic and acetabular surgery: The value of advanced computerised planning modules. Cimerman, M., Kristan, A. *Injury, Int. J. Care Injured* 38, 2007.
- Citak 2008** Virtual 3D planning of acetabular fracture reduction. Citak, M., Gardner, M.J., Kendoff, D., Tarte, S., Krettek, C., Nolte, L.P., Hüfner, T., *Journal of Orthopaedic Research*, 2008, Vols. Volume 26, Issue 4.
- Dahlen 2001** Computer-Assistierte OP-Planung: 3D Software für den PC. Dahlen, C., Zwipp H. *Unfallchirurg*© Springer-Verlag, 2001, Vol. 104
- Davis 1997** Modelling and visualizing multiple spatial uncertainties. Davis, T.J., Keller, C. P. *Computers & Geosciences*, 23(4):397{408, 1997.
- dePoorter 2008** Gene therapy and cement injection for restabilization of loosened hip prostheses. de Poorter, J. J., Hoeben, R. C., Hogendoorn, S., Mautner, V., Ellis, J., Obermann, W. R., et al. *Human gene therapy*, 19(1), 83-95. (2008).
- DiGioia 2000** Surgical Navigation for Total Hip Replacement with the use of HipNav. DiGioia, A., Jaramaz, B., Nikou, C., Labarca, R., Moody, J., Colgan, B. *Operative Techniques in Orthopaedics*, Vol 10, No 1 (January), 2000: pp 3-8, 2000

- Djurcilov 2001** Volume Rendering Data with Uncertainty Information. Djurcilov, S., Kim, K., Lermusiaux, P.F.J., Pang A. In: Ebert D, Favre JM, Peikert R, editors. Data visualization 2001
- Drapikowski 2008** Surface modeling—Uncertainty estimation and visualization. Drapikowski P. Computerized Medical Imaging and Graphics 32 (2008) 134–139
- Eggl 1998** The value of preoperative planning for total hip arthroplasty. Eggl, S., Pisan, M., Müller, M. E. The Journal of Bone and Joint Surgery, Vols. J Bone Joint Surg [Br] 1998;80-B:382-90.
- Ellis 2005** From Scans to Sutures: Computer-Assisted Orthopedic Surgery in the Twenty-First Century. Ellis, R.E. Shanghai, China : Proceedings of the 2005 IEEE Engineering in Medicine and Biology 27th Annual Conference, 2005.
- Elson 2010** The Principles and Role of Medical Imaging in Surgery. Elson, D., Yang., G.-Z.. [book auth.] H. Debas, A. Darzi T. Athanasiou. Key Topics in Surgical Research and Methodology. Springer-Verlag Heidelberg, 2010.
- Fichtinger 2005** Image overlay for CT-guided needle insertions. Fichtinger, G., DeGuet, A., Fischer, G., Iordachita, I., Balogh, E., Masamune, K., Taylor, R.H., Fayad, L.M., DeOliveira M., Zinreich, S.J. Computer Aided Surgery, July 2005; 10(4): 241–255, 2005
- Franco 2010** Preoperative planning of prosthetic replacement in hip fractures in the elderly. Franco-Ferrando, N., Malik, A., González-Della Valle, A., Salvati, E.A. Revista Española de Cirugía Ortopédica y Traumatología, 2010, Vols. Rev esp. cir. ortop. traumatol. 2010; 54(2):136-145.
- Glinkowski 2008** Computer Enhanced Orthopedics. Glinkowski, W. Information Technology in Biomedicine. Springer-Verlag Berlin Heidelberg, 2008
- Griethe 2005** Visualizing Uncertainty for Improved Decision Making. Griethe H., Schumann H. Proc. of the 4th International Conference on Business Informatics Research, 2005
- Grigoryan 2004** Point-Based Probabilistic Surfaces to Show Surface Certainty. Grigoryan G., Rheingans P. IEEE transactions on Visualization and Computer Graphics, Vol. 10, No.5, September/October 2004
- Handels 2000** Virtual planning of hip operations and individual adaption of endoprotheses in orthopaedic surgery. Handels, H., Ehrhardt, J., Plötz, W., Pöppel, S.J. International Journal of Medical Informatics 58–59 (2000) 21–28, 2000.
- Hemminger 1993** Isoluminance: a color technique for visualizing multivariate medical image data. Hemminger, B. Proc. SPIE 1897, Medical Imaging 1993: Image Capture, Formatting, and Display, 325 (June 30, 1993)
- Herghelegiu 2012** Biopsy Planner-Visual Analysis for Needle Pathway Planning in Deep Seated Brain Tumor Biopsy. Herghelegiu, P.C., Manta, V., Perin, R., Bruckner, S., Gröller, E. Eurographics Conference on Visualizations (EuroVis) 2012, Volume 31 (2012), Number 3.
- Hodgson 2008** Computer-Assisted Orthopedic Surgery (chapter12). Hodgson, A.. Image-guided interventions: technology and application. [book auth.] Kevin R. Cleary Terry M. Peters. Springer Science, 2008
- ISO9241-11/1998** ISO 9241-11:1998 Ergonomic requirements for office work with visual display terminals (VDTs) -- Part 11: Guidance on usability. International Organization for Standardization 1998.
- Jaramaz 2004** Imaging devices, computers, peripherals, interfaces (chapter 5.1). Jaramaz, B. [book auth.] Anthony M. DiGioiaIII, et al., et al. computer and Robotic Assisted Knee and Hip Surgery. Oxford University Press, 2004.
- Jaramaz 2004 (2)** Software infrastructure for computer-assisted orthopedic surgery (chapter 6). Jaramaz, B., Delp, S.L. [book auth.] Anthony M. DiGioiaIII, et al., et al. Computer and Robotic Assisted Knee and Hip Surgery. s.l. : Oxford University Press, 2004
- Jaramaz 2007** Navigation and MIS in Orthopedic Surgery. Jaramaz, B. and DiGioiaIII, A.M. CT-Based Navigation Systems. [book auth.] James B. Stiehl, et al., et al. Springer Medizin Verlag Heidelberg, 2007
- Joskowicz 2001** Computers in Imaging and Guided Surgery. Joskowicz, L., Taylor, R.H. September/October 2001.
- Kazanides 1998** An Integrated System for Cementless Hip Replacement. Kazanides, P., Mittelstadt, B.D., Musits, B.L., Bargar, W.L., Zuhars, J.F., Williamson, B., Cain, P.E., Carbone, E. IEEE Engineering in Medicine and Biology, 1998.
- Knight 1992** Preoperative Planning for Total Hip Arthroplasty: Quantitating Its utility and Precision. Knight, J.L., Atwater R.D. The Journal of Arthroplasty Vol. 7 Supplement, 1992.
- Kowal 2007** Basics of Computer-Assisted Orthopaedic Surgery (chapter 1). Kowal, J., Langlotz, F., Nolte, L.P. [book auth.] James B. Stiehl, et al., et al. Navigation and MIS in Orthopedic Surgery. s.l. : Springer Medizin Verlag Heidelberg, 2007.

- Krekel 2006** Interactive simulation and comparative visualization of the bone-determined range of motion of the human shoulder. Krekel, P., Botha, C., Valstar, E.R., de Bruin, P.W., Rozing, P.M., Post, F.H. 2006.
- Lam 2011** Seven Guiding Scenarios for Information Visualization Evaluation. Lam, H., Bertini, E., Isenberg, P., Plaisant, C., Carpendale, S. Techreport 2011-992-04, Department of Computer Science, University of Calgary, January 2011.
- Langlotz 2002** State-of-the-art in orthopaedic surgical navigation with a focus on medical image modalities. Langlotz, F. The Journal of Visualization and Computer Animation. Vols. J. Visual. Comput. Animat. 2002; 13: 77–83.
- Langlotz 2004** Technical Approaches to Computer-Assisted Orthopedic Surgery. Langlotz, F., Nolte, L.-P. European Journal of Trauma, 2004
- Laramee 2011** How to write a Visualization Research Paper: A Starting Point. Laramee, R. Computer Graphics Forum, vol. 29, no. 8, pp. 2363-2371, Dec. 2010.
- Leschka 2011** C-arm cone beam computed tomography needle path overlay for image-guided procedures of the spine and pelvis. Leschka, S.C., Babic, D., Shikh, S., Wossmann, C., Schumacher, M., Taschner, C.A. Neuroradiology- Springer, 2011.
- Levkowitz 1992** The design and evaluation of color scales for image data. Levkowitz H., Herman, G.T. IEEE Computer Graphics and Applications. Vol.12, No.1, pp.72-80, January 1992
- Lodha 1996** UFLOW: Visualizing Uncertainty in Fluid Flow. Lodha S., Pang A., Sheehan R. , Wittenbrink C.M. IEEE Visualization 1996 Conference Proceedings, 1996, pp. 249-254.
- Lundström 2007** Uncertainty Visualization in Medical Volume Rendering Using Probabilistic Animation. Lundström C., Ljung P., Persson A., Ynnerman A. IEEE Transactions on Visualization and Computer Graphics, Vol.13, No.6, November/December 2007
- Ma 2010** Novel 3D Reconstruction Modeling Contributes to Development of Orthopaedic Surgical Interventions. Ma, X., Wu, X., Liu, J., Wu, Y., Sun, L. IEEE, 2010.
- MacEachren2005** Visualizing Geospatial Information Uncertainty: What We Know and What We Need to Know. MacEachren A.M., Robinson A., Hopper S., Gardner S., Murray R., Gahegan M., Hetzler E. Cartography and Geographic Information Science, Vol. 32, No. 3, 2005, pp. 139-160
- Malan 2012** Voxel classification and graph cuts for automated segmentation of pathological periprosthetic hip anatomy. Malan, D.F., Botha, C.P., Valstar, E.R. Int J CARS, January 2012
- Moreland 2009** Diverging Colormaps for Scientific Visualization. Moreland, K. In Proceedings of the 5th International Symposium on Visual Computing. December 2009.
- Munzner 2008** Process and Pitfalls in Writing Information Visualization Research Papers. Munzner, T. Information Visualization, Human Centered Issues and Perspectives (A. Kerren et al. Eds) 134-153 (2008).
- Munzner 2009** A Nested Model for Visualization Design and Validation. Munzner, T. IEEE J VCG, 2009.
- Newman 2004** On Visualizing Uncertainty in Volumetric Data: Techniques and their Evaluation. Newman, T.S., Lee, W. Journal of Visual Languages and Computing 15 (2004) 463-491.
- Otten 2010** Trends in the number of knee and hip arthroplasties: considerably more knee and hip prostheses due to osteoarthritis in 2030. Otten, R., van Roermund, PM., Picavet, HS. Ned Tijdschr Geneesk. 2010; 154:A1534.
- Pang 1997** Approaches to Uncertainty Visualization. Pang, A.T., Wittenbrink, C.M., Lodha S.K. The Visual Computer, Vol.13, No.8 (1997), 370-390
- Picard 2004** Computer and Robotic Assisted Knee and Hip Surgery. Picard, F., et al., et al. History of computer assisted orthopaedic surgery of hip and knee (chapter1). [book auth.] Antony M. DiGioia, et al., et al.. Oxford University Press, 2004.
- Plaisant 2004** The Challenge of Information Visualization Evaluation. Plaisant, C. IEEE Proc. of AVI 2004.
- Prince 2006** Medical Imaging Signals and Systems. Prince J.L., Links J.M. ©2006 Pearson Education, Pearson Prentice Hall. (§5.3.4 Film Characteristics, pages 162-164)
- Racadio 2007** Live 3D Guidance in the Interventional Radiology Suite. Racadio, J.M., Babic, D., Homan, R., Ramptom, J.W., Patel, M.N., Racadio J.M., Johnson N.D. Interventional Radiology-American Roentgen Ray Society, 2007, Vols. AJR 2007; 189:W357–W364.
- Rheingans 1999** Task-Based Colormap Design. Rheingans, P. Proc. Applied Image and Pattern Recognition.pp.35-43. 1999
- Rhodes 2003** Uncertainty Visualization Methods in Isosurface Volume Rendering. Rhodes, P.J., Laramee, R.S., Bergeron D., Sparr T.M. *s.l.* : EUROGRAPHICS 2003
- Robb 1996** Computer-Aided Surgery Planning and Rehearsal at Mayo Clinic. Robb, R.A., Hanson, D.P., Camp, J.J. IEEE Xplore, 1996.

- Sariali 2009** Accuracy of reconstruction of the hip using computerised three-dimensional pre-operative planning and a cementless modular neck. Sariali, E., Mouttet, A., Pasquier, G., Durante, E., Catone, Y. *The Journal of Bone and Joint Surgery*, 2009.
- Schlenzka 2000** Computer-assisted spine surgery. Schlenzka, D., Laine, T., Lund, T. *Eur Spine J* (2000) 9 (Suppl 1) :S57–S64; Springer- Verlag, 2000.
- Simon 1998** Medical Imaging, Visualization and Registration in Computer-Assisted Surgery. Simon, D.A., Lavalle, S. *Clinical Orthopaedics & Related Research: September 1998 - Volume 354 - Issue - pp 17-27*, Symposium: Computer Assisted Orthopaedic Surgery: Medical Robotics and Image Guided Surgery
- Stiehl 2010** Computer-Assisted Orthopedic Surgery: Pros and Cons. Stiehl, J.B. *Minimally Invasive Surgery in Orthopedics*. Springer Science + Business Media, 2010.
- Suero 2010** Use of a virtual 3D software for planning of tibial plateau fracture reconstruction. Suero, E. M., Hüfner, T., Stübig, T., Krettek, C., Citak, M. *Injury, Int. J. Care Injured* 41 (2010) 589–591, 2010.
- Sugano 1998** Computed-Tomography-Based Computer Preoperative Planning for Total Hip Arthroplasty. Sugano, N., Ohzono, K., Nishii, T., Keiji H., Takashi S., Ochi, T. *Vols. Computer Aided Surgery* 3:320–324 (1998).
- Sugano 2003** Computer-assisted orthopedic surgery. Sugano, N. *J Orthop Sci* (2003) 8:442–448, 2003.
- Taylor 2001** Computer-Integrated Surgery and Medical Robotics. Taylor, R., Joskowicz, L. 2001
- Tory 2004** Human Factors in Visualization Research. Tory, M., Möller, T. *IEEE transactions on visualization and computer graphics*. Vol.10, No.1, January/February 2004.
- Trumbo 1981** Theory for Coloring Bivariate Statistical Maps. Trumbo, B.E. *The American Statistician*. vol35., no.4, pp.220-226, 1981
- Twiddy 1994** Restrorer: A visualization technique for handling missing data. Twiddy, R., Cavallo, J., Shiri, S.M., *IEEE Visualization '94*, pages 212{216, October 1994. ISBN 0-8186-6627-7.
- Vancamberg 2011** Needle path planning for digital breast tomosynthesis biopsy using a heterogeneous model. Vancamberg L., Sahbani A., Muller S., Morel G. *Imaging* (2011), 5749-5755.
- Wade 1998** Pre-operative planning in orthopaedics: a study of surgeons' opinions. Wade, R. H., Kevu, J., Doyle, J. *Injury* Vol. 29, No. 10, pp. 785-786, 1998
- Wilkinson 2011** Bisphosphonates in orthopedic applications. Wilkinson, J.M., Littlec, D.G. *Bone*, Volume 49, Issue 1, July 2011, Pages 95–102.
- Wittenbrink 1996** Glyphs for Visualizing Uncertainty in Vector Fields. Wittenbrink, C.M., Pang, A.T., Lodha, S.K. *IEEE Transactions on Visualization and ComputerGraphics*, Vol.2, No.3, September 1996.
- Woodruff 2009** Value-by-Alpha-maps: an alternative techniqe to the cartogram. Woodruff A., Roth R., Johnson Z. 2009 online
- Woolf 2003** Burden of major musculoskeletal conditions. Woolf, D.A., Pfleger, B. *Bulletin of the World Health Organization*, 2003.

Appendix A

In this Appendix, we provide some additional figures related to our work.

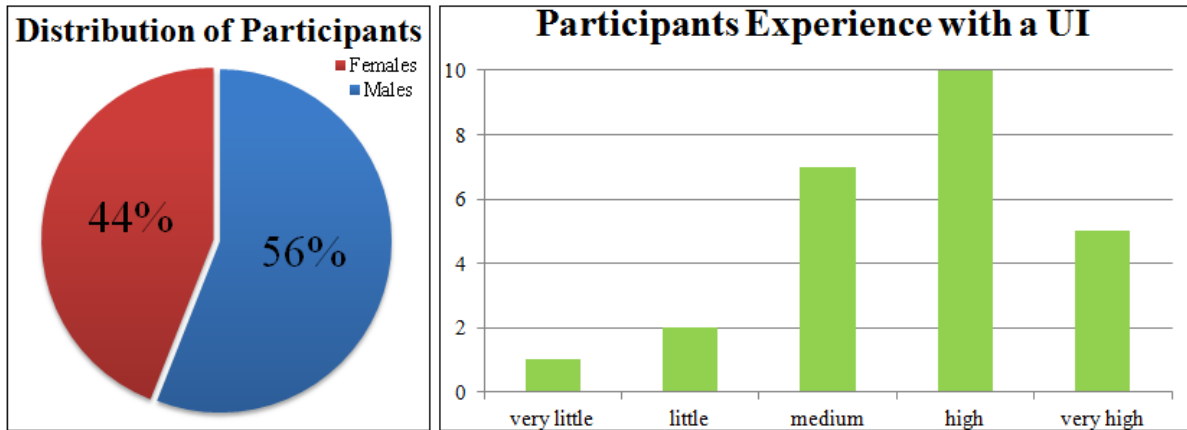


Figure A.1: Distribution of the participants based on sex and experience with user interfaces.

	Strongly disagree				Strongly agree
1. I think that I would like to use this system frequently	1	2	3	4	5
2. I found the system unnecessarily complex	1	2	3	4	5
3. I thought the system was easy to use	1	2	3	4	5
4. I think that I would need the support of a technical person to be able to use this system	1	2	3	4	5
5. I found the various functions in this system were well integrated	1	2	3	4	5
6. I thought there was too much inconsistency in this system	1	2	3	4	5
7. I would imagine that most people would learn to use this system very quickly	1	2	3	4	5
8. I found the system very cumbersome to use	1	2	3	4	5
9. I felt very confident using the system	1	2	3	4	5
10. I needed to learn a lot of things before I could get going with this system	1	2	3	4	5

Figure A.2: Adapted SUS-System Usability Score Scale (SUS: Digital Equipment Corporation ©, 1986)

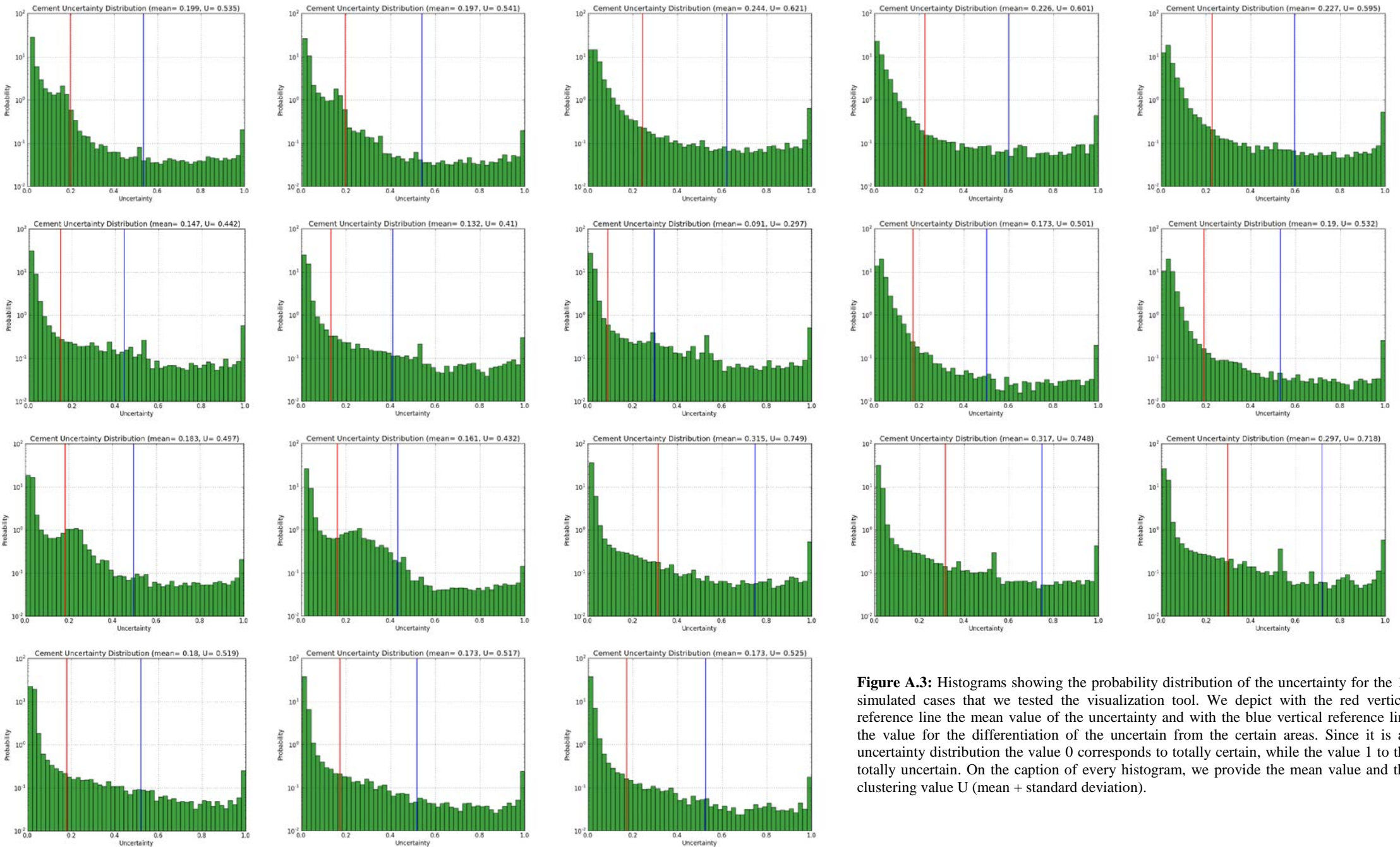


Figure A.3: Histograms showing the probability distribution of the uncertainty for the 18 simulated cases that we tested the visualization tool. We depict with the red vertical reference line the mean value of the uncertainty and with the blue vertical reference line the value for the differentiation of the uncertain from the certain areas. Since it is an uncertainty distribution the value 0 corresponds to totally certain, while the value 1 to the totally uncertain. On the caption of every histogram, we provide the mean value and the clustering value U (mean + standard deviation).

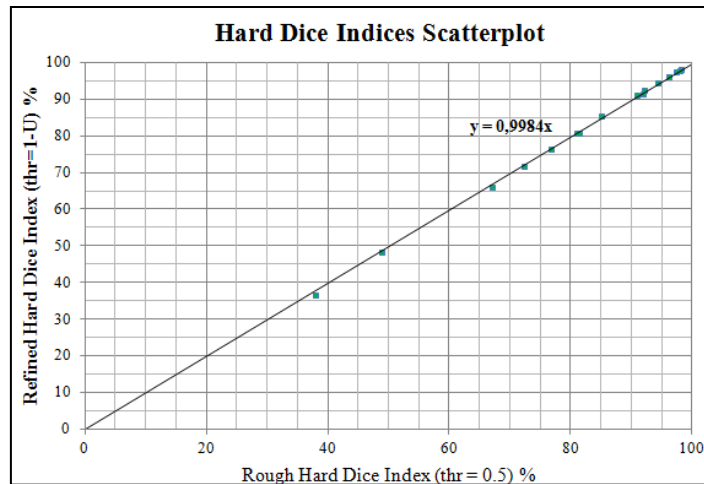


Figure A.4: Scatterplot showing the linear relationship between the two Hard Dice Indices given by the equation $y=0,9984x$

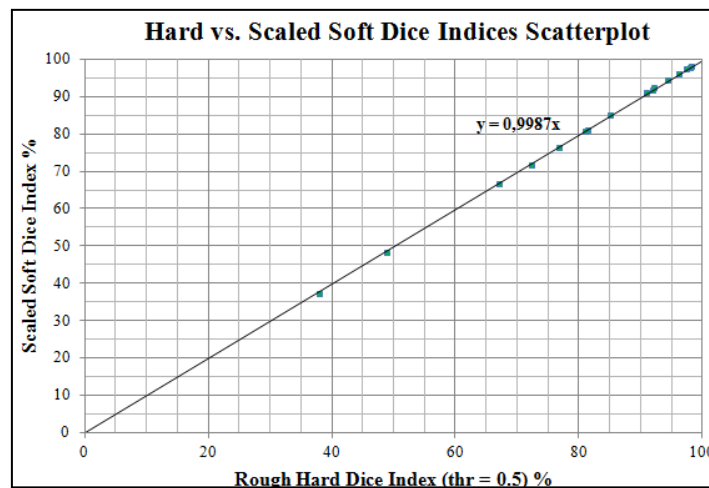


Figure A.5: Scatterplot showing the linear relationship between the Rough Hard Dice and the Soft Scaled Dice Index given by the equation $y=0,9987x$

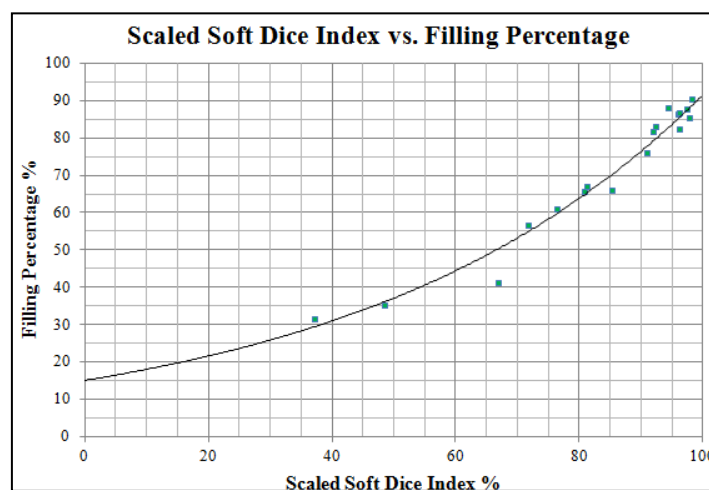


Figure A.6: Scatterplot showing the exponential relationship between the Scaled Soft Dice Index and the Cement filling percentage, as calculated from the system for each one of the simulations.

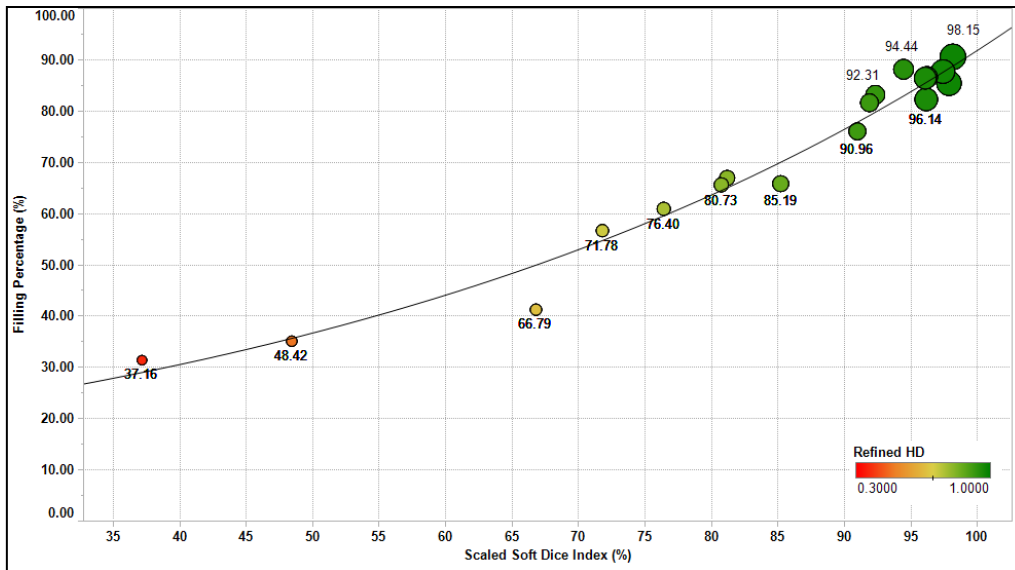


Figure A.7: Scatterplot showing the exponential relationship between the Scaled Soft Dice Index and the Cement filling, as well as with both Hard Dice Indices. The Refined Hard Index is mapped to the traffic-light color scale. The Rough Hard Index is mapped to the circles size.

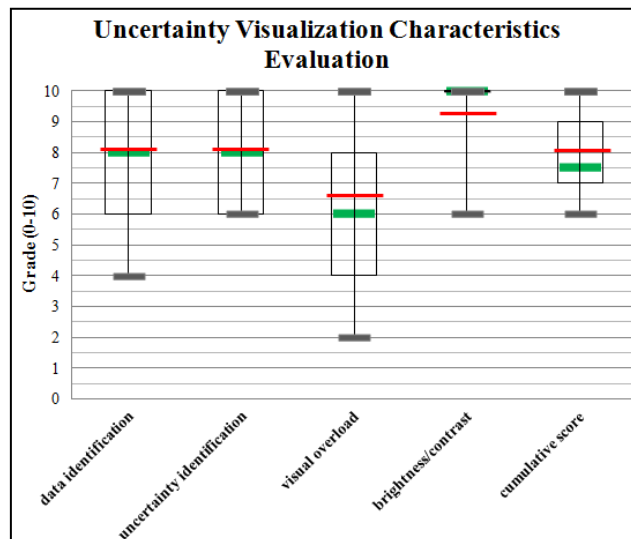


Figure A.8: Boxplots of the four characteristics scores and the cumulative (average of the four characteristics) score of the uncertainty visualization. We present with the red lines the mean value, with the green lines the median and with the grey lines the minimum/maximum values. The first and third quartiles are also visible.

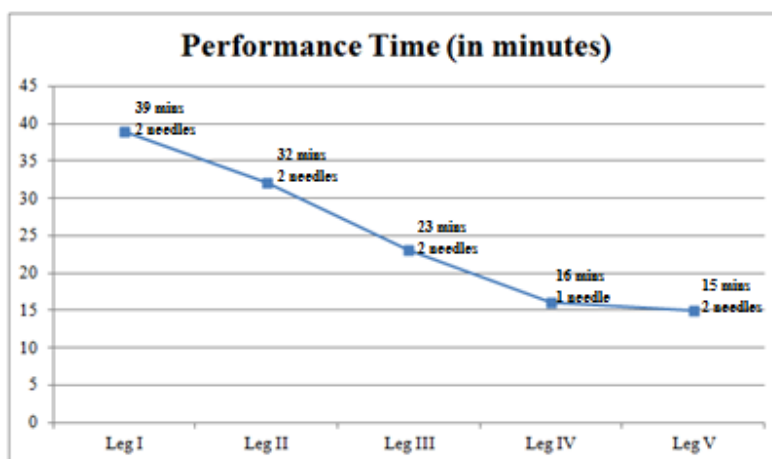


Figure A.9: Performance time reduction for the 5 subjects of the cadaver experiment, with the use of HipRFX.

Glossary

In this appendix we give an overview of frequently used terms and abbreviations.

CA(O)S: Computer Assisted(Orthopedic) Surgery

CAD: Computer Aided Design

CT: Computed Tomography

DoFs: Degrees of Freedom

DRR: Digitally Reconstructed Radiograph

MRI: Magnetic Resonance Imaging

OR: Operation Room

PMMA: polymethylmethacrylate

ROM: Range of Motion